ATG9 vesicles are a subtype of intracellular nanovesicle

Mary Fesenko [1], Daniel J. Moore [1], Peyton Ewbank[1], Elizabeth Courthold [1], and Stephen J. Royle [1,✉]

[1]Centre for Mechanochemical Cell Biology and Division of Biomedical Sciences, Warwick Medical School, University of Warwick, Coventry, UK

Cells are filled with thousands of vesicles, which mediate protein transport and ensure homeostasis of the endomembrane system. Distinguishing these vesicles functionally and molecularly represents a major challenge. Intracellular nanovesicles (INVs) are a large class of transport vesicles that likely comprises of multiple subtypes. Here, we define the INV proteome and find that it is molecularly heterogeneous, and enriched for transmembrane cargo molecules including integrins, transporters, and ATG9A, a lipid scramblase associated with autophagy. ATG9A is known to reside in 'ATG9 vesicles': small vesicles that contribute to autophagosome formation. Using in-cell vesicle capture assays we found that ATG9A, as well as other ATG9 vesicle cargos, were in INVs. Quantitative analysis showed that virtually all ATG9 vesicles are INVs, but that only ∼20 % of INVs are ATG9 vesicles, suggesting that ATG9 vesicles are in fact a subtype of INV, which we term ATG9A-flavor INVs. Finally, we show that perturbing ATG9A-flavor INVs impaired the autophagy response induced by starvation.

autophagy | transport vesicle | proteomics | cargo | membrane traffic
Correspondence: ***s.j.royle@warwick.ac.uk***

Introduction

Membrane trafficking is a fundamental cellular process by which cargo molecules are moved between compartments via vesicular carriers. Several types of vesicle have been identified so far. Well-studied examples include those identified by their electron dense coat: clathrin-coated vesicles or COPII-coated vesicles (Bonifacino and Glick, 2004). However, the cell is filled with thousands of small, uncoated vesicles, whose roles in intracellular trafficking are poorly understood. We recently described a novel type of transport vesicle, intracellular nanovesicles (INVs). They are small (∼35 nm diameter), uncoated vesicles that are defined by the presence of Tumor Protein D52-like (TPD52-like) protein family members on their surface (Larocque et al., 2020, 2021; Larocque and Royle, 2022). INVs are an integral part of the intracellular trafficking network and they transport cargo on the anterograde and recycling pathways, mainly moving by diffusion (Larocque and Royle, 2022; Sittewelle and Royle, 2024). Importantly, INVs are likely a superfamily of vesicles with different identities, or flavors. For example, they collectively contain at least 16 different Rab GTPases and a minimum of four different R-SNAREs, which suggest the vesicles have diverse origins (Larocque et al., 2020). Disambiguation of the different flavors of INVs is therefore a major challenge.

There are four TPD52-like proteins (TPD52, TPD53/TPD52L1, TPD54/TPD52L2, TPD55/TPD52L3) that each contain a coiled-coil domain through which they can homo- or hetero-dimerize (Byrne et al., 1998), and four amphipathic helices, with a preference for high curvature membranes (Reynaud et al., 2022; Larocque et al., 2021). The third amphipathic helix in TPD54 conforms to an amphipathic lipid packing sensor (ALPS) motif, and mutation of a single positively charged residue in this region (R159E) prevents the otherwise tight association of TPD54 with INVs (Reynaud et al., 2022; Larocque et al., 2021). Due to its high expression among TPD52-like proteins, TPD54 is used as a marker for INVs (Larocque et al., 2020).

Autophagy, the cellular process responsible for clearing unnecessary or dysfunctional components, relies on the formation of autophagosomes. These specialized organelles encapsulate targeted cargoes and transport them to lysosomes for degradation. Of the core set of Atg proteins that are essential for autophagy, Atg9/ATG9A is the only transmembrane protein (Nishimura and Tooze, 2020), and functions as a lipid scramblase (Maeda et al., 2020; Guardia et al., 2020; Matoba et al., 2020). In mammalian cells, ATG9A resides on small uncoated vesicles, termed 'ATG9 vesicles', that cycle between the *trans*-Golgi network, the plasma membrane and the endosomal system (Orsi et al., 2012; Popovic and Dikic, 2014; Young et al., 2006). During autophagy, ATG9 vesicles move to the phagophore assembly site, where they contribute to phagophore formation through mechanisms that are still being determined (Orsi et al., 2012; Karanasios et al., 2016; Olivas et al., 2023; Broadbent et al., 2023). ATG9 vesicles are formed at the *trans*-Golgi network (TGN) via the recruitment of adaptor proteins, of which the AP-4 dependent mechanism is the best characterized (Davies et al., 2018; Mattera et al., 2017). Neurological diseases associated with AP-4 deficiency, might therefore be explained by dysregulation of autophagy caused by mistrafficking of ATG9A. Finally, ATG9 vesicles may have additional, autophagy-independent functions. For example, in plasma membrane repair (Claude-Taupin et al., 2021), in mobilization of lipids from lipid droplets to mitochondria (Mailler et al., 2021), and in integrin trafficking during cell migration (Campisi et al., 2022). At

least superficially, ATG9 vesicles resemble INVs: their size, lack of coat, their diffusive movement through the cytoplasm and their involvement in exocytosis and integrin recycling (Broadbent et al., 2023; Holzer et al., 2024; Sittewelle and Royle, 2024; Larocque et al., 2021).

To determine the different molecular identities of INV and how these subtypes might relate to other vesicle types, we set out to determine the INV proteome. Analysis of the proteome underscored the molecular heterogeneity of this class of transport vesicle. The presence of ATG9A and other ATG9 vesicle cargos in the proteome prompted us to investigate whether ATG9 vesicles could be one flavor of INV. We show that a fraction of INVs can account for the majority of ATG9 vesicles and that perturbing INVs results in impaired autophagy.

Results

Determining the INV proteome

Our previous work suggested that INVs could be immunoisolated from cells and analyzed proteomically (Larocque et al., 2020, 2021). We therefore optimized an INV immunoisolation procedure from cells permeabilized with low concentrations of digitonin, and using a GFP nanobody (GFP-Trap) to isolate the INVs by virtue of the marker protein GFP-TPD54. For optimization, three different cell backgrounds were used, either parental HeLa cells (control), HeLa cells stably expressing GFP-TPD54 (WT) or a GFP-TPD54 mutant (R159E) that cannot bind INVs (Figure 1A-D). The immunoisolated material from GFP-TPD54 WT cells was significantly enriched for 111 or 120 proteins when compared with control or cells expressing GFP-TPD54 R159E, respectively (Figure 1B,D). The enriched proteins included all TPD52-like proteins expressed in HeLa cells (TPD54, TPD52, and TPD53) as well as various Rabs, VAMPs and cargo proteins, suggesting successful purification of INVs. By contrast, immunoisolated material from cells expressing GFP-TPD54 R159E did not isolate INVs, with only 17 proteins alongside TPD54 significantly enriched compared to control (Figure 1C and S1A,B). Nine of these proteins were known contaminants in affinity purification experiments (Mellacheruvu et al., 2013). This suggests that the majority of proteins enriched following immunoisolation from GFP-TPD54 WT expressing cells are *bona fide* INV proteins and are not, for example, binding directly to TPD54.

With this method in hand, we extended the approach to large-scale isolation of INVs from a knock-in GFP-TPD54 HeLa cell line. This allowed us to isolate endogenous INVs via GFP-Trap and compare to a control IP from a single cell line source (Figure 1E). Analysis of these experiments yielded 525 proteins that were significantly enriched compared to the control (Figure 1F-G). Again, TPD52-like proteins, Rabs and cargo were present alongside other proteins indicating deeper coverage with this strategy. We combined the data from both approaches to obtain a list of 602 proteins that we consider a first INV proteome (Supplementary Table S1).

Exploring the INV proteome

To begin exploring the INV proteome, we used PANTHER protein classification to categorize INV proteins (Figure 2A and Supplementary Table S2). The "membrane traffic protein" class and "G-protein" subclass were both large with 35 proteins each. The INV proteome contains 17 Rab GTPases (Rab1A-C, Rab2A, Rab5A-C, Rab6A, Rab7A, Rab8A-B, Rab10, Rab11A-B, Rab14, Rab21, and Rab34), 4 VAMPs (VAMP2, VAMP3, VAMP7, and VAMP8) as well as TPD52-like proteins; which is consistent with previous vesicle trapping experiments (Larocque et al., 2020). Aside from dynamin-2 (DNM2) and coatomer subunit-beta (COPB1), there was an absence of machinery associated with classical coated vesicles. The largest category was without PANTHER protein classification (Unclassified) and this contained many secreted proteins (see below). When used as bait in proximity biotinylation proteomics studies, a number of INV proteins, including DNAJC5, LAMTOR1, LAMP2, RhoB, Rab2, Rab5C, Rab11A, and NRAS, have each identified TPD54 as their enriched putative interactor (Barker et al., 2024; Wilson et al., 2023; Go et al., 2021; Adhikari and Counter, 2018), giving confidence to our dataset.

Cargo proteins dominate the proteome. Across multiple categories, receptors, transporters and other transmembrane cargo proteins feature strongly. Examples include the transferrin receptor (TFRC), mannose-6-phosphate receptors (M6PR, IGF2R), and integrins (ITGA3, ITGA5, ITGA6, ITGAV, ITGA11, ITGB1) some of which have previously been shown to be trafficked via INVs (Larocque et al., 2020, 2021).

We found that the INV proteome had a significant enrichment of secreted proteins (10.5 % vs 7.2 %, χ^2 = 7.66, p = 5.7×10^{-3}) and of proteins with one or more transmembrane (TM) domains (28.0 % vs 17.0 %, χ^2 = 39.9, p = 2.7×10^{-10}), which is consistent with their previously characterized role as transport vesicles on the anterograde and recycling pathways (Figure 2B). Of the INV proteins that have TM domains, there was a notable enrichment of proteins with either 1, 4, or 12 TM domains (Figure 2C). The single pass protein group was the largest and was heterogeneous. However, the 12 TM domain proteins were all transporters (SLC12A2, SLC12A4, SLC16A1, SLC16A3, SLC2A1, SLC2A13, SLC7A11, SLC7A5, SPNS1), while the 4 TM domain proteins include tetraspanins (CD63, TSPAN6), and the secretory carrier-associated membrane proteins (SCAMP1, SCAMP2, SCAMP3), synaptogyrin-2 (SYNGR2), and synaptophysin-like protein 1 (SYPL1) whose neuronal counterparts are usually associated with synaptic vesicles. Gene Ontology (GO) enrichment analysis highlighted the cellular components secretory vesicle and secretory granule among other terms in-

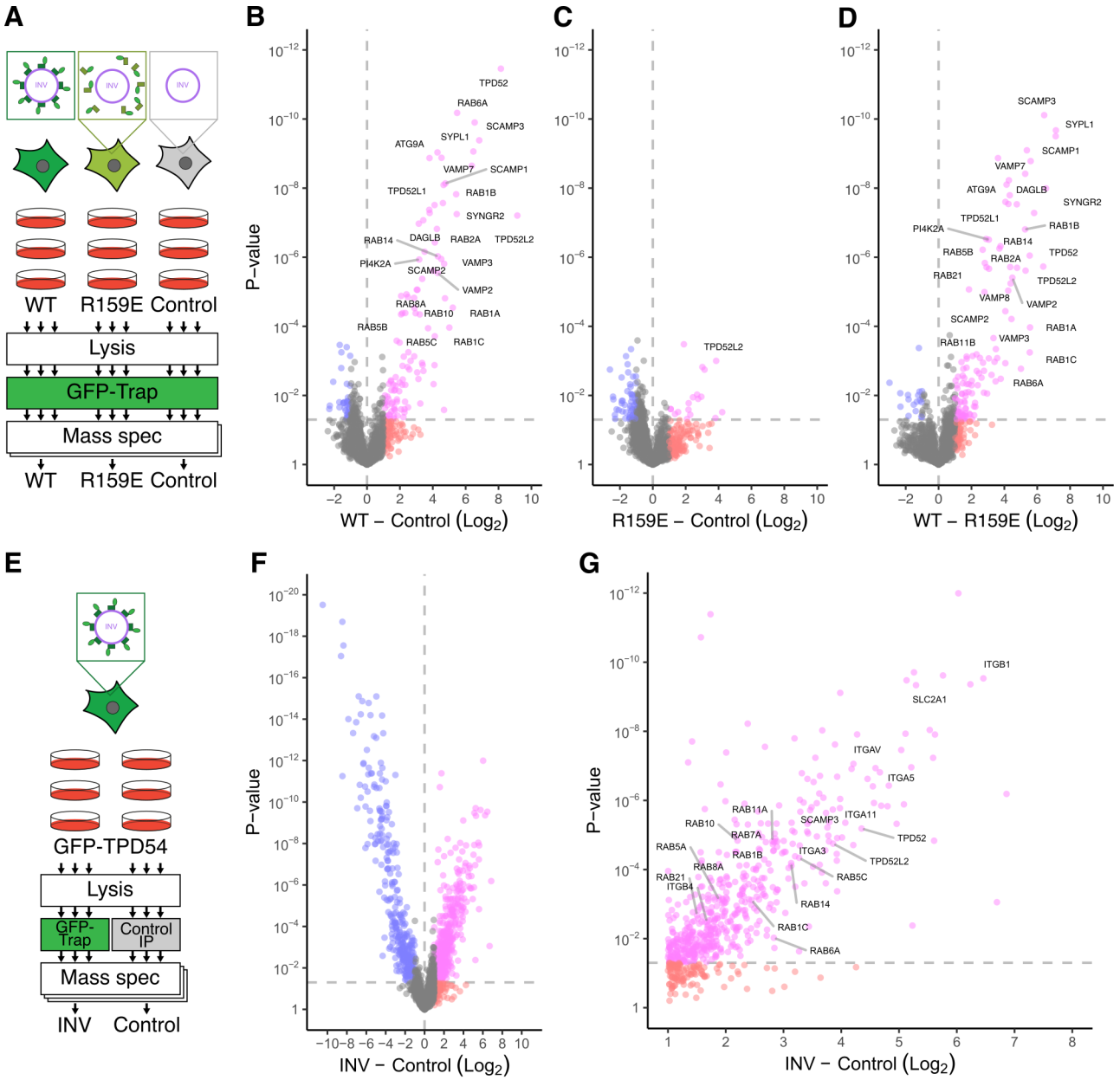

Figure 1. Determining the INV proteome.
(**A**) Schematic diagram of INV immunoisolation: GFP-Trap pulldown from HeLa cells stably expressing GFP-TPD54 WT, GFP-TPD54 R159E, or untransfected Hela cells (Control). (**B-D**) Volcano plots to show comparisons of (B) WT and Control, (C) R159E and Control, or (D) WT and R159E. Data are from two independent runs consisting of three replicates each. (**E**) Schematic diagram of INV immunoisolation: GFP-Trap or control IP pulldown from GFP-TPD54 knock-in HeLa cells. (**F**) Volcano plot to show the comparison of INV and Control isolation. (**G**) Expanded view of F. Data are from three independent runs of three replicates each. Colors indicate: pink, fold-change > 2 and p < 0.05; red, fold-change > 2 and p > 0.05; blue, fold-change < 2 and p < 0.05; gray, remainder.

cluding cell migration, cell adhesion, and GTPase binding (Figure 2D).

We next compared the INV proteome with previously published vesicle proteomic datasets. The presence of VAMP2, SCAMPs, SYNGR2 and SYPL-1, together with vacuolar-type ATPase subunits (ATP6V0A1, ATP6V0D1) was intriguing, especially since TPD52-like proteins are abundant in published synaptic vesicle proteomes (Bradberry et al., 2022; Biesemann et al., 2014). This likely reflects the fraction of INVs that are exocytosed, as we previously demonstrated (Sittewelle and Royle, 2024). First, given the non-neuronal origin of our INV proteome we compared our data with that from synaptic-like microvesicles from PC12 cells, rather than synaptic vesicles (Salazar et al., 2005). We found significant enrichment in the INV proteome for proteins from this dataset (5.5 % vs 1.8 %, χ^2 = 28.44, p = 9.653×10^{-8}); with 27.5 % of SLMV proteins featured in the INV proteome (Supplementary Figure S2A, D).

Since the lipid scramblase ATG9A was also among the cargo proteins in the INV proteome we next compared our data to an ATG9 vesicle proteome (Judith et al., 2019). We found a significant enrichment in the INV proteome for proteins in the ATG9 vesicle dataset (23.8 % vs 10.7 %, χ^2 = 78.73, p < 2.2×10^{-16}). Moreover, the intensity or enrichment of common proteins from the two

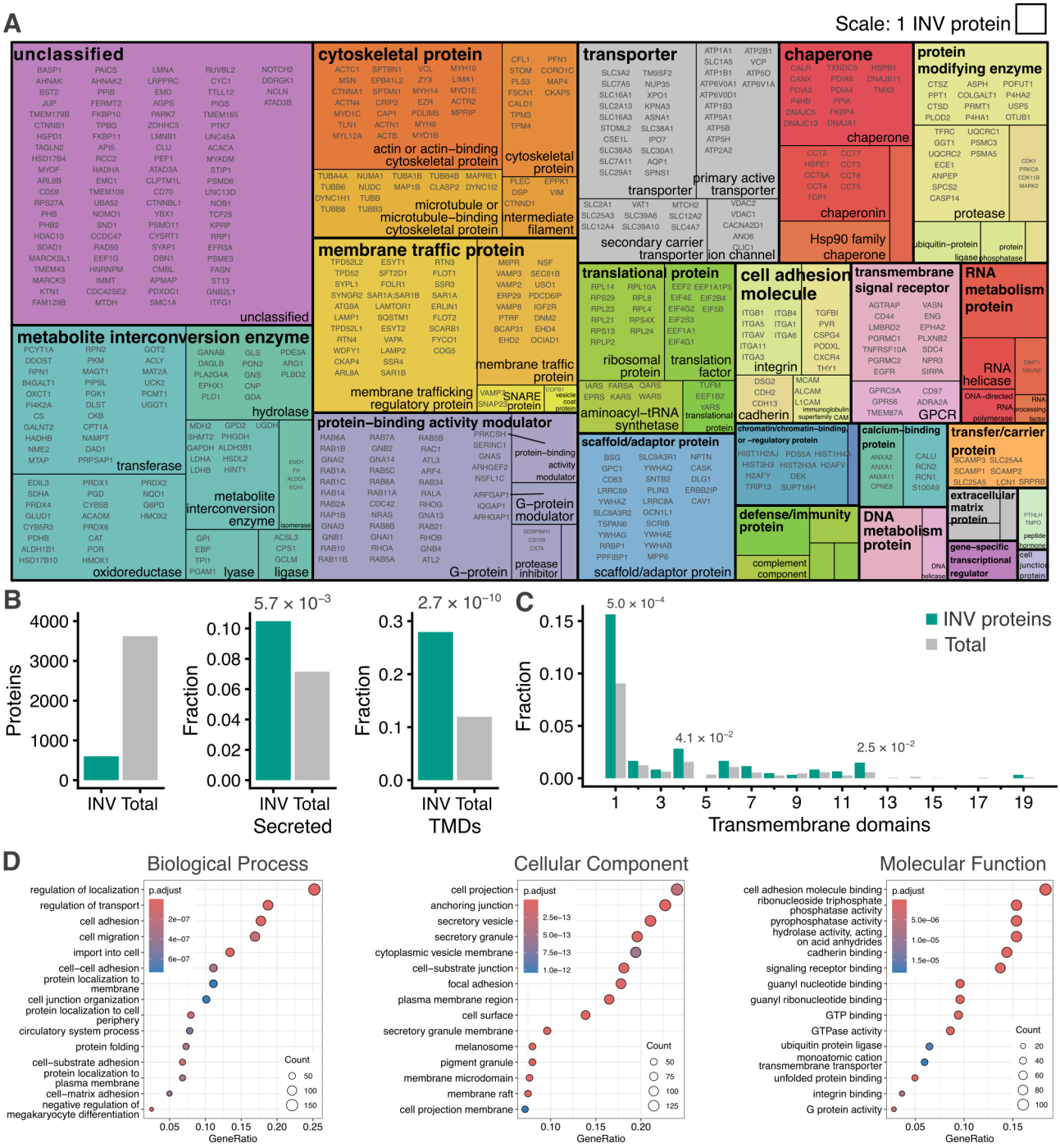

Figure 2. Composition of the INV proteome.

(**A**) Treemap visualization of classification of 602 INV proteins. Two levels of PANTHER classification are shown (for details see Materials and Methods, for full list see Supplementary Table S2). (**B**) Bar charts showing the INV proteins versus all proteins detected (Total), and the fractions of INV or total proteins, which are designated as secreted or which contained one or more transmembrane domain (TMD). Enrichment of secreted or TMD-containing proteins in INVs versus total is indicated, p-values from Pearson's Chi-squared test. (**C**) Fractions of proteins with the indicated number of transmembrane domains. Significant enrichment is indicated by p-values from Pearson's Chi-squared test. (**D**) Gene Ontology (GO) term enrichment analysis for 602 INV proteins versus total.

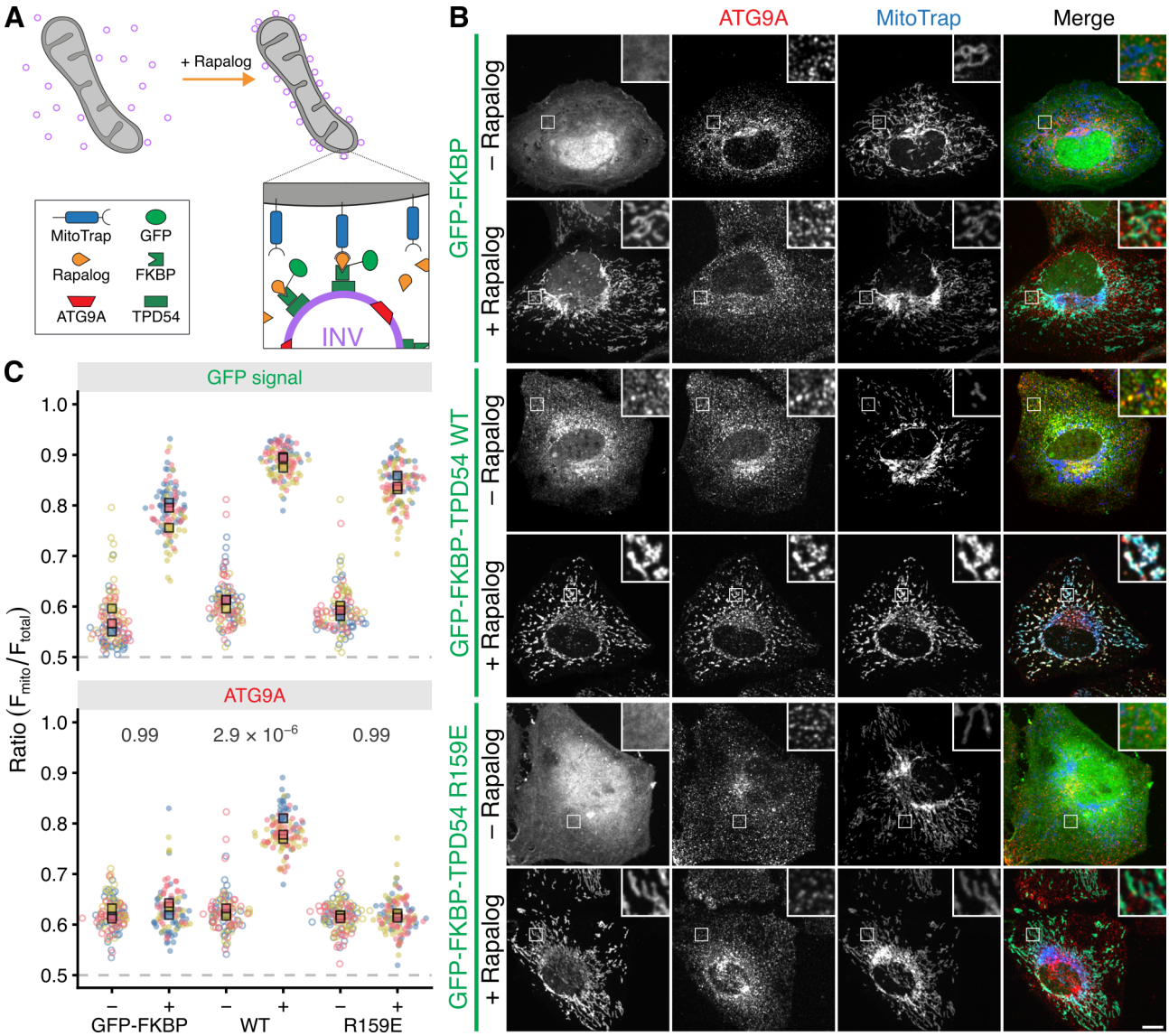

Figure 3. ATG9A is in intracellular nanovesicles.
(**A**) Schematic diagram of vesicle capture at mitochondria as a test for co-relocation. MitoTrap is an FRB domain targeted to mitochondria, GFP-FKBP-TPD54 is coexpressed and, when rapalog is added, the INVs associated with TPD54 become trapped at the mitochondria. Any protein that is also in the INVs is co-relocated with TPD54 (Larocque et al., 2020). (**B**) Representative confocal images of HeLa cells expressing MitoTrap (pMito-mCherry-FRB T2098L, blue) and either GFP-FKBP, GFP-FKBP-TPD54 WT, or GFP-FKBP-TPD54 R159E (green), stained with AF647-conjugated anti-ATG9A antibody (red). Cells were treated with rapalog (5 µM, 5 min) or not, as indicated. Scale bar, 10 µm; insets, 4 × zoom. (**C**) Superplot to show the relocalization of GFP-FKBP or GFP-FKBP-tagged TPD54 construct and the extent of co-relocation of ATG9A. Data are expressed as a fraction of the total fluorescence per cell that is at the mitochondria. Spots indicate individual cell measurements (n = ∼50 per repeat), colors indicate independent experimental repeats (n = 3), squares show the mean value for each replicate. P-values, two-way ANOVA with Tukey's HSD post-hoc test.

datasets were correlated ($\rho = 0.21$, $p < 0.011$, Supplementary Figure S2B, D). Interestingly, in the ATG9 dataset, the INV marker protein TPD54 was one of the most enriched proteins in conditions that upregulate autophagy (Judith et al., 2019), yet the majority of the proteins common to the two datasets were de-enriched upon starvation (Supplementary Figure S2C). Finally, as a control, we tested for enrichment in the INV proteome for proteins in a CCV proteomic dataset (Borner et al., 2012) and found no enrichment (1.5 % vs 1.7 %, $\chi^2 = 0.02$, $p = 0.89$, Supplementary Figure S2D).

In summary, this analysis strengthens the view that INVs are a mix of different subtypes. The enrichment of ATG9 vesicle proteins in the INV proteome and the differential response of the INV proteome to starvation indicated to us that ATG9 vesicles could be a subtype of INV.

ATG9A is in intracellular nanovesicles

To investigate whether ATG9A is in INVs, we used a vesicle capture imaging assay. Here, INVs are captured at the mitochondria using induced heterodimerization between the FKBP-tagged INV marker protein (GFP-FKBP-TPD54) and MitoTrap (Mito-mCherry-FRB[T2098L]) with rapalog (AP21967, 5 µM). The co-relocation of another protein coincident with TPD54 indicates it is present in INVs (Figure 3A). Detection of endogenous ATG9A by immunofluorescence showed that

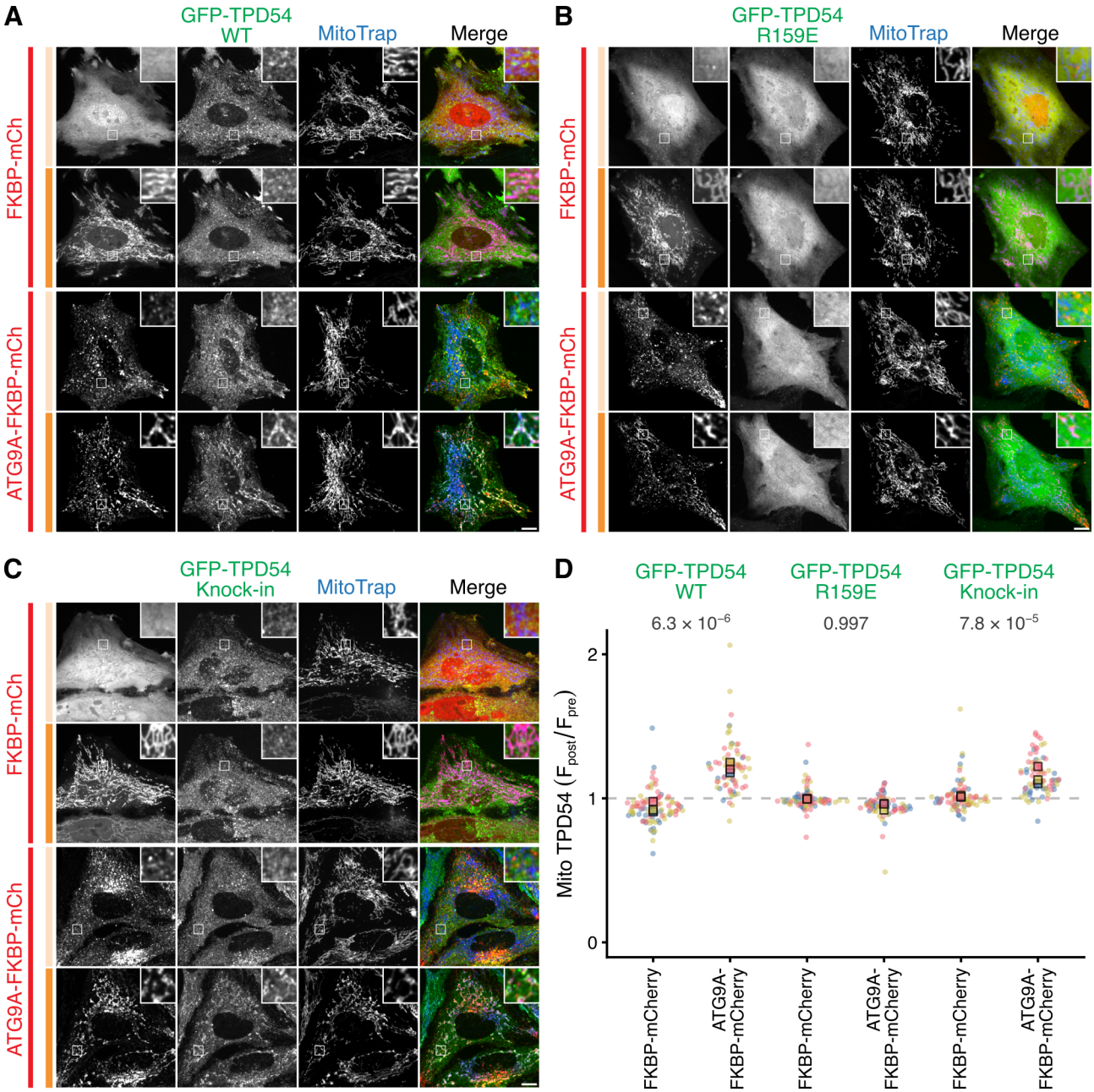

Figure 4. ATG9 vesicles have the INV marker TPD54.
(**A-C**) Representative confocal images of HeLa cells expressing MitoTrap (pMito-EBFP2-FRB T2098L, blue) and either FKBP-mCherry or ATG9A-FKBP-mCherry (red). Cells are co-expressing GFP-TPD54 WT (A), GFP-TPD54 R159E (B), or endogenous GFP-TPD54 knock-in (C) (green). For each condition, the same cell is shown pre- (pale orange bar) and post-treatment (dark orange bar) with rapalog (5 µM, 5 min). Scale bar, 10 µm; insets, 4 × zoom. (**D**) Superplot to show the ratio of mitochondrial fluorescence of GFP-TPD54 post- vs pre-rapalog treatment. Spots indicate individual cell measurements (n = 21 - 69 per repeat), colors indicate independent experimental repeats (n = 3), squares show the mean value for each replicate. P-values, two-way ANOVA with Tukey's HSD post-hoc test. Confirmation of FKBP-mCherry and ATG9A-FKBP-mCherry relocalization is shown in Supplementary Figure S3.

it was strongly co-relocated to the mitochondria when GFP-FKBP-TPD54 WT was relocalized there; but not when GFP-FKBP or GFP-FKBP-TPD54 R159E mutant were relocalized (Figure 3B). Quantification of the ratio of mitochondrial fluorescence versus the total fluorescence per cell demonstrated successful relocalization of the GFP-FKBP tagged proteins to the mitochondria in each case and underscored that co-relocation of ATG9A only occurred with TPD54 WT (Figure 3C). These results indicate that endogenous ATG9A is found in INVs in cells.

ATG9 vesicles are INVs

Next, we performed the reciprocal test: relocalizing ATG9A and asking if TPD54 is co-relocated. To do this, ATG9A-containing vesicles were captured at the mitochondria using ATG9A-FKBP-mCherry with MitoTrap (Mito-EBFP2-FRB T2098L). Using this approach we found that GFP-TPD54 WT but not the R159E mutant was co-relocated to the mitochondria, when ATG9A-FKBP-mCherry was relocalized (Figure 4A,B). This result indicates that GFP-TPD54 WT is present on the same vesicle as ATG9A-FKBP-mCherry by virtue

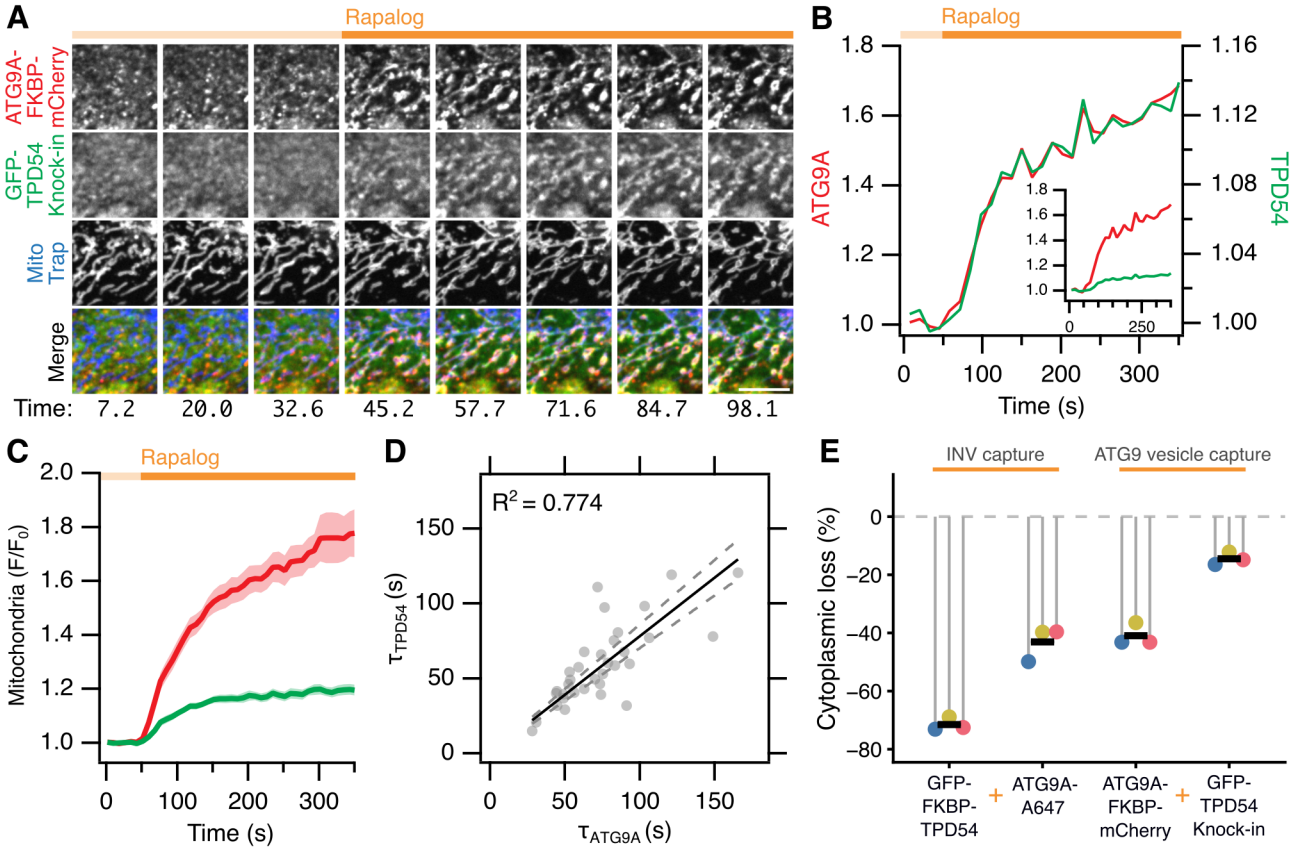

Figure 5. ATG9 vesicles are a subset of INVs.
(**A**) Cropped stills from a movie of GFP-TPD54 (green) knock-in cells expressing ATG9A-FKBP-mCherry (red) and MitoTrap (blue); capture of ATG9A-positive vesicles at the mitochondria is induced by rapalog (5 µM at 40 s). Scale bar, 5 µm. See Supplementary Video SV1. (**B**) Quantification of mitochondria fluorescence of ATG9A-FKBP-mCherry (left axis) and GFP-TPD54 (right axis) for the cell shown in A. Plot shows fluorescence divided by initial fluorescence (F/F_0) Inset: traces shown on same scale. (**C**) Average mitochondrial ATG9A-FKBP-mCherry and GFP-TPD54 signal for 34 cells, from 3 independent experiments (mean ±sem). (**D**) Plot of the time constant (Tau) for single exponential fits to the ATG9A-FKBP-mCherry and the GFP-TPD54 traces. Lines show a linear fit to the data and 95 % confidence bands; R^2 value for the fit through the origin is shown. (**E**) Loss of cytoplasmic signal following relocalization. Lollipops show the average decrease per experimental repeat (n = 31 - 52 cells), bar shows the mean (n = 3 independent repeats). Data are calculated from experiments in Figures 3 and 4.

of membrane-binding rather than by an association with ATG9A itself. Moreover, endogenous TPD54 (in GFP-TPD54 knock-in cells) was also co-relocated with ATG9A-FKBP-mCherry, indicating that co-relocation was not a result of overexpression of GFP-TPD54 (Figure 4C). Importantly, the co-relocation of TPD54 was dependent on ATG9A-containing vesicle capture, because relocalization of FKBP-mCherry had no effect on GFP-TPD54 localization (Figure 4A,C). Quantification of the ratio of mitochondrial TPD54 fluorescence post- versus pre-rapalog treatment confirmed the specific co-relocation of TPD54 with ATG9A relocalization (Figure 4D). The results indicate that relocalization–co-relocation of ATG9A and TPD54 was reciprocal.

The most likely interpretation of these experiments is that the two proteins are present in the same vesicles. Since our analysis was done at two discrete time points, it is formally possible that distinct INVs were captured secondarily to the trapping of ATG9 vesicles at the mitochondria. To address this point, we used live-cell imaging to study the kinetics of ATG9A-FKBP-mCherry relocalization and endogenous GFP-TPD54 co-relocation to the mitochondria in response to 5 µM rapalog (Figure 5A-D, Supplementary Movie SV1). Analysis of the mitochondrial fluorescence of each protein as a ratio of the pre-rapalog fluorescence, revealed a jump in fluorescence which was coincident in both channels (Figure 5A-C). The kinetics of relocalization and co-relocation were highly similar: the time-constant (τ) of a single exponential function fitted to each protein co-varied across 34 cells from three experiments ($R^2 = 0.774$, Figure 5D). This strengthens the evidence that the two proteins are on the same vesicles and argues against the secondary capture of a distinct vesicle type. This analysis also revealed a disparity in the extent of co-relocation of TPD54 compared to the amount of ATG9A that was relocalized (see below). Together these results indicate that TPD54 is found in ATG9A-containing vesicles in cells. Since our definition of INVs is that they contain TPD54, then it follows that ATG9 vesicles are actually INVs.

ATG9A-containing vesicles are subset of INVs

In the relocalization–co-relocation experiments, the loss of protein from the cytoplasm can be quantified in order to estimate the sizes of the vesicle pools that are captured at the mitochondria. We therefore compared the loss of fluorescence in the cytoplasm after adding ra-

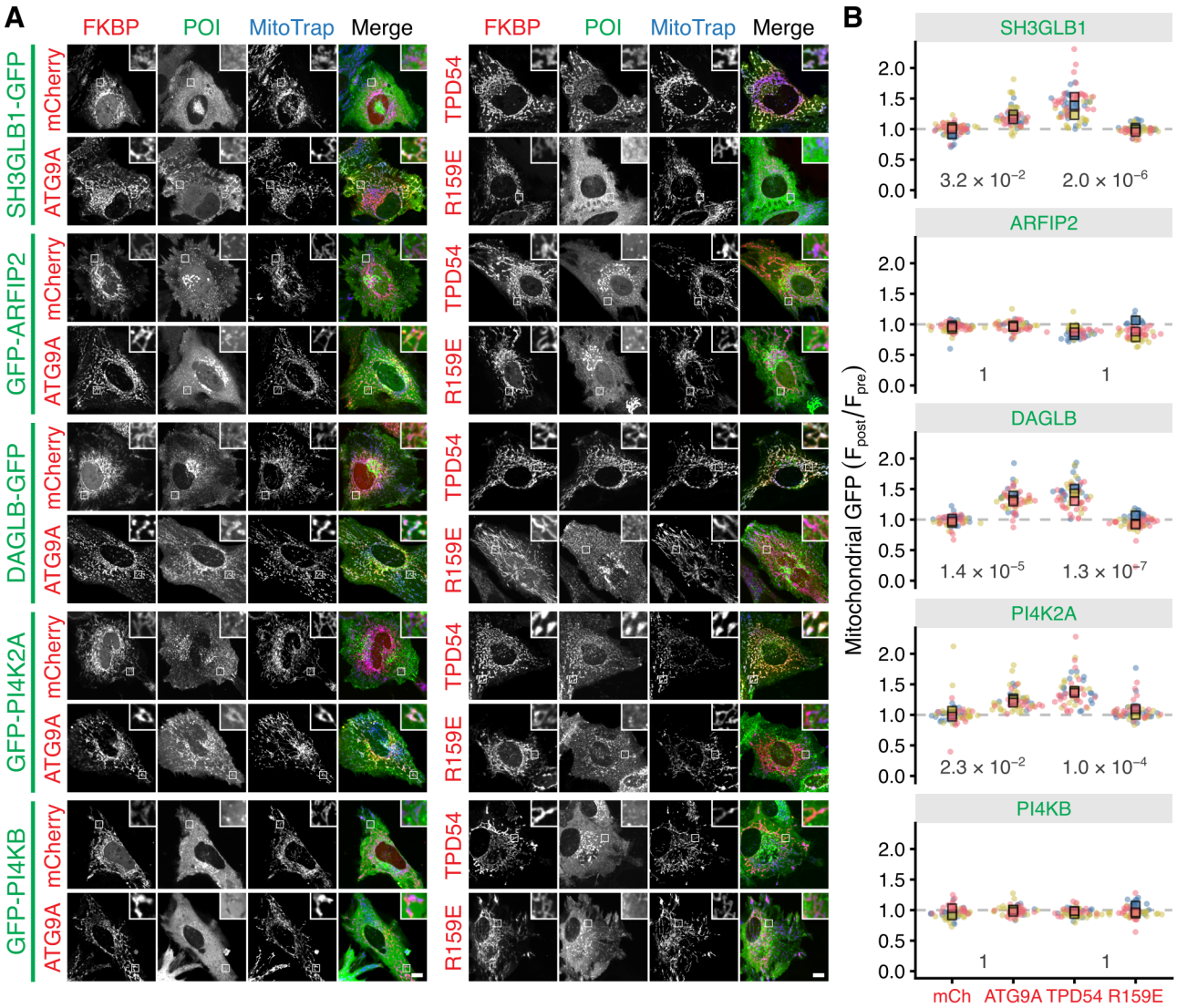

Figure 6. ATG9A-flavor INVs have ATG9 vesicle cargos.
(**A**) Representative confocal images of HeLa cells expressing MitoTrap (pMito-EBFP2-FRB T2098L, blue) and either FKBP-mCherry, ATG9A-FKBP-mCherry, mCherry-FKBP-TPD54 WT, or mCherry-FKBP-TPD54 R159E (red). Cells are co-expressing GFP-tagged SH3GLB1, ARFIP2, DAGLB, PI4K2A, or PI4KB as indicated (green). For each condition, only the post-rapalog (5 µM, 5 min) treatment images are shown, for the pre-treatment images see Supplementary Figure S4. Scale bar, 10 µm; insets, 4 × zoom. (**B**) Superplots to show the ratio of mitochondrial fluorescence of the indicated GFP-tagged protein post- vs pre-rapalog treatment. Spots indicate individual cell measurements (n = 10 - 28 cells per repeat), colors indicate independent experimental repeats (n = 3), squares show the mean value for each replicate.

palog as a percentage of its steady-state localization. During INV capture – when TPD54 was relocalized and ATG9A co-relocated – there was a 71.5 % decrease in cytosoplasmic TPD54 resulting in a 43.1 % decrease in endogenous ATG9A signal (Figure 5E). During capture of vesicles containing ATG9A – when ATG9A was relocalized and TPD54 co-relocated – we found a 41.0 % decrease in cytoplasmic ATG9A causing only a 14.5 % decrease of the endogenous TPD54. This means that the size of the pool of vesicles that can be relocalized is ∼70 % for TPD54 and ∼40 % for ATG9A. Therefore, the capture of INVs results in trapping of the entire ATG9 vesicle pool; whereas only ∼20 % of the INV pool was trapped when all of the ATG9A-positive vesicles were captured. That is, all ATG9 vesicles are INVs, but not all INVs are ATG9 vesicles. We conclude that ATG9 vesicles are a subset of INVs and we term them ATG9A-flavor INVs.

ATG9 vesicle cargo is also in INVs

If ATG9 vesicles are ATG9A-flavor INVs, then we would predict that other ATG9 vesicle cargos would also be found in INVs. To test this possibility, we examined the co-relocation of five candidate proteins reported to be present on ATG9 vesicles: SH3GLB1, ARFIP2, DAGLB, PI4K2A, PI4KB (Takahashi et al., 2011; Judith et al., 2019; Davies et al., 2022). Of these, DAGLB and PI4K2A were enriched in the INV proteome (Supplementary Table S1). We performed vesicle capture using relocalization of either ATG9A-FKBP-mCherry or mCherry-FKBP-TPD54 to MitoTrap and used FKBP-mCherry or mCherry-FKBP-TPD54 R159E mutant as the respective negative controls for the specificity of cargo co-relocation due to vesicle capture. For GFP-

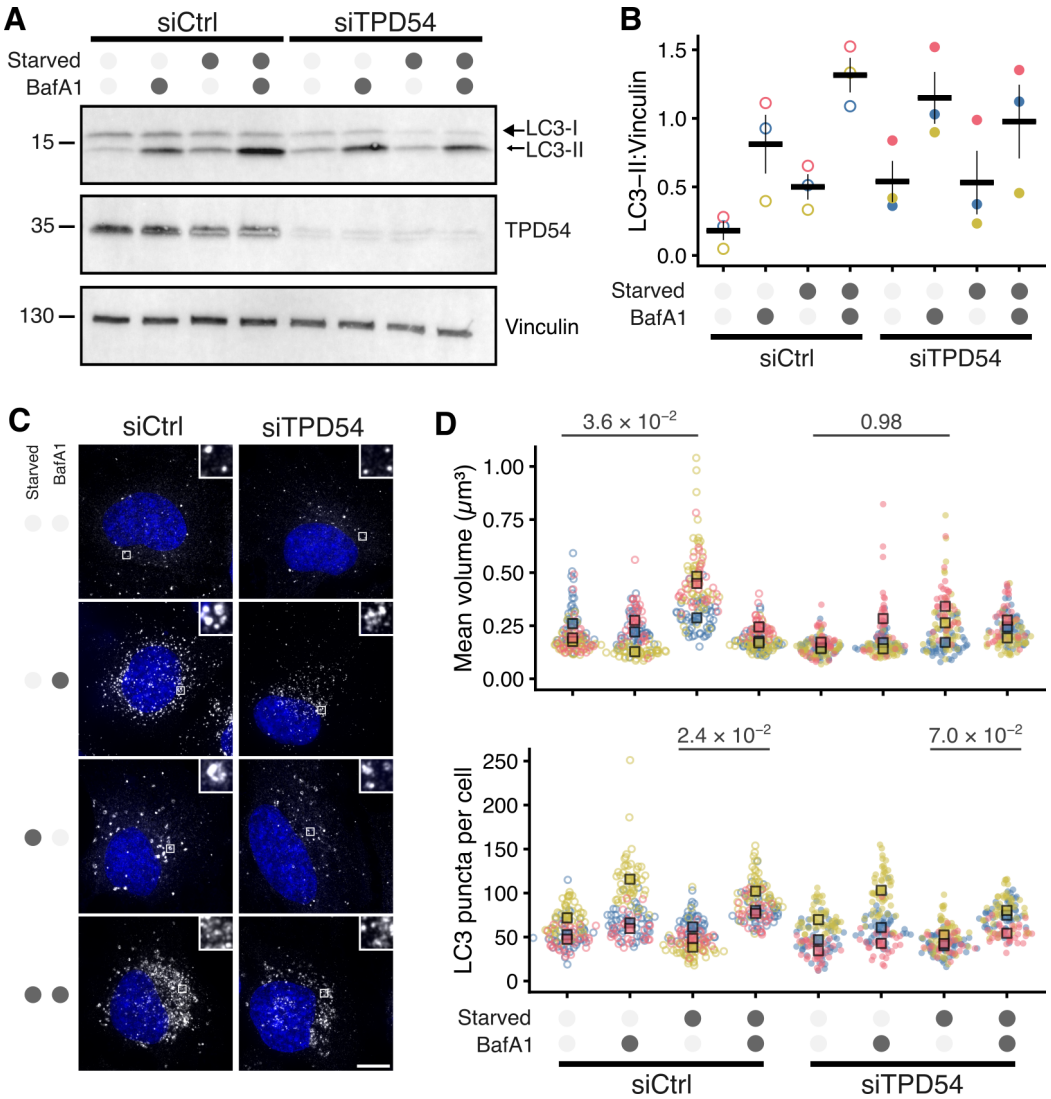

Figure 7. Depletion of TPD54 impairs the autophagy response.
HeLa cells were transfected with control (GL2, siCtrl) or TPD54 (siTPD54) siRNA, then either starved (3 h) or not and either treated with BafA1 (100 μM) or not, as indicated. (**A**) Western blot showing levels of LC3B, TPD54 and vinculin (loading control). Result is typical of three repeats shown in Supplementary Figure S6. (**B**) Quantification of LC3B-II signal normalized to vinculin. Dots show experimental repeats and bars shown mean ± sem. (**C**) Representative maximum intensity z-projections showing LC3 immunofluorescence (white) and DAPI (blue). Scale bar, 10 μm; insets, 5 × zoom. TPD54 depletion for these experiments was confirmed by Western blot (Supplementary Figure S7). (**D**) Superplots to show the average volume and number of LC3 puncta. Spots indicate individual cell measurements (n = 30 - 50 cells per repeat), colors indicate independent experimental repeats (n = 3), squares show the mean value for each replicate. P-values from Tukey's HSD post hoc test, following two-way ANOVA.

tagged SH3GLB1, DAGLB and PI4K2A, we observed robust co-relocation that was caused by the relocalization of ATG9A or of TPD54 (Figure 6A,B). No co-relocation was observed for GFP-tagged ARFIP2 nor for PI4KB when either ATG9A-FKBP-mCherry or mCherry-FKBP-TPD54 was relocalized to mitochondria (Figure 6B). This was unexpected because ARFIP2 and PI4KB strongly colocalized with ATG9A at the TGN prior to relocalization (Supplementary Figure S4). This might indicate that these two proteins are associated with ATG9A at the TGN and that this pool of ATG9A is not relocalized in our experiments, or they are not stably associated with vesicles, such that they fall off during vesicle trapping. Where co-relocation of cargo proteins was observed, it was specific because relocalization of FKBP-mCherry or mCherry-FKBP-TPD54 R159E had no effect any of the candidates. The finding that the same candidate proteins were co-relocated by relocalization of ATG9A or of TPD54 underscores the idea ATG9 vesicles are ATG9A-flavor INVs. The magnitude of co-relocation of SH3GLB1, DAGLB and PI4K2A was greater with relocalization of TPD54 than with ATG9A, which indicates that these proteins may be on other INV subtypes in addition to ATG9A-flavor INVs.

ATG9A-flavor INVs can be distinguished from another INV subtype by selective transport

RUSC2 overexpression induces a striking aggregation of AP4-derived vesicles and their cargoes, including ATG9A, at the edges of the cell (Davies et al., 2018; Guardia et al., 2021). To test if ATG9A-flavor INVs respond to HA-RUSC2 overexpression in the same way, we examined vesicle distributions in GFP-TPD54

knock-in HeLa cells in these conditions by microscopy. Large accumulations of HA-RUSC2 at the cell periphery were found in the majority of cells, and these accumulations were positive for GFP-TPD54 and ATG9A immunofluorescence (Supplementary Figure S5. Another INV cargo – CIMPR/IGF2R – did not accumulate at HA-RUSC2/TPD54 vesicle aggregations (Supplementary Figure S5. CIMPR is found in our INV proteome and we have previously shown that CIMPR-containing INVs can be relocalized to the mitochondria by INV trapping (Larocque et al., 2020). Therefore, these results suggest two things. First, that endogenous ATG9A-flavor INVs behave in the same way as ATG9 vesicles; second, the selectivity of this manipulation highlights that not all INVs are ATG9A-flavor INVs, and that other subtypes of INV behave differently.

Depletion of TPD54 impairs the autophagy response

Having established that ATG9 vesicles are a subset of INVs, we next tested whether these INVs were functional during autophagy. To do this, we depleted TPD54 using RNAi and examined the levels of the autophagy marker protein LC3B/MAP1LC3B in HeLa cells under fed or starvation conditions, with or without bafilomycin A1 (BafA1, 100 nM). Western blotting revealed that in control RNAi cells, the level of LC3B-II – the lipidated form of LC3B – was low in basal conditions (fed, no BafA1) and increased with BafA1 treatment, indicating a functional basal autophagic flux response (Figure 7A,B). When autophagy was upregulated by amino acid and growth factor starvation, the amount of LC3B-II increased by 2.8-fold, as expected. The level of LC3B-II increased further in cells that were starved and treated with BafA1, indicating the expected higher autophagic flux in response to starvation-induced autophagy upregulation. In TPD54-depleted cells, the level of LC3B-II was higher in basal conditions, but the rate of basal autophagic flux was unchanged when compared to control RNAi cells. However, we did not observe further increases in the levels of LC3B-II in response to starvation in TPD54-depleted cells, and induced autophagic flux was also dampened, relative to that in control RNAi cells (Figure 7A,B).

Under the same conditions, we also directly visualized autophagosome formation using immunofluorescence detection of LC3B. Starvation resulted in an increase in the mean volume of LC3 puncta per cell, but this increase was less pronounced in TPD54-depleted cells (Figure 7C,D). The mean volume of LC3 puncta in starved cells was 24.0–40.2 % lower in TPD54-depleted cells than controls, indicating inhibition of autophagosome formation (Figure 7D). Basal autophagic flux, assessed by quantifying numbers of LC3 puncta per cell was unaffected by TPD54 RNAi, however autophagic flux induced by starvation was lower in TPD54 depleted cells. BafA1 treatment of starved, control RNAi cells resulted in a 0.3- to 1.6-fold accumulation of smaller

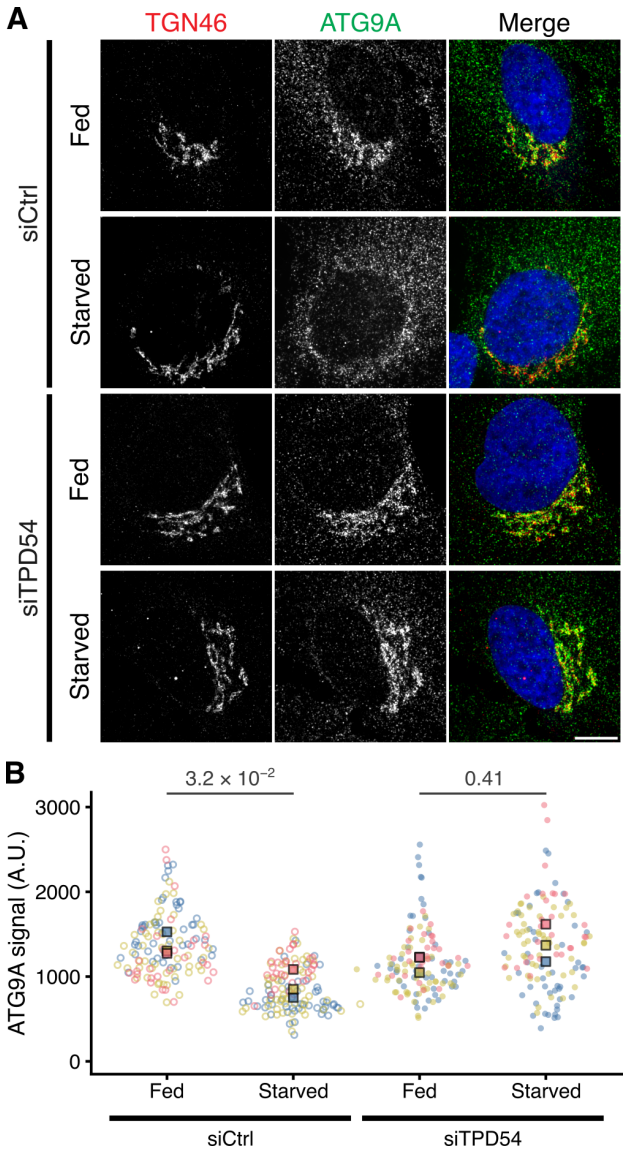

Figure 8. Starvation-induced loss of ATG9A from the TGN is blocked by TPD54 depletion.
(**A**) Representative confocal micrographs of HeLa cells transfected with control (GL2, siCtrl) or TPD54-targeting siRNA (siTPD54) in either fed or starved (3 h) conditions as indicated, stained for TGN46 (red) and ATG9A (green). Scale bar, 10 µm. TPD54 depletion was confirmed by Western blot (Supplementary Figure S7). (**B**) Superplot to show the ATG9A immunofluorescence signal at the Golgi. Spots indicate individual cell measurements (n = 30 - 50 per repeat), colors indicate independent experimental repeats (n = 3), squares show the mean value for each replicate. P-values from Tukey's HSD post hoc test, following two-way ANOVA.

LC3 puncta. In TPD54-depleted cells, the LC3 puncta accumulation in starved, BafA1-treated cells was less pronounced and the mean number of LC3 puncta per cell was 6.8–29.3 % lower than in control RNAi cells (Figure 7D). Together, these data indicate that ATG9A-flavor INVs are functionally equivalent to previously described ATG9 vesicles during amino acid and growth factor starvation-induced autophagy. Perturbing INV function through TPD54 depletion inhibited autophagosome formation and impedes autophagic flux, identifying TPD54 as a novel molecular regulator of autophagy.

Cellular origin of ATG9A-flavor INVs

ATG9A has been shown to be redistributed from the TGN upon starvation (Orsi et al., 2012). We therefore tested whether INVs were involved in this phenomenon by examining the effect of TPD54 depletion on starvation-induced ATG9A redistribution. Using immunofluorescence of ATG9A and TGN46, we saw that under fed conditions, a fraction of ATG9A overlaps with the TGN (Figure 8A). Following 3 h amino acid and growth factor starvation, the ATG9A signal at the TGN was significantly lower in control RNAi conditions, confirming the redistribution phenomenon (Figure 8A,B). However in TPD54-depleted cells, this redistribution was blocked and the levels of ATG9A at the TGN in starved cells were not significantly different to those in fed conditions (Figure 8A,B). If the redistribution of ATG9A from the TGN during starvation represents the exit ATG9A in new ATG9A-flavor INVs to mediate autophagosome formation, and this is blocked by TPD54 depletion, then it suggests that TPD54 is involved in their formation.

Discussion

Understanding the functions and identities of the thousands of uncoated vesicles inside cells is a major challenge. Here, we described the proteome of intracellular nanovesicles and found that this is a large, molecularly diverse class of vesicles, likely comprising of multiple INV subtypes. We showed that ATG9 vesicles – a key membrane source during autophagy – are a subtype of INV, and confirmed that it is these ATG9A-flavor INVs that are important for autophagic flux.

ATG9 vesicles have been classically defined by the presence of the transmembrane Atg gene product, ATG9A or ATG9B in humans. Our finding, that these vesicles are actually a subtype of INV, is based on multiple lines of evidence. First, ATG9A and other ATG9 vesicle cargos are found in the INV proteome, and the INV marker, TPD54, is found in an ATG9 vesicle proteome (Judith et al., 2019). Second, ATG9A is in INVs and ATG9 vesicles have an INV marker, as revealed by the reciprocal relocalization–co-relocation of ATG9A and TPD54 in cells. Third, some ATG9 vesicle cargos were also confirmed to be present in INVs using INV capture at the mitochondria. Fourth, depletion of TPD54 impaired the autophagy response: decreased LC3B lipidation, reduced autophagosome size and inhibition of subcellular redistribution of ATG9A. Fifth, comparison of vesicle capture efficiency suggests that approximately 20 % of INVs are ATG9A-flavor, whereas all ATG9 vesicles that could be captured are INVs. Finally, ATG9A-flavor INVs could be redistributed selectively to the cell periphery by RUSC2 overexpression, whereas a CIMPR-flavor of INV was unaffected. These findings are supplemented by other evidence such as the similar diffusivity of ATG9A-containing vesicles and INVs (Sittewelle and Royle, 2024; Broadbent et al., 2023).

The established function of ATG9 vesicles is as a membrane reservoir for autophagosome formation during autophagy. Accordingly, we found that depletion of TPD54 impeded autophagosome formation and autophagic flux in starved cells. In addition, the loss of ATG9A from the TGN upon starvation was also inhibited by TPD54 depletion. This suggests that TPD54 may be involved in the formation of ATG9A-flavor INVs at the TGN. Previous work indicates that ATG9 vesicles form at the TGN by an AP-4-dependent mechanism (Davies et al., 2018; Guardia et al., 2021). Beyond a preference for high curvature membranes there has yet to be a function ascribed to TPD54, so it is unclear if it has a role in vesicle formation. A stringent analysis of proteins in dynamic organellar maps which are altered in response to loss of AP-4, identified TPD54 (Davies et al., 2022). This identification might simply reflect the effect of AP-4 knockout on ATG9A-flavor INVs, but it may also suggest that TPD54 works together with AP-4 in vesicle formation at the TGN. In support of this, the increase in LC3B lipidation upon depletion of TPD54 is reminiscent to that seen following knockout of AP-4 subunits AP4E1 and AP4B1 (Davies et al., 2018). On the other hand, an AP-4-specific function for TPD54 seems unlikely since depletion of TPD54 affects many other membrane trafficking steps – for example, recycling of integrins and transferrin receptor, anterograde traffic – which are not governed by AP-4 and would argue for a more ubiquitous role for this protein during vesicle formation (Larocque et al., 2020, 2021).

While ATG9 vesicles have been synonymous with autophagy, there has been a growing appreciation of their autophagy-independent functions. ATG9 vesicles have been shown to be involved in plasma membrane repair following exotoxin injury, and also in lipid mobilization from lipid droplets through association with the lipid transferase TMEM41B (Claude-Taupin et al., 2021; Mailler et al., 2021). In addition, Campisi et al. (2022) described a role for ATG9 vesicles in integrin trafficking during cell migration; a function which is remarkably similar to that attributed to INV-mediated integrin recycling in our previous work (Larocque et al., 2021). Rather than an autophagy-specific vesicle type, the classification of ATG9A-flavor INVs as a vesicle subtype with lipid scramblase activity that can participate in a wide range of cell biological activities is probably a more accurate definition.

If ∼80 % of INVs are not ATG9A-flavor, then what are the other flavors of INV? The INV proteome highlights a number of interesting cargos which might constitute new subtypes of INVs. For example, glucose transporter 1 (SLC2A1), is a typical cargo sorted by retromer (Steinberg et al., 2013). Vesicles containing such cargos may constitute novel INV flavors. Conversely, other small uncoated vesicles that have been previously been described may actually be flavors of INV. For example, synaptic-like microvesicles (SLMVs) are synaptic vesicle-sized secretory vesicles found in non-neuronal

cells (Clift-O'Grady et al., 1990; Cameron et al., 1991; Régnier-Vigouroux et al., 1991). We found considerable overlap of the INV proteome with a SLMV dataset (Salazar et al., 2005), due to the presence of synaptic vesicle proteins and paralogs (SCAMP1, SCAMP2, SCAMP3, SYNGR2, SYPL1) in the INV proteome. An SLMV-flavor of INV would be in keeping with the observation of fusion of synaptophysin-containing INVs at the cell surface (Sittewelle and Royle, 2024). Intriguingly, classic work showed that expression of synaptophysin in non-neuronal cells causes the aggregation of SLMVs (Cameron et al., 1991). Recently, coexpression of synapsin and synaptophysin was shown to enhance the clustering of SLMVs (Park et al., 2021) and that ATG9 vesicles and SLMVs are each present in the synapsin clusters, yet remain separate (Park et al., 2023). Our work suggests that these vesicles – collectively – are INVs, and that this is strong evidence that separate INV flavors do exist and can remain segregated.

Exploring the variety of INV flavors and determining any interplay between them is an important goal in order to understand the roles of INVs in membrane trafficking in health and disease.

Methods

Molecular biology

The following plasmids were available from previous work: GFP-FKBP-TPD54, mCherry-FKBP-tagged TPD54 WT and R159E mutant, GFP-FKBP and mCherry-MitoTrap (Larocque et al., 2021); ATG9A-GFP (Sittewelle and Royle, 2024). HA-RUSC2 was a kind gift from Alex Davies (Davies et al., 2018).

For low expression of GFP-TPD54 WT or R159E in HeLa cells, a pEGFP-C1 plasmid with the CMV promoter exchanged for PGK was used, and a TPD54 cDNA was subcloned into this plasmid using XhoI and MfeI sites; and then the R159E mutation was introduced by site-directed mutagenesis. GFP-FKBP-TPD54 R159E was made by cloning TPD54 R159E into pEGFP-FKBP-C1 at XhoI and MfeI sites.

ATG9A-FKBP-mCherry was constructed by first making ATG9A-FKBP-GFP by amplification of human ATG9A and insertion at EcoRI and SalI sites in pFKBP-GFP-C1, followed by replacement of GFP with mCherry using NheI and NotI sites. Tagging ATG9A at the C-terminus was shown previously to be sufficient to functionally complement knockout of ATG9A (Mailler et al., 2021). FKBP-mCherry was made by replacing GFP in pFKBP-GFP-C1 with mCherry using NheI and NotI; FKBP-mCherry was cloned in place of mCherry using NheI/MfeI into a pmCherry-N1 vector with a crippled CMV promoter in order to reduce expression levels in cells. MitoTrap constructs were converted to the rapalog-specific FRB T2098L form by site directed mutagenesis of mCherry-MitoTrap and conversion to blue form by replacing mCherry with EBFP2 at AgeI/BrGI (Bayle et al., 2006). SH3GLB1-GFP, GFP-ARFIP2, DAGLB-GFP, GFP-PI4K2A, and GFP-PI4KB were each made by custom synthesis and cloning in pmEGFP-C1 or pmEGFP-N1 at EcoRI/SalI, EcoRI/KpnI, HindIII/SalI, EcoRI/SalI, and BglII/SalI sites respectively.

Cell culture

Wild-type HeLa cells (HPA/ECACC 93021013) or GFP-TPD54 knock-in (clone 35) HeLa cells (Larocque et al., 2020) were maintained in DMEM with GlutaMAX and 25 mM HEPES (Thermo Fisher, 32430100) supplemented with 10 % FBS, and 100 U mL^{-1} penicillin/streptomycin. All cells were kept in a humidified incubator at 37 °C and 5 % CO_2; and were routinely tested for mycoplasma contamination by PCR.

To generate cell lines stably expressing GFP-TPD54 WT or GFP-TPD54 R159E under a PGK promoter, HeLa cells were seeded at 50 % confluency in a 75 cm^2 flask and transfected with 5 µg of the respective plasmid, using Genejuice (Merck). After 48 h, media was changed to complete media supplemented with 500 µg mL^{-1} geneticin (Thermo Fisher, 10131035). Following selection, cells were assessed for GFP fluorescence by microscopy, expanded and were frozen down as stably transfected populations.

For transient transfection, 1.4×10^5 cells were plated onto either coverslips or 35 mm glass bottom dishes (WPI – FD35-100). Plasmids were transfected using Genejuice and cells analyzed 36–48 h after transfection. For depletion of TPD54, siTPD54 (GUCCUACCUGUUACGCAAU) or siGL2 (CGUACGCGGAAUACUUCGA) as a control were used (Larocque et al., 2020). Transfection of siRNA was by Lipofectamine RNAiMax according to the manufacturer's instructions, with cells typically analyzed 48 h post-transfection.

Isolation of intracellular nanovesicles

HeLa cells (14×10^6) were seeded onto a 24.5 × 24.5 cm plate (Corning, 431110). Typically one plate per condition, per replicate was set up and left to grow until 80–100 % confluent. For harvest, plates were placed on ice, cells were washed three times with 10 mL ice cold PBS and scraped into 5 mL PBS using a bisected rubber stopper. Cells were pelleted by centrifugation at 4200 *g* for 2 min at 4 °C and then lysed via resuspension of the cell pellet in 1 mL INV release buffer (20 mM Tris-Cl, 300 mM NaCl, 5 µg mL^{-1} digitonin, 0.2 mM PMSF, with cOmplete EDTA free proteinase inhibitor (Roche, 4693132001), pH 7.5) in a pre-cooled microcentrifuge tube. Cells were lysed on ice for 30 min, with gentle pipetting every 10 min using a 1 mL tip. During lysis, GFP-Trap Agarose beads (chromotek, gta-20), 25 µL per reaction, were prepared by washing three times with 500 mL INV release buffer with spins at 2500 *g* for 2 min at 4 °C before final resuspension in INV release buffer (50 µL per reaction). For experiments where a control IP was performed, Rho1D4 MagBeads (Genaxxon, S5394.0005) were used, and magnetic isolation per-

formed. Lysates were then centrifuged at 20 000 *g* for 15 min at 4 ℃, 50 µL supernatant was reserved for analysis and the remainder was incubated with GFP-Trap beads (50 µL per reaction) in a pre-cooled microcentrifuge tube and incubated with end-over-end rotation at 4 ℃ for 1 h. The bead-lysate mixture was centrifuged at 20 000 *g* for 2 min at 4 ℃ to pellet the beads. The supernatant was retained for analysis and the INVs on beads were washed three times with INV release buffer. Digitonin in the washes reduced background but potentially interfered with mass spectrometry so was omitted for some experiments. Captured material was eluted by resuspending beads in 50 µL 2× laemmli buffer (Alfa Aesar, J60015.AD) and heating to 95 ℃ for 5 min.

Mass spectrometry

Samples were loaded onto a 4–15 % precast polyacrylamide gel (Bio-Rad, #4561084) and run at constant voltage until all proteins had migrated into the resolving gel. The gel was stained with InstantBlue protein stain (Abcam, ab119211) for 1 h at room temperature (RT) with gentle agitation. Individual lanes were excised and diced (2–4 mm) and transferred to 1.5 mL microcentrifuge tubes per lane. Gel pieces were washed three times with 1 mL 50 % ethanol (EtOH), 50 mM ammonium bicarbonate (ABC) for 20 min at RT with shaking at 650 rpm. The fragments were then dehydrated with 200 µL 100 % EtOH for 5 min at RT. For efficient reduction of disulphide bridges and alkylation of cysteines, the gel pieces were next rehydrated in 100 µL 10 mM TCEP, 55 mM CAA in 50 mM ABC and incubated for 30 min at 70 ℃ with shaking at 650 rpm. Slices were washed a further three times in 1 mL 50 % EtOH, 50 mM ABC for 20 min at RT with shaking at 650 rpm before dehydration with 200 µL 100 % EtOH for 5 min at RT. Trypsin was made up to 2.5 ng μL^{-1} in 50 mM ABC and 80 µL was used to rehydrate the gel pieces for 10 min at RT. Buffer volume was increased by adding additional 50 mM ABC to ensure all pieces were submerged followed by digestion overnight at 37 ℃. The following day, the solution around the gel containing the peptides was collected. Gel pieces were submerged in 25 % ACN 5 % formic acid solution and sonicated in a water bath for 10 min at RT. This process was performed three times with solution collection and pooling per sample. Finally, the solutions were filtered using a Costar Spin-X centrifuge tube filter (Sigma, CLS8169) to remove any residual gel and then peptides were concentrated in a speed-vacuum for 3 h at 45 ℃ and resuspended in 50 µL 2 % acetonitrile, 0.1 % trifluoracetic acid (TFA) before being transferred to mass spectrometry vials. Samples were stored at –20 ℃ until running on either a timsTOF or Orbitrap mass spectrometer (Proteomics Facility, University of Warwick).

LC-MS/MS raw data files were processed using MaxQuant (v2.0.1) (Max Planck Institute of Biochemistry). The peptide lists were searched against the reviewed UniProt human proteome database (retrieved May 2021) supplemented with the sequence of GFP-TPD54 and the MaxQuant common contaminant database. Peptide abundance was quantified using the MaxQuant Label-Free Quantification (LFQ) algorithm. Enzyme specificity for trypsin was selected with the allowance of up to two missed cleavages. All searches were performed with cysteine carbamidomethylation set as the fixed modification and oxidation of methionine and acetylation of the protein N-terminus set as the variable modifications. The initial precursor mass deviation was set as 20 ppm and the fragment mass deviation set as 20 ppm. For label-free quantification, we set a minimum ratio count of 2 with 3 minimum and 6 average comparisons.

Cell treatments

To capture vesicles at the mitochondria, an inducible heterodimerization approach was used as described previously, with minor modifications (Larocque et al., 2020). Briefly, cells expressing FKBP-tagged proteins and FRB T2098L-MitoTrap constructs were treated with rapalog AP21967 (A/C Heterodimerizer, TaKaRa Bio, 635056 or 635057) at a final concentration of 5 µM in media. Rapamycin induces autophagy and, although this occurs on a much longer timescale than our experiments, rapalog was used in place of rapamycin for induced heterodimerization. For fixed cell experiments, rapalog application was via complete exchange of media and a time point of 5 min was used for fixation. For live cell imaging, cells were in Leibovitz L-15 media supplemented with 10 % FBS immediately prior to imaging and rapalog application was done using a 1:5 addition of a 5X stock in L-15 media with FBS.

Autophagy was induced by 3 h starvation in HBSS (Sigma Aldrich, H6648) or EBSS (Thermo Fisher, 24010043). To assess autophagic flux, bafilomycin A1 (Sigma Aldrich, SML1661) was applied at a final concentration of 100 nM during this incubation. Control conditions were treated with a 1:1600 dilution of DMSO.

Immunofluorescence

Cells on glass cover slips were fixed using 3 % PFA/4 % sucrose in PBS for 15 min. After fixation, cells were washed with PBS and then incubated in permeabilization buffer (0.1 % v/v Triton X-100 in 1xPBS) for 10 min. Cells were washed twice with PBS, before 45–60 min blocking (3 % BSA, 5 % goat serum in 1xPBS). Antibody dilutions were prepared in blocking solution. After blocking, cells were incubated for 2 h with primary antibody, PBS washed (3 washes, 5 min each), 1 h secondary antibody incubation (not required for directly conjugated primaries), 5 min each PBS wash (3 washes), mounting with ProLong Gold or Vectashield vibrance. Primary antibodies used: anti-ATG9A [EPR2450(2)], rabbit (Abcam, ab108338 or ab206253); anti-LC3B [EPR18709], rabbit (Abcam, ab192890); anti-CIMPR [2G11], mouse (Abcam, ab2733); anti-TGN46 , sheep (Bio-RAD, AHP500G); anti HA [6E2], mouse (Cell Sig-

naling, 2367); anti-HA [C29F4], rabbit (Cell Signaling, 3724); anti-GFP, rabbit, conjugated to Alexa Fluor488 (Thermo Fisher, A-21311). Secondary antibodies were Alexa Fluor568 or 647 conjugated goat anti-rabbit or anti-mouse, and donkey anti-sheep Alexa Fluor568, all highly cross-adsorbed (Thermo-Fisher). Note, for anti-LC3B staining, ice-cold methanol was used as a fixative (10 min) with the permeabilization step omitted.

Western blotting

For Western blotting, cells were washed with ice-cold PBS and pelleted at 300 *g* for 5 min at 4 ℃. Lysates were prepared using RIPA buffer (Thermo Fisher, 89900) supplemented with cOmplete EDTA-free protease inhibitor cocktail tablet (Roche, 11836170001), 0.2 mM PMSF and DNAse I (New England Biolabs, M0303L) 150 µL per 10 mL; for 30 min at 4 ℃ with gentle agitation. Protein concentrations were determined using the BCA assay, and samples were heated at 65 ℃ or 95 ℃ in Laemmli buffer for 5 min, and resolved on a precast 4–15 % polyacrylamide gel (Bio-Rad). Proteins were transferred to nitrocellulose or PVDF using a iBlot2 Dry Blotting System (Bio-Rad). Following blocking in 5 % w/v non-fat milk (Merck, 70166) in TBST buffer (20 mM Tris, 150 mM NaCl, 0.1 % v/v Tween-20, pH 7.6), membranes were incubated with primary antibodies: rat monoclonal anti-GFP (Proteintech, 3H9), rabbit polyclonal anti-vinculin (Sigma Aldrich, V4139), rabbit polyclonal anti-LC3B (Merck, L7543) or rabbit polyclonal anti-TPD54 (Dundee Cell Products) at 1:1000 in 2 % Milk TBST for 2 h at RT or at 4 ℃ overnight with agitation. After three washes in TBST, secondary antibodies, HRP-conjugated goat anti-rat IgG (Sigma Aldrich, A9037) or mouse anti-rabbit IgG (Santa Cruz Biotechnology, sc-2357) at 1:5000 in 2 % milk TBST were applied for 1 h at RT with agitation. Blots were imaged using Amersham ECL Prime Western Blotting Detection Reagent (Cytiva, RPN2236) on a ChemiDoc MP (Bio-RAD) digital imaging system.

Microscopy

All images were captured using a Nikon CSU-W1 spinning disc confocal system with SoRa upgrade (Yokogawa) with a Nikon, 100×, 1.49 NA, oil, CFI SR HP Apo TIRF with optional 2.8× intermediate magnification and a 95B Prime camera (Photometrics). The system has a CSU-W1 (Yokogawa) spinning disk unit with 50 µm and SoRa disks (SoRa disk used), Nikon Perfect Focus autofocus, Okolab microscope incubator, Nikon motorized xy stage and Nikon 200 µm z-piezo. Excitation was via 405 nm, 488 nm, 561 nm and 638 nm lasers with 405/488/561/640 nm dichroic and Blue, 446/60; Green, 525/50; Red, 600/52; FRed, 708/75 emission filters. Acquisition and image capture was via NiS Elements software (Nikon). All microscopy data was stored via automated nightly upload to an OMERO database in the native file format (nd2).

Data analysis

Data from MaxQuant (proteinGroups.txt files) were processed using VolcanoPlot in Igor Pro 9 (Royle, 2024). Processing in this package mimics the workflow in Perseus however, it allows multiple proteinGroups files to be easily combined. For the WT vs R159E vs Control INV comparisons, two files of three replicates of three conditions each were processed together. For the GFP-TPD54 knock-in INV isolation, three files of three replicates of two conditions each where the GFP-Trap isolation was compared to a Rho1D4-MagBead control isolation, were processed together. We used a cut-off of two-fold enrichment and $p < 0.05$ to determine INV proteins.

The outputs from VolcanoPlot were used for further analysis in R. Briefly, the two INV proteomes and their respective backgrounds were consolidated. For each protein, the subcellular location of "secreted" and the count of transmembrane domains in each group was retrieved from Uniprot. To classify INV proteins, PANTHER 18.0 protein classifications were retrieved using Bioconductor/PANTHER.db (Muller, 2017). The two topmost hierarchies of classification (below protein class) were used to construct the treemap. Many characterized proteins have no PANTHER classification, and so some "unclassified" proteins were manually assigned. Enriched analysis of Gene Ontology (GO) terms was done using Bioconductor package clusterProfiler (Wu et al., 2021).

For comparison with SLMV, ATG9 vesicle and CCV datasets, we used published data and read the data into R (Judith et al., 2019; Salazar et al., 2005; Borner et al., 2012). For SLMV data, we mapped all rat proteins to their human counterparts; for ATG9 data, we used 0.5 (log2) difference to remove background; and for all datasets we used Gene Name to match co-occurrence in datasets.

For relocalization–co-relocation analysis, three-channel images (FKBP protein, POI, Mitotrap) were first registered with NanoJ using TetraSpeck bead images (Laine et al., 2019). The mitochondrial channel was segmented using a Labkit classifier trained on MitoTrap images (Arzt et al., 2022). A 'cytoplasm' mask was then made by excluding the mitochondrial mask from a duplicate mask that had been dilated eight times. Measures of the FKBP and POI channels were taken in these two regions and background-subtracted to give the fluorescence of those two regions (F_{mito} and F_{cyto}). Relocalization and co-relocation are shown in two ways. First, for live cell experiments, the fluorescence in the mitochondrial region post-treatment is divided by the pre-treatment value (F_{post}/F_{pre}), for each cell. Second, for fixed cell experiments where this is not possible, rapalog-treated cells are compared to control cells using the fluorescence at the mitochondria divided by the sum of the fluorescence in mitochondrial and cytoplasmic regions (F_{mito}/F_{total}). In each case, any negative responding cells ($F_{mito}/F_{cyto} < 1$, FKBP channel, post-treatment)

were removed from the analysis. In order to compare cytoplasmic loss of fluorescence due to relocalization–co-relocation, F_{cyto}/F_{total} was calculated from fixed cell or live cell data using rapalog-treated cells. Where dynamic live cell data was quantified, the mitochondrial fluorescence was read in IgorPro and used for curve fitting using equation 1.

$$y_0 + Aexp\frac{x - x_0}{\tau} \quad \textbf{(1)}$$

Traces are presented as the mitochondrial fluorescence (F) divided by the fluorescence at the beginning of the recording (F_0), as F/F_0.

For LC3 puncta quantification, normalized image stacks were segmented in Fiji using the Labkit plugin. The stacks were scaled isotropically, the segmented puncta were labeled using 'connected components' and their statistics retrieved using CLIJ (Haase et al., 2020). LC3 puncta were defined as >0.012 μm^3. To quantify ATG9A at the Golgi, the two fluorescence channels were first registered using NanoJ using TetraSpeck bead images (Laine et al., 2019). The TGN46 channel was normalized and segmented in Fiji using a Labkit classifier trained on a subset of images. The resulting masks were used to quantify the mean pixel density in the ATG9A channel. Unless stated otherwise, image analysis outputs from ImageJ were read into R, analyzed and plotted using custom-written scripts.

Data and software availability

All code used in the manuscript is available at https://github.com/quantixed/p064p037.

ACKNOWLEDGEMENTS

We thank Sean Munro and Jerôme Cattin-Ortolá for sharing unpublished data with us, and Sharon Tooze for sharing reagents and helpful discussions. We are indebted to Cleidi Zampronio in the Proteomics Facility RTP and to the Computing and Advanced Microscopy Unit (CAMDU) for their help and support. We are grateful to all members of the Royle lab for feedback and critical discussion. The work was supported by grants from UKRI-BBSRC (BB/V003062/1) and Human Frontier Science Program (HFSP RGP25/2022). MF and DJM were supported by UKRI-MRC Studentships (MR/N014294/1). We thank Julius Muller for updating PANTHER.db to work with the latest PANTHER version. For the purpose of open access, the authors have applied a Creative Commons Attribution (CC BY) license to any Author Accepted Manuscript version arising

AUTHOR CONTRIBUTIONS

MF, all ATG9 cell biological experiments, data analysis, programming; DJM, developed INV isolation and proteomic methods; PE, deep INV proteomic dataset; EC, LC3 western blotting; SJR, data analysis, programming, wrote the manuscript.

COMPETING FINANCIAL INTERESTS

The authors declare no conflict of interest.

References

Adhikari, H. and Counter, C. M. (2018). Interrogating the protein interactomes of RAS isoforms identifies PIP5K1A as a KRAS-specific vulnerability. *Nat Commun*, 9(1):3646. doi: 10.1038/s41467-018-05692-6.

Arzt, M., Deschamps, J., Schmied, C., Pietzsch, T., Schmidt, D., Tomancak, P., Haase, R., and Jug, F. (2022). LABKIT: Labeling and Segmentation Toolkit for Big Image Data. *Front. Comput. Sci.*, 4:777728. doi: 10.3389/fcomp.2022.777728.

Barker, E., Milburn, A., Helassa, N., Hammond, D., Sanchez-Soriano, N., Morgan, A., and Barclay, J. (2024). Proximity labelling reveals effects of disease-causing mutation on the DNAJC5/cysteine string protein α interactome. *Biochem J*, 481(3):141–160. doi: 10.1042/BCJ20230319.

Bayle, J. H., Grimley, J. S., Stankunas, K., Gestwicki, J. E., Wandless, T. J., and Crabtree, G. R. (2006). Rapamycin analogs with differential binding specificity permit orthogonal control of protein activity. *Chem Biol*, 13(1):99–107. doi: 10.1016/j.chembiol.2005.10.017.

Biesemann, C., Grønborg, M., Luquet, E., Wichert, S. P., Bernard, V., Bungers, S. R., Cooper, B., Varoqueaux, F., Li, L., Byrne, J. A., Urlaub, H., Jahn, O., Brose, N., and Herzog, E. (2014). Proteomic screening of glutamatergic mouse brain synaptosomes isolated by fluorescence activated sorting. *EMBO J*, 33(2):157–170. doi: 10.1002/embj.201386120.

Bonifacino, J. S. and Glick, B. S. (2004). The mechanisms of vesicle budding and fusion. *Cell*, 116(2):153–166. doi: 10.1016/s0092-8674(03)01079-1.

Borner, G. H. H., Antrobus, R., Hirst, J., Bhumbra, G. S., Kozik, P., Jackson, L. P., Sahlender, D. A., and Robinson, M. S. (2012). Multivariate proteomic profiling identifies novel accessory proteins of coated vesicles. *J Cell Biol*, 197(1):141–160. doi: 10.1083/jcb.201111049.

Bradberry, M. M., Mishra, S., Zhang, Z., Wu, L., McKetney, J. M., Vestling, M. M., Coon, J. J., and Chapman, E. R. (2022). Rapid and Gentle Immunopurification of Brain Synaptic Vesicles. *J Neurosci*, 42(17):3512–3522. doi: 10.1523/JNEUROSCI.2521-21.2022.

Broadbent, D. G., Barnaba, C., Perez, G. I., and Schmidt, J. C. (2023). Quantitative analysis of autophagy reveals the role of ATG9 and ATG2 in autophagosome formation. *J Cell Biol*, 222(7):e202210078. doi: 10.1083/jcb.202210078.

Byrne, J. A., Nourse, C. R., Basset, P., and Gunning, P. (1998). Identification of homo- and heteromeric interactions between members of the breast carcinoma-associated D52 protein family using the yeast two-hybrid system. *Oncogene*, 16(7):873–881. doi: 10.1038/sj.onc.1201604.

Cameron, P. L., Südhof, T. C., Jahn, R., and De Camilli, P. (1991). Colocalization of synaptophysin with transferrin receptors: implications for synaptic vesicle biogenesis. *J Cell Biol*, 115(1):151–164. doi: 10.1083/jcb.115.1.151.

Campisi, D., Desrues, L., Dembélé, K.-P., Mutel, A., Parment, R., Gandolfo, P., Castel, H., and Morin, F. (2022). The core autophagy protein ATG9A controls dynamics of cell protrusions and directed migration. *J Cell Biol*, 221(3):e202106014. doi: 10.1083/jcb.202106014.

Claude-Taupin, A., Jia, J., Bhujabal, Z., Garfa-Traoré, M., Kumar, S., da Silva, G. P. D., Javed, R., Gu, Y., Allers, L., Peters, R., Wang, F., da Costa, L. J., Pallikkuth, S., Lidke, K. A., Mauthe, M., Verlhac, P., Uchiyama, Y., Salemi, M., Phinney, B., Tooze, S. A., Mari, M. C., Johansen, T., Reggiori, F., and Deretic, V. (2021). ATG9A protects the plasma membrane from programmed and incidental permeabilization. *Nat Cell Biol*, 23(8):846–858. doi: 10.1038/s41556-021-00706-w.

Clift-O'Grady, L., Linstedt, A. D., Lowe, A. W., Grote, E., and Kelly, R. B. (1990). Biogenesis of synaptic vesicle-like structures in a pheochromocytoma cell line PC-12. *J Cell Biol*, 110(5):1693–1703. doi: 10.1083/jcb.110.5.1693.

Davies, A. K., Itzhak, D. N., Edgar, J. R., Archuleta, T. L., Hirst, J., Jackson, L. P., Robinson, M. S., and Borner, G. H. H. (2018). AP-4 vesicles contribute to spatial control of autophagy via RUSC-dependent peripheral delivery of ATG9A. *Nat Commun*, 9(1):3958. doi: 10.1038/s41467-018-06172-7.

Davies, A. K., Alecu, J. E., Ziegler, M., Vasilopoulou, C. G., Merciai, F., Jumo, H., Afshar-Saber, W., Sahin, M., Ebrahimi-Fakhari, D., and Borner, G. H. H. (2022). AP-4-mediated axonal transport controls endocannabinoid production in neurons. *Nat Commun*, 13(1):1058. doi: 10.1038/s41467-022-28609-w.

Go, C. D., Knight, J. D. R., Rajasekharan, A., Rathod, B., Hesketh, G. G., Abe, K. T., Youn, J.-Y., Samavarchi-Tehrani, P., Zhang, H., Zhu, L. Y., Popiel, E., Lambert, J.-P., Coyaud, E., Cheung, S. W. T., Rajendran, D., Wong, C. J., Antonicka, H., Pelletier, L., Palazzo, A. F., Shoubridge, E. A., Raught, B., and Gingras, A.-C. (2021). A proximity-dependent biotinylation map of a human cell. *Nature*, 595(7865):120–124. doi: 10.1038/s41586-021-03592-2.

Guardia, C. M., Christenson, E. T., Zhou, W., Tan, X.-F., Lian, T., Faraldo-Gómez, J. D., Bonifacino, J. S., Jiang, J., and Banerjee, A. (2020). The structure of human ATG9A and its interplay with the lipid bilayer. *Autophagy*, 16(12):2292–2293. doi: 10.1080/15548627.2020.1830522.

Guardia, C. M., Jain, A., Mattera, R., Friefeld, A., Li, Y., and Bonifacino, J. S. (2021). RUSC2 and WDR47 oppositely regulate kinesin-1-dependent distribution of ATG9A to the cell periphery. *Mol Biol Cell*, 32(21):ar25. doi: 10.1091/mbc.E21-06-0295.

Haase, R., Royer, L. A., Steinbach, P., Schmidt, D., Dibrov, A., Schmidt, U., Weigert, M., Maghelli, N., Tomancak, P., Jug, F., and Myers, E. W. (2020). CLIJ: GPU-accelerated image processing for everyone. *Nat Methods*, 17(1):5–6. doi: 10.1038/s41592-019-0650-1.

Holzer, E., Martens, S., and Tulli, S. (2024). The Role of ATG9 Vesicles in Autophagosome Biogenesis. *J Mol Biol*, page 168489. doi: 10.1016/j.jmb.2024.168489.

Judith, D., Jefferies, H. B. J., Boeing, S., Frith, D., Snijders, A. P., and Tooze, S. A. (2019). ATG9A shapes the forming autophagosome through Arfaptin 2 and phosphatidylinositol 4-kinase IIIβ. *J Cell Biol*, 218(5):1634–1652. doi: 10.1083/jcb.201901115.

Karanasios, E., Walker, S. A., Okkenhaug, H., Manifava, M., Hummel, E., Zimmermann, H., Ahmed, Q., Domart, M.-C., Collinson, L., and Ktistakis, N. T. (2016). Autophagy initiation by ULK complex assembly on ER tubulovesicular regions marked by ATG9 vesicles. *Nat Commun*, 7:12420. doi: 10.1038/ncomms12420.

Laine, R. F., Tosheva, K. L., Gustafsson, N., Gray, R. D. M., Almada, P., Albrecht, D., Risa, G. T., Hurtig, F., Lindås, A.-C., Baum, B., Mercer, J., Leterrier, C., Pereira, P. M., Culley, S., and Henriques, R. (2019). NanoJ: a high-performance open-source super-resolution microscopy toolbox. *J Phys D Appl Phys*, 52(16):163001. doi: 10.1088/1361-6463/ab0261.

Larocque, G. and Royle, S. J. (2022). Integrating intracellular nanovesicles into integrin trafficking pathways and beyond. *Cell Mol Life Sci*, 79(6):335. doi: 10.1007/s00018-022-04371-6.

Larocque, G., La-Borde, P. J., Clarke, N. I., Carter, N. J., and Royle, S. J. (2020). Tumor protein D54 defines a new class of intracellular transport vesicles. *J Cell Biol*, 219(1):e201812044. doi: 10.1083/jcb.201812044.

Larocque, G., Moore, D. J., Sittewelle, M., Kuey, C., Hetmanski, J. H. R., La-Borde, P. J., Wilson, B. J., Clarke, N. I., Caswell, P. T., and Royle, S. J. (2021). Intracellular nanovesicles mediate α5β1 integrin trafficking during cell migration. *J Cell Biol*, 220(10):e202009028. doi: 10.1083/jcb.202009028.

Maeda, S., Yamamoto, H., Kinch, L. N., Garza, C. M., Takahashi, S., Otomo, C., Grishin, N. V., Forli, S., Mizushima, N., and Otomo, T. (2020). Structure, lipid scrambling activity and role in autophagosome formation of ATG9A. *Nat Struct Mol Biol*, 27(12):1194–1201. doi: 10.1038/s41594-020-00520-2.

Mailler, E., Guardia, C. M., Bai, X., Jarnik, M., Williamson, C. D., Li, Y., Maio, N., Golden, A., and Bonifacino, J. S. (2021). The autophagy protein ATG9A enables lipid mobilization from lipid droplets. *Nat Commun*, 12(1):6750. doi: 10.1038/s41467-021-26999-x.

Matoba, K., Kotani, T., Tsutsumi, A., Tsuji, T., Mori, T., Noshiro, D., Sugita, Y., Nomura, N., Iwata, S., Ohsumi, Y., Fujimoto, T., Nakatogawa, H., Kikkawa, M., and Noda, N. N. (2020). Atg9 is a lipid scramblase that mediates autophagosomal membrane expansion. *Nat Struct Mol Biol*, 27(12):1185–1193. doi: 10.1038/s41594-020-00518-w.

Mattera, R., Park, S. Y., De Pace, R., Guardia, C. M., and Bonifacino, J. S. (2017). AP-4 mediates export of ATG9A from the trans-Golgi network to promote autophagosome formation. *Proc Natl Acad Sci U S A*, 114(50):E10697–E10706. doi: 10.1073/pnas.1717327114.

Mellacheruvu, D., Wright, Z., Couzens, A. L., Lambert, J.-P., St-Denis, N. A., Li, T., Miteva, Y. V., Hauri, S., Sardiu, M. E., Low, T. Y., Halim, V. A., Bagshaw, R. D., Hubner, N. C., Al-Hakim, A., Bouchard, A., Faubert, D., Fermin, D., Dunham, W. H., Goudreault, M., Lin, Z.-Y., Badillo, B. G., Pawson, T., Durocher, D., Coulombe, B., Aebersold, R., Superti-Furga, G., Colinge, J., Heck, A. J. R., Choi, H., Gstaiger, M., Mohammed, S., Cristea, I. M., Bennett, K. L., Washburn, M. P., Raught, B., Ewing, R. M., Gingras, A.-C., and Nesvizhskii, A. I. (2013). The CRAPome: a contaminant repository for affinity purification-mass spectrometry data. *Nat Methods*, 10(8):730–736. doi: 10.1038/nmeth.2557.

Muller, J. PANTHER.db, (2017). URL https://bioconductor.org/packages/PANTHER.db.

Nishimura, T. and Tooze, S. A. (2020). Emerging roles of ATG proteins and membrane lipids in autophagosome formation. *Cell Discov*, 6(1):32. doi: 10.1038/s41421-020-0161-3.

Olivas, T. J., Wu, Y., Yu, S., Luan, L., Choi, P., Guinn, E. D., Nag, S., De Camilli, P. V., Gupta, K., and Melia, T. J. (2023). ATG9 vesicles comprise the seed membrane of mammalian autophagosomes. *J Cell Biol*, 222(7):e202208088. doi: 10.1083/jcb.202208088.

Orsi, A., Razi, M., Dooley, H. C., Robinson, D., Weston, A. E., Collinson, L. M., and Tooze, S. A. (2012). Dynamic and transient interactions of Atg9 with autophagosomes, but not membrane integration, are required for autophagy. *Mol Biol Cell*, 23(10):1860–1873. doi: 10.1091/mbc.E11-09-0746.

Park, D., Wu, Y., Lee, S.-E., Kim, G., Jeong, S., Milovanovic, D., De Camilli, P., and Chang, S. (2021). Cooperative function of synaptophysin and synapsin in the generation of synaptic vesicle-like clusters in non-neuronal cells. *Nat Commun*, 12(1):263. doi: 10.1038/s41467-020-20462-z.

Park, D., Wu, Y., Wang, X., Gowrishankar, S., Baublis, A., and De Camilli, P. (2023). Synaptic vesicle proteins and ATG9A self-organize in distinct vesicle phases within synapsin condensates. *Nat Commun*, 14(1):455. doi: 10.1038/s41467-023-36081-3.

Popovic, D. and Dikic, I. (2014). TBC1D5 and the AP2 complex regulate ATG9 trafficking and initiation of autophagy. *EMBO Rep*, 15(4):392–401. doi: 10.1002/embr.201337995.

Reynaud, A., Magdeleine, M., Patel, A., Gay, A.-S., Debayle, D., Abelanet, S., and Antonny, B. (2022). Tumor protein D54 binds intracellular nanovesicles via an extended amphipathic region. *J Biol Chem*, 298(7):102136. doi: 10.1016/j.jbc.2022.102136.

Royle, S. quantixed/VolcanoPlot: First release for zenodo, (2024). URL https://zenodo.org/doi/10.5281/zenodo.12570017.

Régnier-Vigouroux, A., Tooze, S. A., and Huttner, W. B. (1991). Newly synthesized synaptophysin is transported to synaptic-like microvesicles via constitutive secretory vesicles and the plasma membrane. *EMBO J*, 10(12):3589–3601. doi: 10.1002/j.1460-2075.1991.tb04925.x.

Salazar, G., Craige, B., Wainer, B. H., Guo, J., De Camilli, P., and Faundez, V. (2005). Phosphatidylinositol-4-kinase type II alpha is a component of adaptor protein-3-derived vesicles. *Mol Biol Cell*, 16(8):3692–3704. doi: 10.1091/mbc.e05-01-0020.

Sittewelle, M. and Royle, S. J. (2024). Passive diffusion accounts for the majority of intracellular nanovesicle transport. *Life Sci Alliance*, 7(1):e202302406. doi: 10.26508/lsa.202302406.

Steinberg, F., Gallon, M., Winfield, M., Thomas, E. C., Bell, A. J., Heesom, K. J., Tavaré, J. M., and Cullen, P. J. (2013). A global analysis of SNX27-retromer assembly and cargo specificity reveals a function in glucose and metal ion transport. *Nat Cell Biol*, 15(5):461–471. doi: 10.1038/ncb2721.

Takahashi, Y., Meyerkord, C. L., Hori, T., Runkle, K., Fox, T. E., Kester, M., Loughran, T. P., and Wang, H.-G. (2011). Bif-1 regulates Atg9 trafficking by mediating the fission of Golgi membranes during autophagy. *Autophagy*, 7(1):61–73. doi: 10.4161/auto.7.1.14015.

Wilson, B., Flett, C., Gemperle, J., Lawless, C., Hartshorn, M., Hinde, E., Harrison, T., Chastney, M., Taylor, S., Allen, J., Norman, J. C., Zacharchenko, T., and Caswell, P. T. (2023). Proximity labelling identifies pro-migratory endocytic recycling cargo and machinery of the Rab4 and Rab11 families. *J Cell Sci*, 136(12):jcs260468. doi: 10.1242/jcs.260468.

Wu, T., Hu, E., Xu, S., Chen, M., Guo, P., Dai, Z., Feng, T., Zhou, L., Tang, W., Zhan, L., Fu, X., Liu, S., Bo, X., and Yu, G. (2021). clusterProfiler 4.0: A universal enrichment tool for interpreting omics data. *Innovation (Camb)*, 2(3):100141. doi: 10.1016/j.xinn.2021.100141.

Young, A. R. J., Chan, E. Y. W., Hu, X. W., Köchl, R., Crawshaw, S. G., High, S., Hailey, D. W., Lippincott-Schwartz, J., and Tooze, S. A. (2006). Starvation and ULK1-dependent cycling of mammalian Atg9 between the TGN and endosomes. *J Cell Sci*, 119(Pt 18):3888–3900. doi: 10.1242/jcs.03172.

Supplementary Information

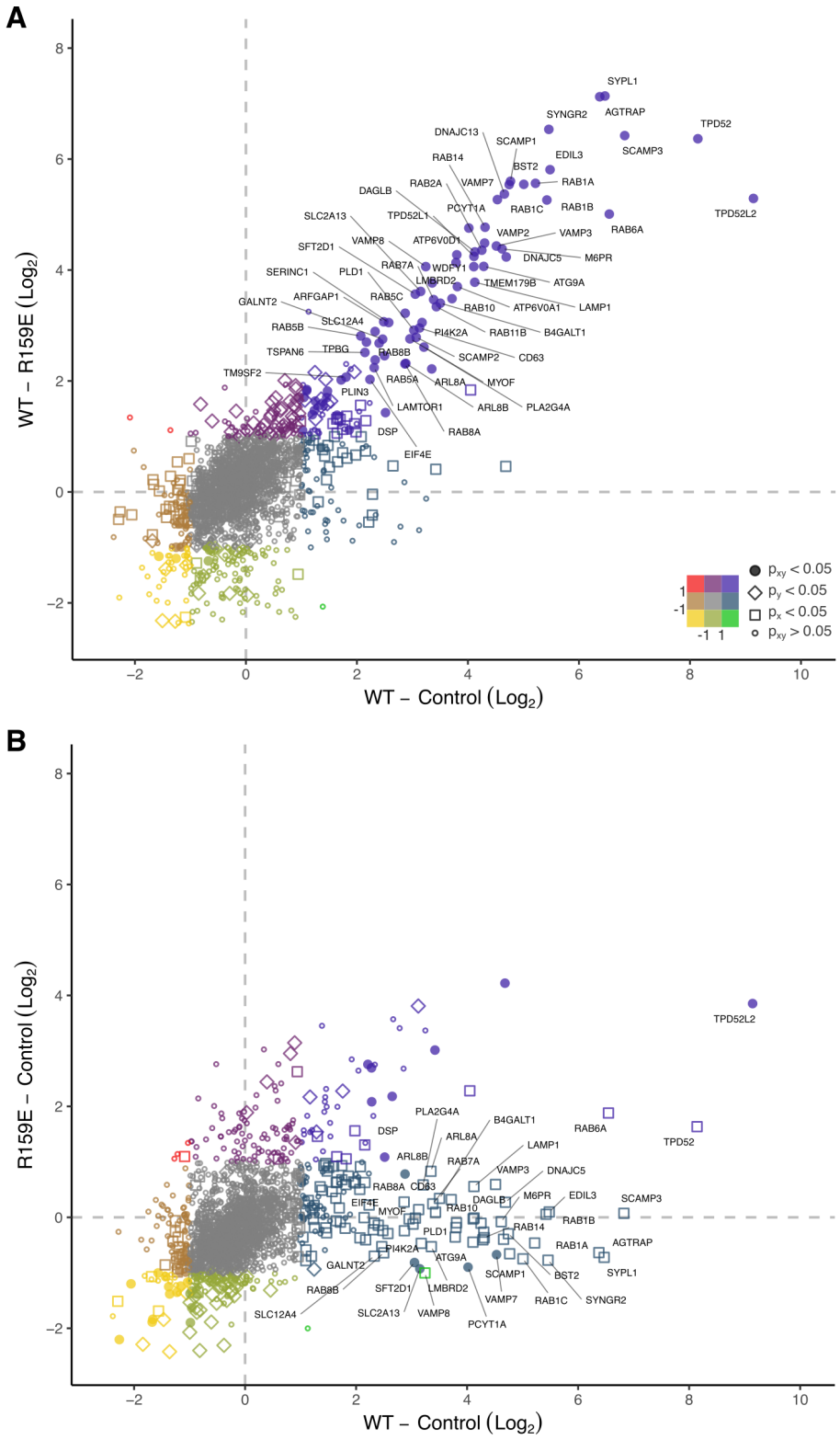

Figure S1. Verifying the INV proteome.
(**A,B**) INV protein enrichment data. Data from Figure 1 replotted to compare enrichment in WT vs R159E against WT vs Control pulldown (A), or R159E vs Control against WT vs Control pulldown (B). Proteins significantly enriched in WT vs Control are labeled sparsely. Colors indicate the fold-enrichment (log2) while shapes indicate p-values of the comparison, as indicated.

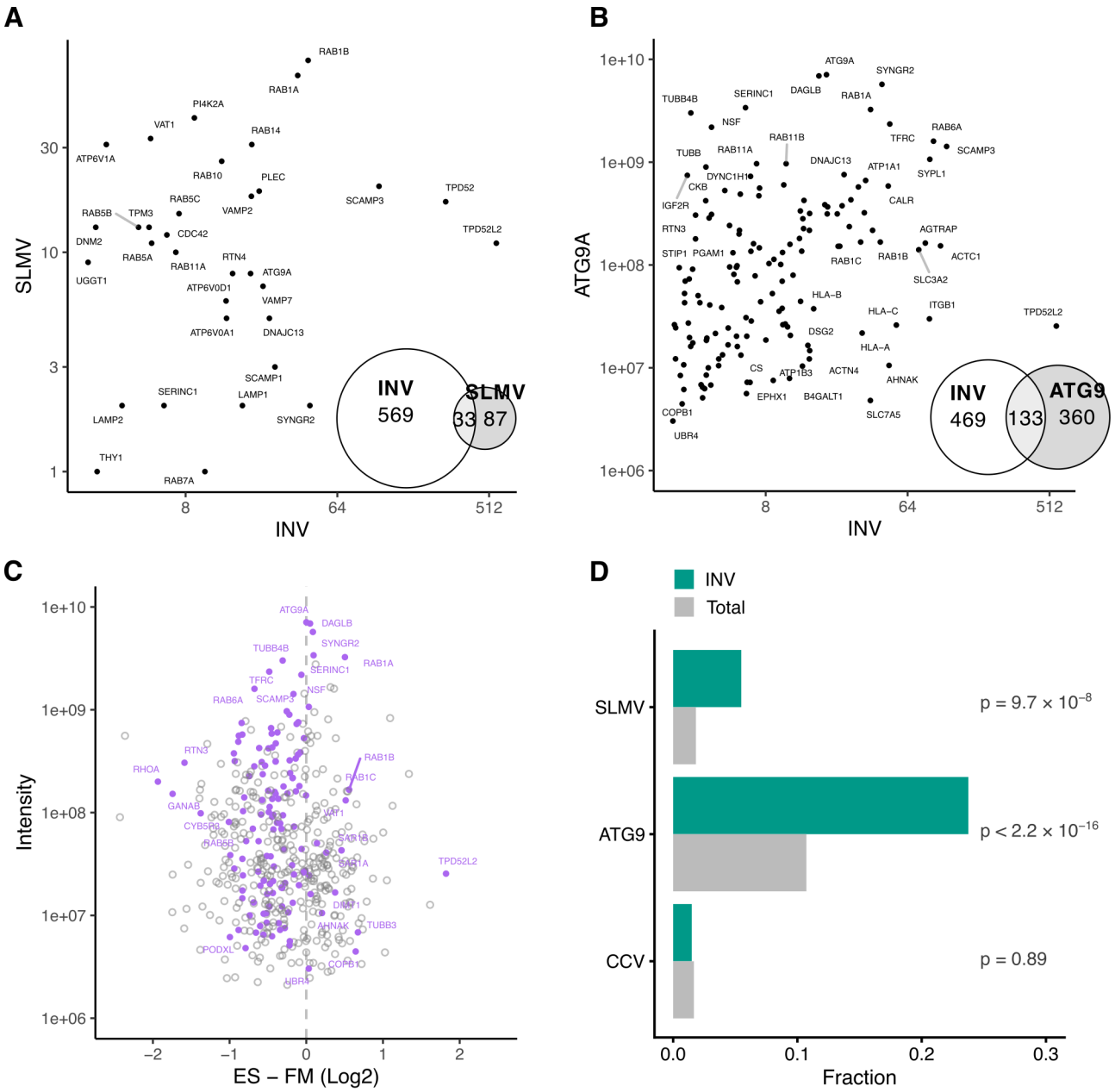

Figure S2. Comparison of the INV proteome with published vesicle datasets.
(**A**) Comparison of INV enrichment data with SLMV proteomic dataset (Salazar et al., 2005). Log-log plot of SMLV peptide values vs INV enrichment data. (**B**) Comparison of INV enrichment data with ATG9 proteomic dataset (Judith et al., 2019). Log-log plot of ATG9 intensity values vs INV enrichment data. Insets: Euler plot to show the the number of proteins in each dataset and their overlap. (**C**) Proteins associated with ATG9A-positive membranes from cells incubated in full media (FM) or EBSS for amino acid depletion (ES). Proteins that are enriched in the INV dataset are highlighted purple. (**D**) Fractions of INV proteins and of total proteins that were featured in the indicated dataset. Enrichment of dataset proteins in INVs versus total is indicated, p-values from Pearson's Chi-squared test.

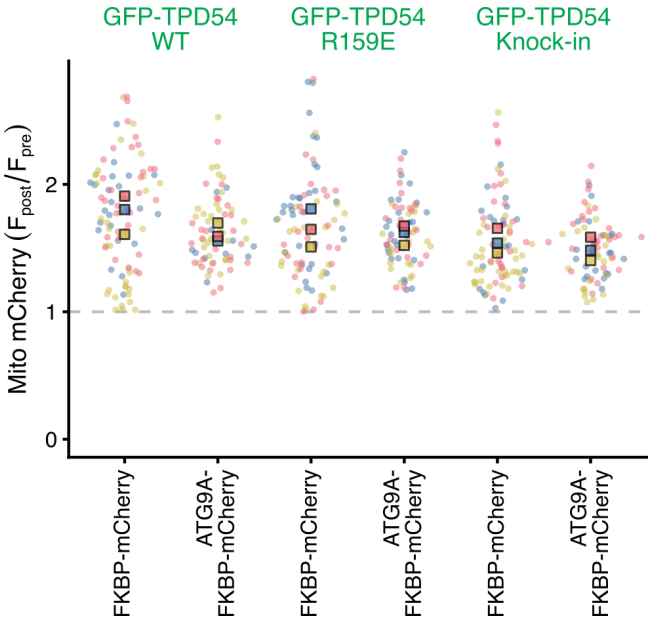

Figure S3. Relocalization of FKBP-mCherry or ATG9A-FKBP-mCherry.
Superplot to show the ratio of mitochondrial fluorescence of FKBP-mCherry or ATG9A-FKBP-mCherry post- vs pre-rapalog treatment. Spots indicate individual cell measurements (n = 21 - 69 per repeat), colors indicate independent experimental repeats (n = 3), squares show the mean value for each replicate. Co-relocation results for the green channel are shown in Figure 4.

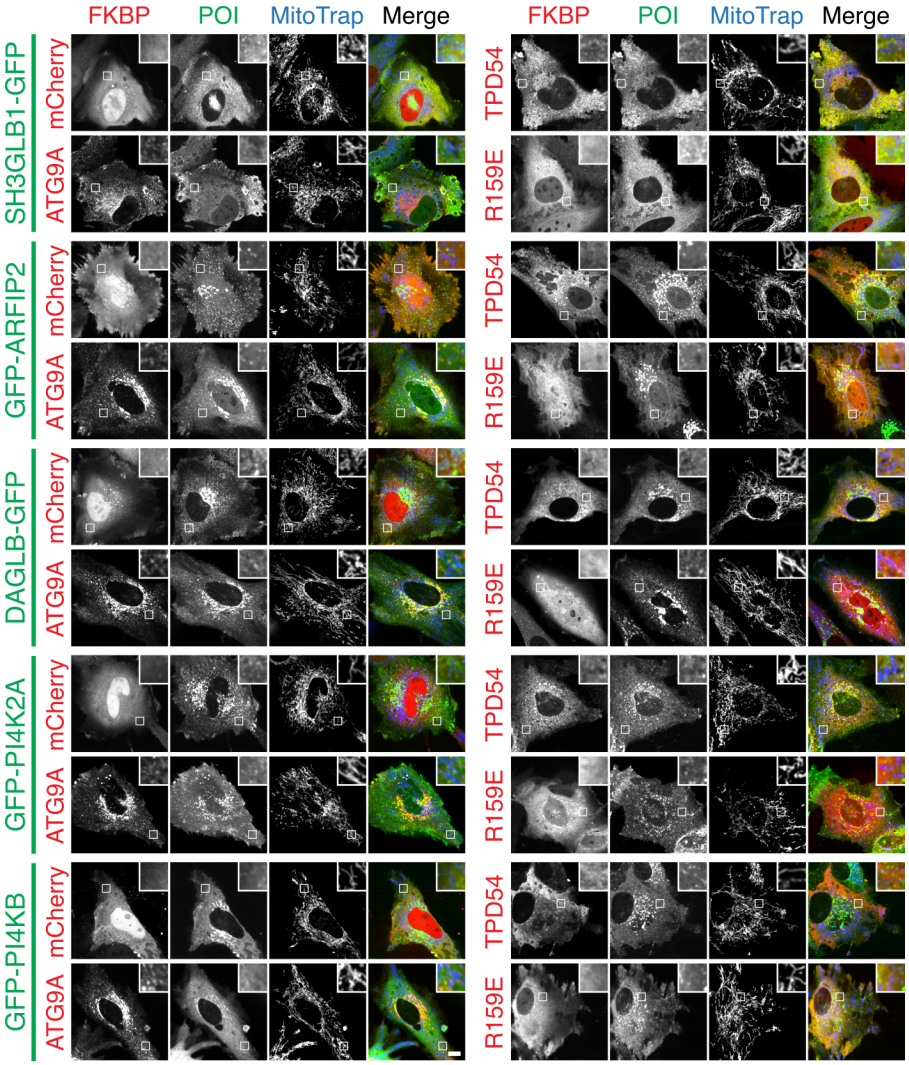

Figure S4. ATG9A-flavor INVs have ATG9 vesicle cargos – pre-rapalog images.

(**A**) Representative confocal images of HeLa cells expressing MitoTrap (pMito-EBFP2-FRB T2098L, blue) and either FKBP-mCherry, ATG9A-FKBP-mCherry, mCherry-FKBP-TPD54 WT, or mCherry-FKBP-TPD54 R159E (red). Cells are co-expressing GFP-tagged SH3GLB1, ARFIP2, DAGLB, PI4K2A, or PI4KB as indicated (green). For each condition, only the pre-treatment image is shown, for the post-rapalog images see Figure 6. Scale bar, 10 µm; insets, 4 × zoom.

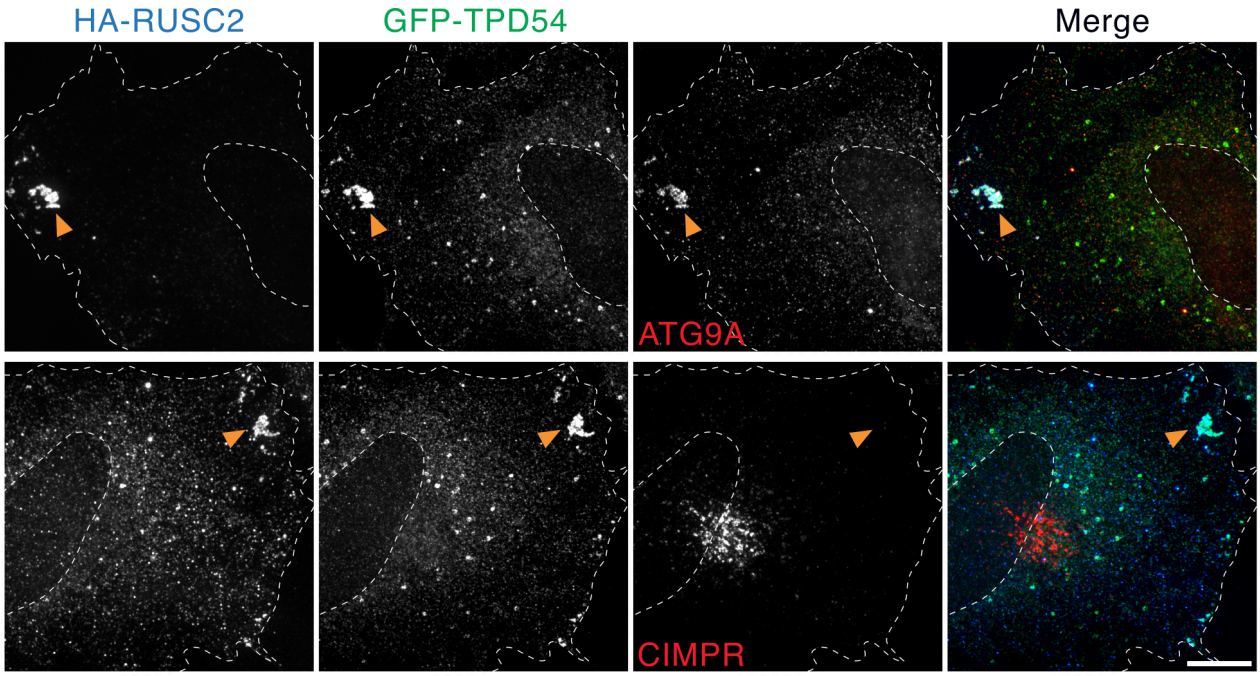

Figure S5. Selective relocalization of ATG9A-flavor INVs using RUSC2.
Representative confocal micrographs of GFP-TPD54 (green) knock-in HeLa cells overexpressing HA-RUSC2 (blue). Cells were fixed and stained for ATG9A or CIMPR (red, as indicated), anti-HA as well as GFP boost. Orange arrowheads indicate accumulation of vesicular material at the cell periphery. Scale bar, 10 µm.

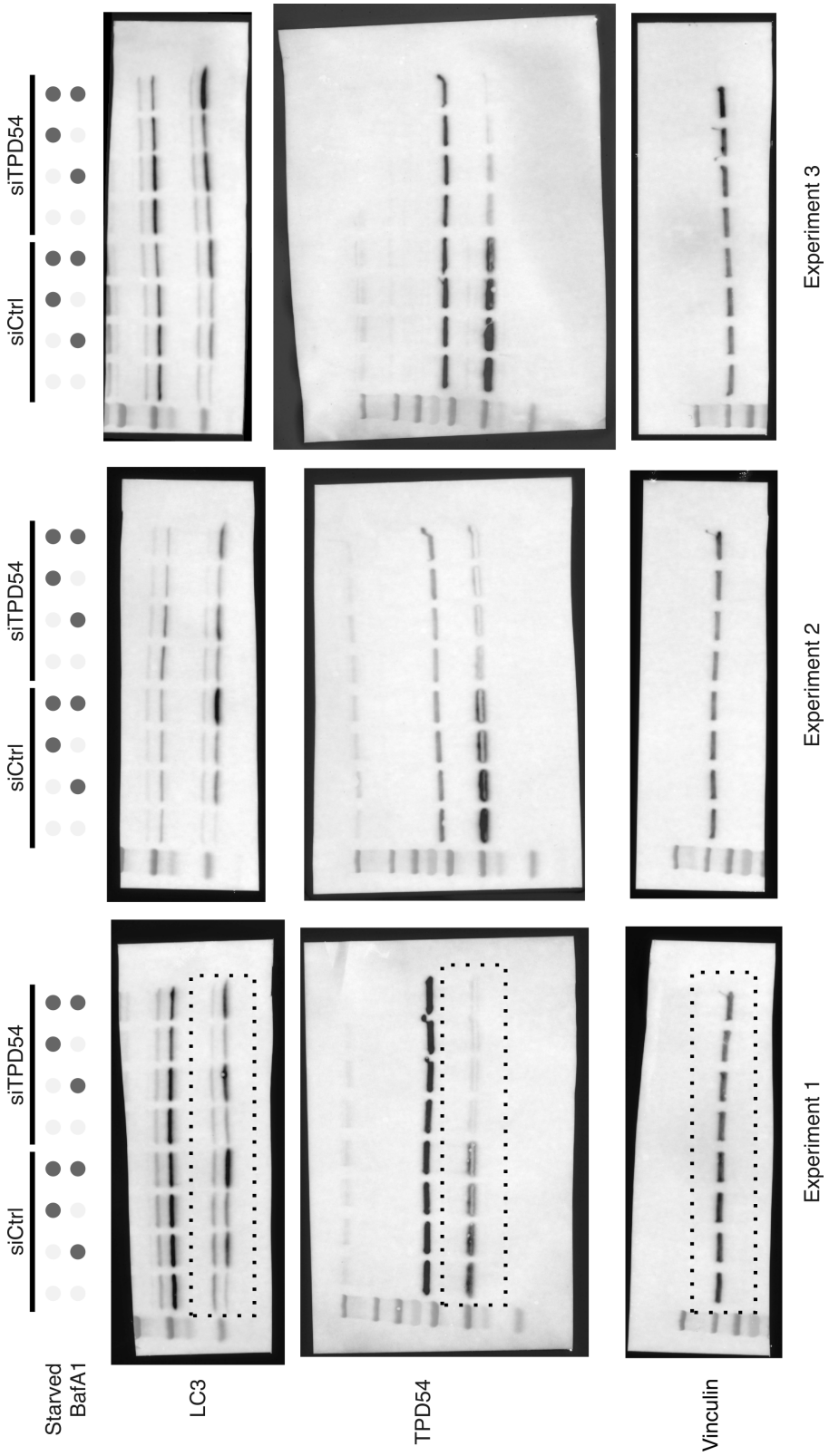

Figure S6. Effect of TPD54 depletion on LC3 lipidation under starvation.
Three experiments where cells were transfected with siCtrl or siTPD54, starved (3 h) or not (fed) and either treated with BafA1 (100 µM) or not (DMSO), as indicated. LC3 was detected with anti-LC3B antibody, endogenous TPD54 was detected using an anti-TPD54 antibody; detection of Vinculin was used as a loading control. Dotted lines indicate the crops shown in Figure 7.

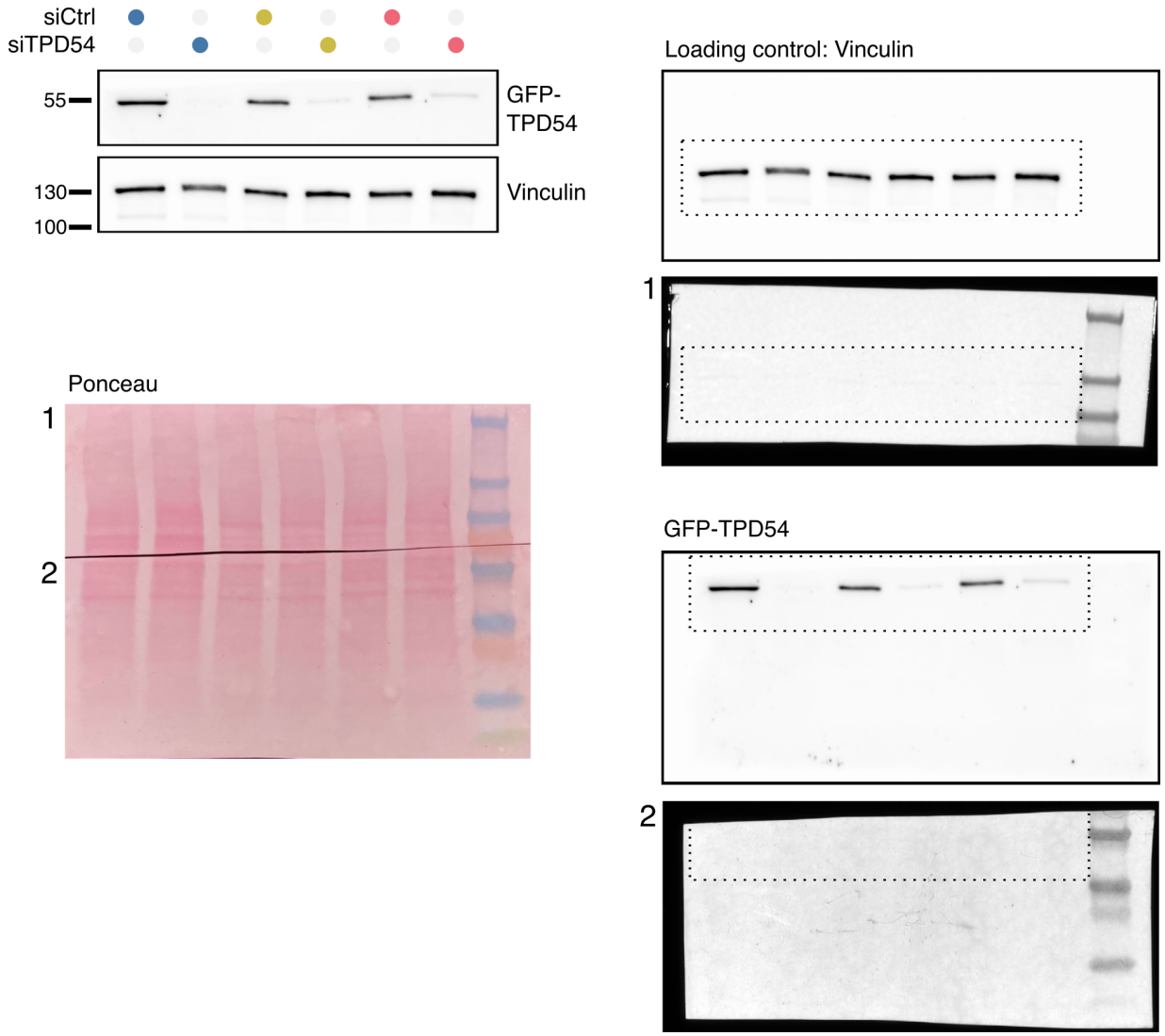

Figure S7. Depletion of TPD54 using RNAi.
Western blot to show knock-down of TPD54 in the experiments shown in Figures 7 and 8). Endogenous GFP-TPD54 was detected using an anti-GFP antibody and vinculin was used as a loading control. Markers in kDa, colors indicate experimental repeats in Figures 7 and 8) and siRNA treatment. Other panels show the full Ponceau stained membrane and the full imaged area.

Supplementary References

Judith, D., Jefferies, H. B. J., Boeing, S., Frith, D., Snijders, A. P., and Tooze, S. A. (2019). ATG9A shapes the forming autophagosome through Arfaptin 2 and phosphatidylinositol 4-kinase IIIβ. *J Cell Biol*, 218(5):1634–1652. doi: 10.1083/jcb.201901115.

Salazar, G., Craige, B., Wainer, B. H., Guo, J., De Camilli, P., and Faundez, V. (2005). Phosphatidylinositol-4-kinase type II alpha is a component of adaptor protein-3-derived vesicles. *Mol Biol Cell*, 16(8):3692–3704. doi: 10.1091/mbc.e05-01-0020.

Supplementary Videos

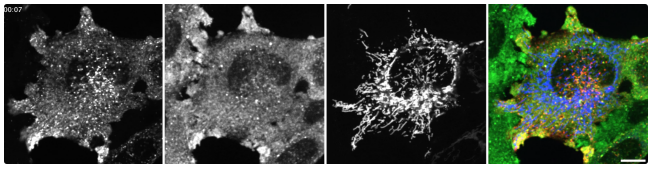

Figure SV1. Reclocalization of ATG9A-FKBP-mCherry causes co-relocalization of endogenous GFP-TPD54. Movie of GFP-TPD54 (panel 2, green) knock-in cells expressing ATG9A-FKBP-mCherry (panel 1, red) and MitoTrap (panel 3, blue); capture of ATG9A-positive vesicles at the mitochondria is induced by rapalog (5 µM at 40 s). Time, mm:ss. Playback, 10 fps. Scale bar, 10 µm.

Supplementary Tables

Table S1. The INV proteome A consolidated list of INV proteins determined by proteomics ranked by their fold enrichment over control. 602 proteins that had a fold change of > 2 and p < 0.05 are included. The enrichment in WT, R159E and/or knock-in over their respective controls is indicated as WT, R159E, and/or INV, respectively.

Rank	Gene name	Protein name	Protein ID	Fold change	P value	Dataset
1	TPD52L2	Tumor protein D54	O43399	565.5	6.2e-08	WT + INV + R159E
2	TPD52	Tumor protein D52	P55327	282.6	3.5e-12	WT + INV
3	BASP1	Brain acid soluble protein 1	P80723	116.3	6.5e-07	INV
4	SCAMP3	Secretory carrier-associated membrane protein 3	O14828	113.3	4.1e-10	WT + INV
6	RAB6A	Ras-related protein Rab-6A	P20340	93.5	1.3e-10	WT + INV
7	SYPL1	Synaptophysin-like protein 1	Q16563	88.6	8.7e-10	WT
8	ITGB1	Integrin beta-1	P05556	88.0	2.9e-10	INV
9	AGTRAP	Type-1 angiotensin II receptor-associated protein	Q6RW13	82.9	2.3e-09	WT
10	SLC3A2	4F2 cell-surface antigen heavy chain	P08195	75.3	4.4e-10	INV
11	BSG	Basigin	P35613	65.2	1.0e-12	INV
13	TFRC	Transferrin receptor protein 1	P02786	49.3	1.2e-08	INV
14	AHNAK	Neuroblast differentiation-associated protein AHNAK	Q09666	48.7	1.5e-05	INV
15	CALR	Calreticulin	P27797	48.2	5.9e-08	INV
16	ANXA2	Annexin A2	P07355	46.3	9.1e-09	INV
17	EDIL3	EGF-like repeat and discoidin I-like domain-containing protein 3	O43854	44.6	6.6e-11	WT + INV
18	SYNGR2	Synaptogyrin-2	O43760	43.9	5.7e-08	WT + INV
19	RAB1B	Ras-related protein Rab-1B	Q9H0U4	42.9	1.5e-08	WT + INV
21	GNAI2	Guanine nucleotide-binding protein G(i) subunit alpha-2	P04899	38.3	2.0e-10	INV
22	PTHLH	Parathyroid hormone-related protein	P12272	37.6	4.2e-03	INV
23	RAB1A	Ras-related protein Rab-1A	P62820	37.2	2.9e-05	WT + INV
24	SLC7A5	Large neutral amino acids transporter small subunit 1	Q01650	37.1	1.1e-07	INV
25	CD44	CD44 antigen	P16070	35.0	3.3e-10	INV
26	ATP1A1	Sodium/potassium-transporting ATPase subunit alpha-1	P05023	34.6	1.2e-08	INV
27	CANX	Calnexin	P27824	33.9	1.3e-06	INV
29	RAB1C	Putative Ras-related protein Rab-1C	Q92928	32.1	1.1e-04	WT + INV
30	PDIA3	Protein disulfide-isomerase A3	P30101	31.1	4.8e-06	INV
31	MSN	Moesin	P26038	28.3	3.7e-07	INV
32	P4HB	Protein disulfide-isomerase	P07237	27.9	1.5e-06	INV
33	SCAMP1	Secretory carrier-associated membrane protein 1	O15126	27.2	7.3e-09	WT
34	BST2	Bone marrow stromal antigen 2	Q10589	26.8	1.5e-05	WT + INV
35	SLC1A5	Neutral amino acid transporter B(0)	Q15758	25.9	1.4e-06	INV
36	DNAJC5	DnaJ homolog subfamily C member 5	Q9H3Z4	25.8	1.5e-06	WT
37	HIST1H2AJ	Histone H2A type 1-J	Q99878	25.7	2.6e-02	WT + R159E
38	ITGA5	Integrin alpha-5	P08648	25.4	1.5e-07	INV
39	DNAJC13	DnaJ homolog subfamily C member 13	O75165	25.2	8.1e-09	WT
40	M6PR	Cation-dependent mannose-6-phosphate receptor	P20645	24.5	2.7e-08	WT
41	MCAM	Cell surface glycoprotein MUC18	P43121	24.1	1.2e-07	INV
42	GANAB	Neutral alpha-glucosidase AB	Q14697	23.7	1.2e-06	INV
43	JUP	Junction plakoglobin	P14923	23.4	3.9e-07	INV
44	VAMP7	Vesicle-associated membrane protein 7	P51809	23.1	1.3e-09	WT
45	VAMP3	Vesicle-associated membrane protein 3	Q15836	22.8	1.1e-06	WT + INV
46	PLEC	Plectin	Q15149	21.9	2.4e-07	INV
47	RAB14	Ras-related protein Rab-14	P61106	19.8	9.4e-07	WT + INV
48	VAMP2	Vesicle-associated membrane protein 2	P63027	19.7	2.9e-06	WT
49	ATG9A	Autophagy-related protein 9A	Q7Z3C6	19.5	9.2e-10	WT
50	HSP90B1	Endoplasmin	P14625	19.4	1.2e-08	INV
51	RAB2A	Ras-related protein Rab-2A	P61019	19.0	1.5e-07	WT
52	ITGAV	Integrin alpha-V	P06756	18.5	8.8e-08	INV
54	CTNNA1	Catenin alpha-1	P35221	18.1	1.2e-07	INV
55	DAGLB	Sn1-specific diacylglycerol lipase beta	Q8NCG7	17.4	3.7e-07	WT
56	LAMP1	Lysosome-associated membrane glycoprotein 1	P11279	17.4	1.9e-04	WT + INV
57	TPD52L1	Tumor protein D53	Q16890	17.3	3.1e-08	WT
58	TMEM179B	Transmembrane protein 179B	Q7Z7N9	17.2	1.3e-03	WT
59	ATP1B1	Sodium/potassium-transporting ATPase subunit beta-1	P05026	16.8	4.4e-06	INV
60	HIST3H3	Histone H3.2	Q71DI3	16.5	4.7e-03	WT
61	PCYT1A	Choline-phosphate cytidylyltransferase A	P49585	16.2	2.5e-06	WT
63	CFL1	Cofilin-1	P23528	15.8	7.7e-10	INV
64	RAP1B	Ras-related protein Rap-1b	P61224	15.8	9.1e-07	INV
65	CTNNB1	Catenin beta-1	P35222	15.7	1.7e-06	INV
66	DSG2	Desmoglein-2	Q14126	15.2	1.2e-05	INV
68	RTN4	Reticulon-4	Q9NQC3	15.2	4.3e-04	INV
69	GNAI3	Guanine nucleotide-binding protein G(k) subunit alpha	P08754	15.2	5.5e-05	INV
70	ACTN4	Alpha-actinin-4	O43707	15.2	3.5e-05	INV
71	DDOST	Dolichyl-diphosphooligosaccharide–protein glycosyltransferase 48 kDa subunit	P39656	14.8	2.4e-08	INV
72	LGALS1	Galectin-1	P09382	14.4	1.8e-06	INV
73	ATP6V0A1	V-type proton ATPase 116 kDa subunit a isoform 1	Q93050	14.0	5.2e-08	WT
74	ATP6V0D1	V-type proton ATPase subunit d 1	P61421	13.9	1.3e-09	WT
75	ITGA11	Integrin alpha-11	Q9UKX5	13.9	4.2e-06	INV
77	WDFY1	WD repeat and FYVE domain-containing protein 1	Q8IWB7	13.8	4.2e-08	WT
78	ATP1B3	Sodium/potassium-transporting ATPase subunit beta-3	P54709	13.7	1.0e-05	INV
79	RPN1	Dolichyl-diphosphooligosaccharide–protein glycosyltransferase subunit 1	P04843	13.6	6.1e-06	INV
80	TXNDC5	Thioredoxin domain-containing protein 5	Q8NBS9	13.3	2.3e-06	INV
81	GNB1	Guanine nucleotide-binding protein G(I)/G(S)/G(T) subunit beta-1	P62873	13.3	2.5e-04	INV
82	ENO1	Alpha-enolase	P06733	13.2	2.8e-05	INV

Rank	Gene name	Protein name	Protein ID	Fold change	P value	Dataset
83	RAB10	Ras-related protein Rab-10	P61026	13.1	1.1e-04	WT + INV
84	CDH2	Cadherin-2	P19022	12.9	8.4e-07	INV
85	CTSZ	Cathepsin Z	Q9UBR2	12.7	1.2e-04	INV
86	MYO1C	Unconventional myosin-Ic	O00159	12.4	1.9e-07	INV
87	TLN1	Talin-1	Q9Y490	12.4	7.3e-05	INV
88	PRKCSH	Glucosidase 2 subunit beta	P14314	11.9	1.1e-05	INV
89	GPC1	Glypican-1	P35052	11.9	1.2e-06	INV
91	CKAP4	Cytoskeleton-associated protein 4	Q07065	11.5	2.9e-07	INV
92	SLC16A1	Monocarboxylate transporter 1	P53985	11.4	8.3e-05	INV
94	ACSL3	Long-chain-fatty-acid–CoA ligase 3	O95573	11.0	1.9e-06	INV
95	SLC25A5	ADP/ATP translocase 2	P05141	10.9	4.0e-06	INV
96	MYL12A	Myosin regulatory light chain 12A	P19105	10.8	4.5e-03	INV
97	RAB11B	Ras-related protein Rab-11B	Q15907	10.8	2.0e-03	WT
98	ITGA3	Integrin alpha-3	P26006	10.7	9.0e-06	INV
99	COL8A1	Collagen alpha-1(VIII) chain	P27658	10.7	8.5e-08	WT + R159E
100	TAGLN2	Transgelin-2	P37802	10.7	4.8e-06	INV
101	ERP29	Endoplasmic reticulum resident protein 29	P30040	10.7	2.4e-07	INV
102	STOM	Erythrocyte band 7 integral membrane protein	P27105	10.6	8.0e-06	INV
103	RAB7A	Ras-related protein Rab-7a	P51149	10.4	1.3e-03	WT + INV
104	GNB2	Guanine nucleotide-binding protein G(I)/G(S)/G(T) subunit beta-2	P62879	10.3	2.5e-04	INV
105	LMBRD2	LMBR1 domain-containing protein 2	Q68DH5	10.2	4.2e-06	WT
106	PLS3	Plastin-3	P13797	10.2	1.2e-06	INV
107	ARL8A	ADP-ribosylation factor-like protein 8A	Q96BM9	10.2	1.1e-03	WT
108	PDIA6	Protein disulfide-isomerase A6	Q15084	10.0	1.6e-07	INV
109	HSD17B4	Peroxisomal multifunctional enzyme type 2	P51659	9.8	2.1e-06	INV
112	VAMP8	Vesicle-associated membrane protein 8	Q9BV40	9.5	1.7e-02	WT
113	PLA2G4A	Cytosolic phospholipase A2	P47712	9.2	4.5e-05	WT + INV
115	TUBA4A	Tubulin alpha-4A chain	P68366	9.2	4.1e-05	INV
118	PI4K2A	Phosphatidylinositol 4-kinase type 2-alpha	Q9BTU6	9.0	1.2e-06	WT
119	EPHX1	Epoxide hydrolase 1	P07099	8.9	1.8e-05	INV
120	FSCN1	Fascin	Q16658	8.9	7.5e-06	INV
121	SLC2A13	Proton myo-inositol cotransporter	Q96QE2	8.9	1.1e-07	WT
122	ESYT1	Extended synaptotagmin-1	Q9BSJ8	8.8	4.4e-06	INV
124	CD63	CD63 antigen	P08962	8.7	3.3e-03	WT
125	SLC16A3	Monocarboxylate transporter 4	O15427	8.5	1.8e-04	INV
126	SCAMP2	Secretory carrier-associated membrane protein 2	O15127	8.4	8.8e-06	WT + INV
127	SFT2D1	Vesicle transport protein SFT2A	Q8WV19	8.3	2.2e-03	WT
128	EEF2	Elongation factor 2	P13639	8.2	1.8e-03	INV
129	PLD1	Phospholipase D1	Q13393	8.1	8.7e-06	WT
130	FOLR1	Folate receptor alpha	P15328	8.1	3.1e-05	INV
132	PPT1	Palmitoyl-protein thioesterase 1	P50897	7.9	3.4e-05	INV
133	MYOF	Myoferlin	Q9NZM1	7.8	4.2e-05	WT + INV
135	GNA14	Guanine nucleotide-binding protein subunit alpha-11	P29992	7.5	3.9e-04	INV
136	LRRC59	Leucine-rich repeat-containing protein 59	Q96AG4	7.4	1.5e-05	INV
139	ARL8B	ADP-ribosylation factor-like protein 8B	Q9NVJ2	7.4	3.0e-05	WT
140	CD59	CD59 glycoprotein	P13987	7.4	8.9e-04	INV
141	VDAC2	Voltage-dependent anion-selective channel protein 2	P45880	7.4	4.7e-06	INV
142	CCT2	T-complex protein 1 subunit beta	P78371	7.3	4.5e-04	INV
143	RAB5C	Ras-related protein Rab-5C	P51148	7.3	7.4e-04	WT + INV
144	RAB8A	Ras-related protein Rab-8A	P61006	7.3	1.5e-05	WT + INV
145	RPS27A	Ubiquitin-40S ribosomal protein S27a	P62979	7.2	1.3e-05	INV
146	PDIA4	Protein disulfide-isomerase A4	P13667	7.2	1.5e-05	INV
148	SAR1A;SAR1B	GTP-binding protein SAR1a;GTP-binding protein SAR1b	Q9NR31;Q9Y6B6	7.2	1.9e-02	INV
149	PHB	Prohibitin	P35232	7.1	2.8e-05	INV
150	CTSD	Cathepsin D	P07339	7.1	1.5e-03	INV
153	RAB11A	Ras-related protein Rab-11A	P62491	7.0	1.5e-05	INV
154	ATP2A2	Sarcoplasmic/endoplasmic reticulum calcium ATPase 2	P16615	6.8	1.0e-03	INV
155	VDAC1	Voltage-dependent anion-selective channel protein 1	P21796	6.8	1.1e-04	INV
156	PHB2	Prohibitin-2	Q99623	6.7	1.3e-03	INV
157	PRDX4	Peroxiredoxin-4	Q13162	6.7	6.8e-05	INV
158	SNAP23	Synaptosomal-associated protein 23	O00161	6.7	4.7e-06	INV
159	CSE1L	Exportin-2	P55060	6.6	5.5e-03	INV
160	GGT1	Gamma-glutamyltranspeptidase 1	P19440	6.5	8.2e-03	INV
161	CALU	Calumenin	O43852	6.5	1.6e-05	INV
162	YWHAZ	14-3-3 protein zeta/delta	P63104	6.4	5.9e-04	INV
163	HSPA5	78 kDa glucose-regulated protein	P11021	6.4	2.8e-08	INV
165	ANXA1	Annexin A1	P04083	6.4	1.8e-04	INV
166	SLC38A5	Sodium-coupled neutral amino acid transporter 5	Q8WUX1	6.3	5.2e-04	INV
167	HDAC10	Histone deacetylase 10	Q969S8	6.3	1.0e-03	WT + R159E
168	SDAD1	Protein SDA1 homolog	Q9NVU7	6.2	3.7e-04	INV
169	HDLBP	Vigilin	Q00341	6.2	5.4e-04	INV
170	CDC42	Cell division control protein 42 homolog	P60953	6.2	1.8e-04	INV
171	CACNA2D1	Voltage-dependent calcium channel subunit alpha-2/delta-1	P54289	6.2	1.2e-05	INV
172	GPRC5A	Retinoic acid-induced protein 3	Q8NFJ5	6.1	3.3e-04	INV
173	MARCKSL1	MARCKS-related protein	P49006	6.1	4.6e-06	INV
174	PGRMC1	Membrane-associated progesterone receptor component 1	O00264	6.1	2.8e-04	INV
175	HSP90AB2P	Putative heat shock protein HSP 90-beta 2	Q58FF8	6.0	2.7e-05	INV
176	NRAS	GTPase NRas	P01111	6.0	3.1e-03	INV
177	GAPDH	Glyceraldehyde-3-phosphate dehydrogenase	P04406	6.0	2.5e-05	INV
178	LDHA	L-lactate dehydrogenase A chain	P00338	6.0	7.4e-04	INV + R159E
179	SERINC1	Serine incorporator 1	Q9NRX5	5.9	1.8e-03	WT
180	EPB41L2	Band 4.1-like protein 2	O43491	5.9	7.7e-05	INV
181	TMEM43	Transmembrane protein 43	Q9BTV4	5.9	8.8e-06	INV

Rank	Gene name	Protein name	Protein ID	Fold change	P value	Dataset
182	HSP90AA1	Heat shock protein HSP 90-alpha	P07900	5.9	2.1e-06	INV
183	ASPH	Aspartyl/asparaginyl beta-hydroxylase	Q12797	5.9	2.2e-04	INV
186	MARCKS	Myristoylated alanine-rich C-kinase substrate	P29966	5.8	1.6e-03	INV
187	PPIA	Peptidyl-prolyl cis-trans isomerase A	P62937	5.8	6.1e-04	INV
188	SLC9A3R2	Na(+)/H(+) exchange regulatory cofactor NHE-RF2	Q15599	5.8	6.9e-03	INV
189	KTN1	Kinectin	Q86UP2	5.8	9.4e-05	INV
190	GPR56	G-protein coupled receptor 56	Q9Y653	5.7	1.0e-04	INV
191	DSP	Desmoplakin	P15924	5.7	5.6e-04	WT + R159E
192	RAB8B	Ras-related protein Rab-8B	Q92930	5.6	2.2e-02	WT
193	TNFRSF10A	Tumor necrosis factor receptor superfamily member 10A	O00220	5.6	1.9e-04	INV
194	ARFGAP1	ADP-ribosylation factor GTPase-activating protein 1	Q8N6T3	5.6	1.4e-05	WT
195	CTNND1	Catenin delta-1	O60716	5.6	9.8e-05	INV
197	GALNT2	Polypeptide N-acetylgalactosaminyltransferase 2	Q10471	5.5	1.5e-03	WT + INV
198	GNAI1	Guanine nucleotide-binding protein G(i) subunit alpha-1	P63096	5.4	1.1e-03	INV
199	RHOA	Transforming protein RhoA	P61586	5.4	5.1e-03	INV
200	FAM129B	Niban-like protein 1	Q96TA1	5.4	1.1e-02	INV
201	ATP2B1	Plasma membrane calcium-transporting ATPase 1	P20020	5.3	7.3e-04	INV
202	TMEM87A	Transmembrane protein 87A	Q8NBN3	5.3	1.2e-05	WT
203	CYB5R3	NADH-cytochrome b5 reductase 3	P00387	5.3	2.6e-04	INV
204	IQGAP1	Ras GTPase-activating-like protein IQGAP1	P46940	5.2	8.2e-03	INV
205	PGRMC2	Membrane-associated progesterone receptor component 2	O15173	5.2	5.0e-06	INV
206	PON2	Serum paraoxonase/arylesterase 2	Q15165	5.2	1.3e-02	INV
207	SERPINH1	Serpin H1	P50454	5.2	6.0e-09	INV
208	VCP	Transitional endoplasmic reticulum ATPase	P55072	5.1	2.6e-03	INV
209	YES1	Tyrosine-protein kinase Yes	P07947	5.1	6.1e-03	INV
210	CCT6A	T-complex protein 1 subunit zeta	P40227	5.1	7.4e-05	INV
212	H2AFY	Core histone macro-H2A.1	O75367	5.1	2.2e-03	INV
213	EGFR	Epidermal growth factor receptor	P00533	5.1	1.9e-03	INV
214	PAICS	Multifunctional protein ADE2	P22234	5.1	8.8e-04	INV
215	CALD1	Caldesmon	Q05682	5.0	1.5e-03	INV
216	TNC	Tenascin	P24821	5.0	3.1e-04	INV
217	RAB5A	Ras-related protein Rab-5A	P20339	5.0	4.9e-03	WT + INV
218	SLC12A4	Solute carrier family 12 member 4	Q9UP95	5.0	4.1e-05	WT
219	PTRF	Polymerase I and transcript release factor	Q6NZI2	5.0	1.2e-06	INV
220	ALCAM	CD166 antigen	Q13740	5.0	1.9e-04	INV
221	GNS	N-acetylglucosamine-6-sulfatase	P15586	5.0	1.3e-04	INV
222	LAMTOR1	Ragulator complex protein LAMTOR1	Q6IAA8	5.0	1.5e-02	WT
223	VAT1	Synaptic vesicle membrane protein VAT-1 homolog	Q99536	5.0	5.9e-04	INV
224	CCT4	T-complex protein 1 subunit delta	P50991	4.9	1.5e-03	INV
226	L1CAM	Neural cell adhesion molecule L1	P32004	4.9	1.6e-04	INV
228	AHNAK2	Protein AHNAK2	Q8IVF2	4.9	5.1e-04	INV
229	COLGALT1	Procollagen galactosyltransferase 1	Q8NBJ5	4.9	3.8e-04	INV
230	LCN1	Lipocalin-1	P31025	4.9	2.5e-02	WT + R159E
231	TPM3	Tropomyosin alpha-3 chain	P06753	4.8	3.1e-02	WT + INV + R159E
233	SQSTM1	Sequestosome-1	Q13501	4.8	3.1e-02	INV
234	PPIB	Peptidyl-prolyl cis-trans isomerase B	P23284	4.8	5.6e-04	INV
237	SRP54	Signal recognition particle 54 kDa protein	P61011	4.7	4.6e-03	INV
238	BCAP31	B-cell receptor-associated protein 31	P51572	4.7	7.8e-05	INV
239	EIF4E	Eukaryotic translation initiation factor 4E	P06730	4.7	7.5e-04	WT
240	CRIP2	Cysteine-rich protein 2	P52943	4.7	1.4e-03	INV
241	TPM4	Tropomyosin alpha-4 chain	P67936	4.6	4.3e-02	WT + R159E
242	XRCC5	X-ray repair cross-complementing protein 5	P13010	4.6	1.5e-03	INV
243	GNAS	Guanine nucleotide-binding protein G(s) subunit alpha isoforms short	P63092	4.6	4.7e-03	INV
244	DIMT1	Probable dimethyladenosine transferase	Q9UNQ2	4.6	1.7e-02	INV
245	FERMT2	Fermitin family homolog 2	Q96AC1	4.6	1.8e-03	INV
246	TUBB6	Tubulin beta-6 chain	Q9BUF5	4.6	6.0e-03	INV
247	SLC7A11	Cystine/glutamate transporter	Q9UPY5	4.6	5.0e-03	INV
250	FKBP10	Peptidyl-prolyl cis-trans isomerase FKBP10	Q96AY3	4.5	5.8e-03	INV
251	TPBG	Trophoblast glycoprotein	Q13641	4.5	3.5e-03	WT + INV
252	NME2	Nucleoside diphosphate kinase B	P22392	4.5	1.8e-02	INV
253	EIF4G2	Eukaryotic translation initiation factor 4 gamma 2	P78344	4.5	3.1e-05	INV
254	HSD17B10	3-hydroxyacyl-CoA dehydrogenase type-2	Q99714	4.5	4.6e-03	INV
255	EHD2	EH domain-containing protein 2	Q9NZN4	4.5	2.0e-03	INV
256	MTAP	S-methyl-5-thioadenosine phosphorylase	Q13126	4.5	1.4e-03	WT
257	FKBP11	Peptidyl-prolyl cis-trans isomerase FKBP11	Q9NYL4	4.5	1.1e-05	INV
258	GDA	Guanine deaminase	Q9Y2T3	4.5	4.2e-05	WT
259	RPN2	Dolichyl-diphosphooligosaccharide–protein glycosyltransferase subunit 2	P04844	4.5	3.6e-06	INV
260	API5	Apoptosis inhibitor 5	Q9BZZ5	4.5	8.8e-03	INV
261	EIF2S3	Eukaryotic translation initiation factor 2 subunit 3	P41091	4.4	1.9e-03	INV
262	TSPAN6	Tetraspanin-6	O43657	4.4	4.9e-03	WT
263	DYNC1H1	Cytoplasmic dynein 1 heavy chain 1	Q14204	4.4	4.8e-03	INV
264	ANO6	Anoctamin-6	Q4KMQ2	4.4	1.5e-02	INV
265	CD97	CD97 antigen	P48960	4.3	2.3e-03	INV
266	TCP1	T-complex protein 1 subunit alpha	P17987	4.3	1.3e-02	INV
267	TUBB8	Tubulin beta-8 chain	Q3ZCM7	4.3	1.7e-02	INV
268	YWHAG	14-3-3 protein gamma	P61981	4.2	3.3e-03	INV
269	RPL14	60S ribosomal protein L14	P50914	4.2	1.3e-05	WT
270	RAB5B	Ras-related protein Rab-5B	P61020	4.2	4.5e-05	WT
271	RCC2	Protein RCC2	Q9P258	4.2	2.5e-02	WT
273	SLC29A1	Equilibrative nucleoside transporter 1	Q99808	4.1	2.7e-04	INV
274	CAP1	Adenylyl cyclase-associated protein 1	Q01518	4.1	2.4e-02	INV
275	XRCC6	X-ray repair cross-complementing protein 6	P12956	4.1	3.3e-03	INV
276	CCT7	T-complex protein 1 subunit eta	Q99832	4.1	9.7e-03	INV

Rank	Gene name	Protein name	Protein ID	Fold change	P value	Dataset
278	ADRA2A	Alpha-2A adrenergic receptor	P08913	4.1	1.8e-04	INV
279	EMC1	ER membrane protein complex subunit 1	Q8N766	4.1	3.8e-05	INV
280	SLC39A6	Zinc transporter ZIP6	Q13433	4.0	1.6e-04	INV
281	TGFBI	Transforming growth factor-beta-induced protein ig-h3	Q15582	4.0	4.5e-04	INV
282	PKM	Pyruvate kinase PKM	P14618	4.0	4.1e-08	INV
283	ACTN1	Alpha-actinin-1	P12814	4.0	6.5e-04	INV
284	TMEM109	Transmembrane protein 109	Q9BVC6	4.0	6.7e-03	INV
285	UBA52	Ubiquitin	P62987	4.0	9.0e-04	INV
286	PRDX1	Peroxiredoxin-1	Q06830	4.0	1.1e-06	INV
287	ECE1	Endothelin-converting enzyme 1	P42892	4.0	1.6e-03	INV
288	NUMA1	Nuclear mitotic apparatus protein 1	Q14980	4.0	1.8e-03	INV
289	ARG1	Arginase-1	P05089	4.0	3.0e-04	WT
290	ALDOA	Fructose-bisphosphate aldolase A	P04075	3.9	4.2e-03	WT + INV
291	NOMO1	Nodal modulator 1	Q15155	3.9	8.4e-04	INV
293	HYOU1	Hypoxia up-regulated protein 1	Q9Y4L1	3.9	2.2e-03	INV
294	SND1	Staphylococcal nuclease domain-containing protein 1	Q7KZF4	3.9	9.6e-04	INV
295	RRBP1	Ribosome-binding protein 1	Q9P2E9	3.9	2.4e-04	INV
296	RPS29	40S ribosomal protein S29	P62273	3.9	7.6e-03	WT
297	SRPRB	Signal recognition particle receptor subunit beta	Q9Y5M8	3.9	1.5e-03	INV
298	CD109	CD109 antigen	Q6YHK3	3.9	7.5e-04	INV
299	MAGT1	Magnesium transporter protein 1	Q9H0U3	3.8	6.9e-04	INV
300	CCDC47	Coiled-coil domain-containing protein 47	Q96A33	3.8	3.3e-04	INV
302	VCL	Vinculin	P18206	3.8	9.5e-04	INV
303	RAD50	DNA repair protein RAD50	Q92878	3.8	2.4e-02	INV
304	ZYX	Zyxin	Q15942	3.8	3.9e-03	INV
305	PIPSL	Phosphatidylinositol 4-phosphate 5-kinase type-1 alpha	Q99755	3.8	1.9e-04	INV
306	MYH14	Myosin-14	Q7Z406	3.8	1.9e-02	INV
307	HSP90AB1	Heat shock protein HSP 90-beta	P08238	3.8	3.4e-07	INV
308	LDHB	L-lactate dehydrogenase B chain	P07195	3.8	2.1e-02	INV
309	NUDC	Nuclear migration protein nudC	Q9Y266	3.7	2.0e-04	INV
310	EZR	Ezrin	P15311	3.7	2.6e-04	INV
311	EEF1G	Elongation factor 1-gamma	P26641	3.7	3.1e-05	INV
312	PDLIM5	PDZ and LIM domain protein 5	Q96HC4	3.7	6.3e-04	INV
313	MYH9	Myosin-9	P35579	3.7	6.3e-03	INV + R159E
314	GPI	Glucose-6-phosphate isomerase	P06744	3.7	7.1e-03	INV
315	HNRNPM	Heterogeneous nuclear ribonucleoprotein M	P52272	3.6	3.9e-02	WT
316	NSF	Vesicle-fusing ATPase	P46459	3.6	1.5e-02	INV
317	RAC1	Ras-related C3 botulinum toxin substrate 1	P63000	3.6	2.6e-03	INV
318	IMMT	MICOS complex subunit MIC60	Q16891	3.6	2.6e-03	INV
319	CYB5B	Cytochrome b5 type B	O43169	3.6	2.2e-03	INV
321	PGK1	Phosphoglycerate kinase 1	P00558	3.6	1.7e-02	INV
322	CLIC1	Chloride intracellular channel protein 1	O00299	3.6	3.3e-02	INV
323	CDK1	Cyclin-dependent kinase 1	P06493	3.6	1.2e-02	INV
324	ATL3	Atlastin-3	Q6DD88	3.6	8.8e-03	INV
325	CDC42SE2	CDC42 small effector protein 2	Q9NRR3	3.6	2.9e-02	INV
326	PRKCA	Protein kinase C alpha type	P17252	3.5	3.1e-02	INV
328	TRIP13	Pachytene checkpoint protein 2 homolog	Q15645	3.5	1.3e-02	WT + INV
329	PRMT1	Protein arginine N-methyltransferase 1	Q99873	3.5	1.5e-02	WT
330	DDX39B	Spliceosome RNA helicase DDX39B	Q13838	3.5	3.5e-02	INV + R159E
331	MTDH	Protein LYRIC	Q86UE4	3.5	5.3e-03	INV
332	LMNA	Prelamin-A/C	P02545	3.5	2.6e-03	INV
333	PPFIBP1	Liprin-beta-1	Q86W92	3.5	2.9e-03	INV
335	TM9SF2	Transmembrane 9 superfamily member 2	Q99805	3.5	2.6e-04	WT
336	PFN1	Profilin-1	P07737	3.5	1.7e-02	INV
338	MYO1B	Unconventional myosin-Ib	O43795	3.5	3.2e-03	INV
339	PRDX6	Peroxiredoxin-6	P30041	3.5	4.5e-03	INV
340	ESYT2	Extended synaptotagmin-2	A0FGR8	3.4	6.4e-04	INV
343	SLC39A10	Zinc transporter ZIP10	Q9ULF5	3.4	1.6e-02	INV
344	ARF4	ADP-ribosylation factor 4	P18085	3.4	4.0e-02	INV
345	P4HA1	Prolyl 4-hydroxylase subunit alpha-1	P13674	3.4	1.2e-03	INV
346	B2M	Beta-2-microglobulin	P61769	3.4	1.2e-02	INV
347	SLC9A3R1	Na(+)/H(+) exchange regulatory cofactor NHE-RF1	O14745	3.4	1.8e-03	INV
348	PHGDH	D-3-phosphoglycerate dehydrogenase	O43175	3.4	2.1e-04	INV
349	RPL23	60S ribosomal protein L23	P62829	3.4	1.1e-02	INV
350	VAPA	Vesicle-associated membrane protein-associated protein A	Q9P0L0	3.4	5.9e-03	INV
351	YWHAQ	14-3-3 protein theta	P27348	3.4	5.5e-03	INV
352	GLIPR2	Golgi-associated plant pathogenesis-related protein 1	Q9H4G4	3.4	3.4e-04	INV
353	EMD	Emerin	P50402	3.4	7.8e-03	INV
354	LAMP2	Lysosome-associated membrane glycoprotein 2	P13473	3.3	3.0e-03	WT
355	RPL21	60S ribosomal protein L21	P46778	3.3	5.3e-03	WT
356	VASN	Vasorin	Q6EMK4	3.3	1.7e-03	INV
357	PTPRF	Receptor-type tyrosine-protein phosphatase F	P10586	3.3	8.2e-03	INV
358	SNTB2	Beta-2-syntrophin	Q13425	3.3	1.8e-03	INV
359	TUBB	Tubulin beta chain	P07437	3.3	4.1e-12	INV
360	ARHGAP1	Rho GTPase-activating protein 1	Q07960	3.3	4.9e-03	INV
361	CKB	Creatine kinase B-type	P12277	3.3	7.4e-03	INV
362	ENG	Endoglin	P17813	3.3	1.8e-02	INV
364	NAMPT	Nicotinamide phosphoribosyltransferase	P43490	3.3	1.7e-02	INV
365	PLIN3	Perilipin-3	O60664	3.3	6.9e-03	WT + INV
366	LRRC8A	Volume-regulated anion channel subunit LRRC8A	Q8IWT6	3.3	7.7e-03	INV
367	DAD1	Dolichyl-diphosphooligosaccharide–protein glycosyltransferase subunit DAD1	P61803	3.3	1.8e-03	INV
368	SSR4	Translocon-associated protein subunit delta	P51571	3.3	3.0e-03	INV
369	CD55	Complement decay-accelerating factor	P08174	3.3	1.6e-02	INV
370	FKBP4	Peptidyl-prolyl cis-trans isomerase FKBP4	Q02790	3.2	5.4e-04	INV

Rank	Gene name	Protein name	Protein ID	Fold change	P value	Dataset
371	GCN1L1	Translational activator GCN1	Q92616	3.2	4.1e-03	INV
372	SCRIB	Protein scribble homolog	Q14160	3.2	8.1e-04	INV
373	RPS13	40S ribosomal protein S13	P62277	3.2	2.7e-02	WT
374	CDH13	Cadherin-13	P55290	3.2	7.0e-04	INV
376	PTPRJ	Receptor-type tyrosine-protein phosphatase eta	Q12913	3.2	1.6e-02	INV
377	EPHA2	Ephrin type-A receptor 2	P29317	3.2	5.2e-03	INV
378	MYH10	Myosin-10	P35580	3.2	2.3e-02	INV
379	ITGB4	Integrin beta-4	P16144	3.2	3.3e-03	INV
380	SEC61B	Protein transport protein Sec61 subunit beta	P60468	3.2	1.2e-02	INV
381	PARK7	Protein deglycase DJ-1	Q99497	3.2	4.8e-02	INV
382	ANPEP	Aminopeptidase N	P15144	3.2	3.1e-02	INV
383	SPCS2	Signal peptidase complex subunit 2	Q15005	3.2	7.7e-03	INV
384	ZDHHC5	Palmitoyltransferase ZDHHC5	Q9C0B5	3.2	6.5e-03	INV
385	RPLP2	60S acidic ribosomal protein P2	P05387	3.2	2.2e-02	WT
387	LMNB1	Lamin-B1	P20700	3.1	1.0e-02	INV
388	CLU	Clusterin	P10909	3.1	1.4e-03	INV
389	TPI1	Triosephosphate isomerase	P60174	3.1	2.1e-02	INV
390	CASP14	Caspase-14	P31944	3.1	7.2e-03	WT
391	PEF1	Peflin	Q9UBV8	3.1	4.7e-02	WT
392	PCBP2	Poly(rC)-binding protein 2	Q15366	3.1	1.8e-06	INV
393	NR3C1	Glucocorticoid receptor	P04150	3.1	3.3e-03	INV
394	SRP68	Signal recognition particle subunit SRP68	Q9UHB9	3.1	4.0e-02	WT
395	TUBB3	Tubulin beta-3 chain	Q13509	3.1	1.1e-02	INV
396	ARHGEF2	Rho guanine nucleotide exchange factor 2	Q92974	3.1	8.3e-03	INV
397	YWHAE	14-3-3 protein epsilon	P62258	3.1	1.7e-02	INV
398	LIMA1	LIM domain and actin-binding protein 1	Q9UHB6	3.1	2.0e-02	INV
399	EPPK1	Epiplakin	P58107	3.1	2.1e-02	INV
400	NUP35	Nucleoporin NUP53	Q8NFH5	3.1	1.8e-02	INV
401	HAT1	Histone acetyltransferase type B catalytic subunit	O14929	3.1	8.8e-03	INV
402	SAR1B	GTP-binding protein SAR1b	Q9Y6B6	3.0	1.7e-02	INV
403	ATAD3A	ATPase family AAA domain-containing protein 3A	Q9NVI7	3.0	6.1e-04	INV
404	CLPTM1L	Cleft lip and palate transmembrane protein 1-like protein	Q96KA5	3.0	2.2e-03	INV
405	ADAR	Double-stranded RNA-specific adenosine deaminase	P55265	3.0	4.8e-03	WT
406	RCN2	Reticulocalbin-2	Q14257	3.0	3.1e-04	INV
407	PRPSAP1	Phosphoribosyl pyrophosphate synthase-associated protein 1	Q14558	3.0	2.5e-02	INV
408	CDK11B	Cyclin-dependent kinase 11B	P21127	3.0	5.5e-05	INV
409	PTBP3	Polypyrimidine tract-binding protein 3	O95758	3.0	3.2e-03	INV
410	USO1	General vesicular transport factor p115	O60763	3.0	1.1e-03	INV
411	CCT3	T-complex protein 1 subunit gamma	P49368	3.0	6.6e-05	INV
412	LIN7C	Protein lin-7 homolog C	Q9NUP9	3.0	1.5e-02	INV
413	TUBA1B	Tubulin alpha-1B chain	P68363	3.0	1.9e-11	INV
414	RPL10A	60S ribosomal protein L10a	P62906	3.0	1.6e-02	WT
415	TOP2A	DNA topoisomerase 2-alpha	P11388	3.0	3.0e-02	INV
416	CD70	CD70 antigen	P32970	3.0	3.2e-04	INV
417	EEF1A1	Elongation factor 1-alpha 1	P68104	3.0	3.2e-05	INV
418	POFUT1	GDP-fucose protein O-fucosyltransferase 1	Q9H488	2.9	6.8e-03	INV
420	YWHAB	14-3-3 protein beta/alpha	P31946	2.9	1.3e-02	INV
422	CTNNBL1	Beta-catenin-like protein 1	Q8WYA6	2.9	3.7e-03	INV
423	PVR	Poliovirus receptor	P15151	2.9	2.1e-02	INV
424	VIM	Vimentin	P08670	2.9	1.6e-04	INV
425	P4HA2	Prolyl 4-hydroxylase subunit alpha-2	O15460	2.9	1.5e-03	INV
426	PCBP3	Poly(rC)-binding protein 3	P57721	2.9	2.6e-03	INV
427	RTN3	Reticulon-3	O95197	2.9	2.2e-02	INV
428	PGAM1	Phosphoglycerate mutase 1	P18669	2.9	1.5e-02	INV
429	ACLY	ATP-citrate synthase	P53396	2.9	1.7e-02	INV
430	YBX1	Nuclease-sensitive element-binding protein 1	P67809	2.8	1.7e-02	WT
431	CCT8	T-complex protein 1 subunit theta	P50990	2.8	1.5e-02	INV
432	NSUN2	tRNA (cytosine(34)-C(5))-methyltransferase	Q08J23	2.8	1.7e-02	INV
433	PSMD11	26S proteasome non-ATPase regulatory subunit 11	O00231	2.8	1.1e-02	INV
434	MAT2A	S-adenosylmethionine synthase isoform type-2	P31153	2.8	2.9e-02	WT + INV
435	CD3EAP	DNA-directed RNA polymerase I subunit RPA34	O15446	2.8	3.6e-02	INV
436	RAB34	Ras-related protein Rab-34	Q9BZG1	2.8	7.1e-03	WT + INV
437	RFC1	Replication factor C subunit 1	P35251	2.8	2.8e-02	INV
438	EIF4G1	Eukaryotic translation initiation factor 4 gamma 1	Q04637	2.8	2.7e-02	INV
439	XPO1	Exportin-1	O14980	2.7	3.7e-02	INV
440	CAT	Catalase	P04040	2.7	1.8e-02	INV
441	ALDH3B1	Aldehyde dehydrogenase family 3 member B1	P43353	2.7	1.4e-02	INV
442	RALA	Ras-related protein Ral-A	P11233	2.7	4.0e-03	WT + INV
443	CYSRT1	Cysteine-rich tail protein 1	A8MQ03	2.7	3.0e-02	INV
444	DNAJA1	DnaJ homolog subfamily A member 1	P31689	2.7	4.5e-02	INV
445	RPL8	60S ribosomal protein L8	P62917	2.7	3.7e-03	WT
447	MPP6	MAGUK p55 subfamily member 6	Q9NZW5	2.7	3.0e-02	INV
448	SYAP1	Synapse-associated protein 1	Q96A49	2.7	3.1e-03	INV
449	CORO1C	Coronin-1C	Q9ULV4	2.7	2.6e-02	INV
450	UCK2	Uridine-cytidine kinase 2	Q9BZX2	2.7	6.2e-03	INV
451	DBN1	Drebrin	Q16643	2.7	3.4e-02	INV
452	CCT5	T-complex protein 1 subunit epsilon	P48643	2.7	2.2e-02	INV
453	MCM4	DNA replication licensing factor MCM4	P33991	2.7	4.5e-02	INV
454	ATP6V1A	V-type proton ATPase catalytic subunit A	P38606	2.7	2.0e-02	INV
455	CSPG4	Chondroitin sulfate proteoglycan 4	Q6UVK1	2.7	1.7e-03	INV
456	NPTN	Neuroplastin	Q9Y639	2.7	7.9e-03	INV
457	MAP1B	Microtubule-associated protein 1B	P46821	2.7	1.6e-02	INV
458	EPRS	Bifunctional glutamate/proline–tRNA ligase	P07814	2.7	2.4e-02	INV
459	KPNA3	Importin subunit alpha-4	O00505	2.7	6.4e-03	INV
460	PSMC3	26S protease regulatory subunit 6A	P17980	2.7	6.6e-03	INV

Rank	Gene name	Protein name	Protein ID	Fold change	P value	Dataset
461	CMBL	Carboxymethylenebutenolidase homolog	Q96DG6	2.7	4.8e-02	WT
462	MTCH2	Mitochondrial carrier homolog 2	Q9Y6C9	2.7	2.0e-02	INV
463	PDS5A	Sister chromatid cohesion protein PDS5 homolog A	Q29RF7	2.7	9.6e-03	INV
464	TUBB4B	Tubulin beta-4B chain	P68371	2.7	2.0e-08	INV
465	APMAP	Adipocyte plasma membrane-associated protein	Q9HDC9	2.7	3.3e-03	INV
466	PDXDC1	Pyridoxal-dependent decarboxylase domain-containing protein 1	Q6P996	2.6	3.1e-02	INV
467	CASK	Peripheral plasma membrane protein CASK	O14936	2.6	9.6e-03	INV
468	PLXNB2	Plexin-B2	O15031	2.6	2.4e-02	INV
469	POR	NADPH–cytochrome P450 reductase	P16435	2.6	7.8e-03	INV
470	EEF1A1P5	Putative elongation factor 1-alpha-like 3	Q5VTE0	2.6	6.3e-04	INV
471	UBA1	Ubiquitin-like modifier-activating enzyme 1	P22314	2.6	3.7e-02	WT + INV
472	GCLM	Glutamate–cysteine ligase regulatory subunit	P48507	2.6	6.9e-03	INV
473	PDCD6IP	Programmed cell death 6-interacting protein	Q8WUM4	2.6	4.7e-03	INV
474	SDC4	Syndecan-4	P31431	2.6	1.2e-02	INV
475	ITGA1	Integrin alpha-1	P56199	2.6	8.1e-03	INV
476	FLOT1	Flotillin-1	O75955	2.6	1.8e-02	INV
477	PARP1	Poly [ADP-ribose] polymerase 1	P09874	2.6	4.6e-03	INV
478	SMC1A	Structural maintenance of chromosomes protein 1A	Q14683	2.6	2.7e-02	INV
479	CLASP2	CLIP-associating protein 2	O75122	2.6	2.9e-02	INV
480	SLC12A2	Solute carrier family 12 member 2	P55011	2.6	2.2e-02	INV
481	HSDL2	Hydroxysteroid dehydrogenase-like protein 2	Q6YN16	2.6	9.3e-03	INV
482	FARSA	Phenylalanine–tRNA ligase alpha subunit	Q9Y285	2.6	2.9e-02	INV
483	RUVBL2	RuvB-like 2	Q9Y230	2.6	3.6e-02	WT
484	DLG1	Disks large homolog 1	Q12959	2.6	4.7e-02	INV
485	KARS	Lysine–tRNA ligase	Q15046	2.6	1.4e-02	INV
486	MAP4	Microtubule-associated protein 4	P27816	2.5	1.3e-02	INV
487	HSPB1	Heat shock protein beta-1	P04792	2.5	8.0e-08	INV
488	HMOX1	Heme oxygenase 1	P09601	2.5	1.4e-02	INV
489	ASNA1	ATPase ASNA1	O43681	2.5	1.1e-02	INV
490	IGF2R	Cation-independent mannose-6-phosphate receptor	P11717	2.5	4.6e-03	WT
491	SSR3	Translocon-associated protein subunit gamma	Q9UNL2	2.5	3.6e-03	INV
492	RHOG	Rho-related GTP-binding protein RhoG	P84095	2.5	9.5e-03	INV
493	ERBB2IP	Protein LAP2	Q96RT1	2.5	3.0e-02	INV
495	NPR3	Atrial natriuretic peptide receptor 3	P17342	2.5	4.8e-02	INV
496	TTLL12	Tubulin–tyrosine ligase-like protein 12	Q14166	2.5	2.8e-02	INV
497	PIGS	GPI transamidase component PIG-S	Q96S52	2.5	8.8e-04	INV
498	HIST2H3A	Histone H3.3	P84243	2.5	2.1e-02	INV
499	ANXA11	Annexin A11	P50995	2.5	1.3e-02	INV
500	TMEM165	Transmembrane protein 165	Q9HC07	2.5	2.6e-03	INV
501	PTK7	Inactive tyrosine-protein kinase 7	Q13308	2.5	1.1e-02	INV
502	RPL4	60S ribosomal protein L4	P36578	2.5	1.3e-02	WT
503	SLC38A1	Sodium-coupled neutral amino acid transporter 1	Q9H2H9	2.5	3.3e-02	INV
504	PRDX2	Peroxiredoxin-2	P32119	2.5	2.0e-02	INV
505	MCM6	DNA replication licensing factor MCM6	Q14566	2.5	5.7e-03	INV
506	NOP58	Nucleolar protein 58	Q9Y2X3	2.5	7.2e-03	INV
507	IPO7	Importin-7	O95373	2.4	1.0e-02	INV
508	SAR1A	GTP-binding protein SAR1a	Q9NR31	2.4	4.7e-02	INV
509	RCN1	Reticulocalbin-1	Q15293	2.4	8.0e-03	INV
510	UNC45A	Protein unc-45 homolog A	Q9H3U1	2.4	2.2e-02	INV
511	NEGR1	Neuronal growth regulator 1	Q7Z3B1	2.4	4.5e-02	INV
512	NQO1	NAD(P)H dehydrogenase [quinone] 1	P15559	2.4	4.3e-02	INV
513	PODXL	Podocalyxin	O00592	2.4	4.2e-02	INV
514	PTGFRN	Prostaglandin F2 receptor negative regulator	Q9P2B2	2.4	4.1e-02	INV
515	ERLIN1	Erlin-1	O75477	2.4	2.1e-02	INV
516	CXCR4	C-X-C chemokine receptor type 4	P61073	2.4	1.6e-02	INV
517	CKAP5	Cytoskeleton-associated protein 5	Q14008	2.4	1.7e-02	INV
518	THY1	Thy-1 membrane glycoprotein	P04216	2.4	1.2e-02	INV
519	DEK	Protein DEK	P35659	2.4	4.8e-02	WT
520	CSTA	Cystatin-A	P01040	2.4	1.1e-02	WT
521	EEF1B2	Elongation factor 1-beta	P24534	2.4	3.5e-02	INV
522	EIF2B4	Translation initiation factor eIF-2B subunit delta	Q9UI10	2.4	2.1e-02	INV
523	COPB1	Coatomer subunit beta	P53618	2.4	4.8e-02	INV
524	ACACA	Acetyl-CoA carboxylase 1	Q13085	2.3	1.9e-02	WT
525	DDX47	Probable ATP-dependent RNA helicase DDX47	Q9H0S4	2.3	1.1e-02	INV
526	FLOT2	Flotillin-2	Q14254	2.3	2.6e-02	INV
527	DNM2	Dynamin-2	P50570	2.3	4.7e-02	INV
528	SLC30A1	Zinc transporter 1	Q9Y6M5	2.3	4.7e-02	INV
529	S100A9	Protein S100-A9	P06702	2.3	3.9e-02	WT
530	PSMA5	Proteasome subunit alpha type-5	P28066	2.3	1.1e-02	INV
531	EHD4	EH domain-containing protein 4	Q9H223	2.3	4.0e-02	INV
532	CPNE8	Copine-8	Q86YQ8	2.3	3.7e-02	INV
533	MYADM	Myeloid-associated differentiation marker	Q96S97	2.3	1.6e-02	WT + INV
535	STIP1	Stress-induced-phosphoprotein 1	P31948	2.3	1.7e-02	INV
536	DDX21	Nucleolar RNA helicase 2	Q9NR30	2.3	3.2e-02	INV
537	SLC4A7	Sodium bicarbonate cotransporter 3	Q9Y6M7	2.3	1.0e-03	INV
538	PSMD6	26S proteasome non-ATPase regulatory subunit 6	Q15008	2.2	3.2e-02	INV
539	QARS	Glutamine–tRNA ligase	P47897	2.2	1.3e-02	INV
540	SUPT16H	FACT complex subunit SPT16	Q9Y5B9	2.2	3.4e-02	INV
541	UNC13D	Protein unc-13 homolog D	Q70J99	2.2	1.0e-02	INV
542	NOB1	RNA-binding protein NOB1	Q9ULX3	2.2	1.8e-02	INV
543	CAV1	Caveolin-1	Q03135	2.2	2.5e-02	INV
544	GNA13	Guanine nucleotide-binding protein subunit alpha-13	Q14344	2.2	3.2e-02	INV
545	ITGA6	Integrin alpha-6	P23229	2.2	2.8e-02	INV
546	DNAJB11	DnaJ homolog subfamily B member 11	Q9UBS4	2.2	8.0e-03	INV
547	MYO1E	Unconventional myosin-Ie	Q12965	2.2	2.3e-02	INV + R159E

Rank	Gene name	Protein name	Protein ID	Fold change	P value	Dataset
548	UBA5	Ubiquitin-like modifier-activating enzyme 5	Q9GZZ9	2.2	1.0e-02	INV
549	TCF25	Transcription factor 25	Q9BQ70	2.2	2.2e-02	INV
550	HMX3	Homeobox protein HMX3	A6NHT5	2.2	1.6e-02	INV
551	SCARB1	Scavenger receptor class B member 1	Q8WTV0	2.2	2.1e-03	INV
552	KPRP	Keratinocyte proline-rich protein	Q5T749	2.2	4.2e-02	WT
553	RRP1	Ribosomal RNA processing protein 1 homolog A	P56182	2.2	1.2e-02	INV
554	PCMT1	Protein-L-isoaspartate(D-aspartate) O-methyltransferase	P22061	2.2	4.8e-02	INV
555	FYCO1	FYVE and coiled-coil domain-containing protein 1	Q9BQS8	2.2	2.7e-02	INV
556	AQP1	Aquaporin-1	P29972	2.2	4.0e-02	INV
557	ACTR2	Actin-related protein 2	P61160	2.1	1.3e-02	INV
558	MAPRE1	Microtubule-associated protein RP/EB family member 1	Q15691	2.1	1.2e-02	INV
559	PRKAR2A	cAMP-dependent protein kinase type II-alpha regulatory subunit	P13861	2.1	3.3e-02	INV
560	EFR3A	Protein EFR3 homolog A	Q14156	2.1	2.5e-03	INV
561	RAB21	Ras-related protein Rab-21	Q9UL25	2.1	2.3e-02	WT + INV
562	TMX3	Protein disulfide-isomerase TMX3	Q96JJ7	2.1	1.5e-02	INV
563	GATAD2A	Transcriptional repressor p66-alpha	Q86YP4	2.1	3.4e-02	INV
564	PSME3	Proteasome activator complex subunit 3	P61289	2.1	1.0e-02	WT + INV
565	FASN	Fatty acid synthase	P49327	2.1	1.7e-02	WT
566	SIRPA	Tyrosine-protein phosphatase non-receptor type substrate 1	P78324	2.1	6.8e-03	INV
567	HINT1	Histidine triad nucleotide-binding protein 1	P49773	2.1	1.2e-02	INV
568	ST13	Hsc70-interacting protein	P50502	2.1	6.4e-03	INV
569	RHOB	Rho-related GTP-binding protein RhoB	P62745	2.1	2.5e-02	INV
570	UGGT1	UDP-glucose:glycoprotein glucosyltransferase 1	Q9NYU2	2.1	1.5e-02	INV
571	GNB4	Guanine nucleotide-binding protein subunit beta-4	Q9HAV0	2.1	5.2e-03	INV
572	HIST1H4A	Histone H4	P62805	2.1	1.5e-03	INV
573	UGDH	UDP-glucose 6-dehydrogenase	O60701	2.1	3.3e-02	INV
576	LEPRE1	Prolyl 3-hydroxylase 1	Q32P28	2.1	2.9e-02	INV
577	GLIPR1	Glioma pathogenesis-related protein 1	P48060	2.1	2.3e-02	INV
578	H2AFV	Histone H2A.V	Q71UI9	2.1	1.5e-02	INV
579	USP5	Ubiquitin carboxyl-terminal hydrolase 5	P45974	2.1	4.0e-02	INV
580	MARK2	Serine/threonine-protein kinase MARK2	Q7KZI7	2.1	4.5e-02	INV
581	GNB2L1	Guanine nucleotide-binding protein subunit beta-2-like 1	P63244	2.1	3.3e-02	INV
582	ITFG1	T-cell immunomodulatory protein	Q8TB96	2.1	1.6e-02	WT
583	UBR4	E3 ubiquitin-protein ligase UBR4	Q5T4S7	2.1	4.6e-02	INV
584	ATL2	Atlastin-2	Q8NHH9	2.1	2.0e-02	INV
585	G6PD	Glucose-6-phosphate 1-dehydrogenase	P11413	2.0	1.9e-02	INV
586	COG5	Conserved oligomeric Golgi complex subunit 5	Q9UP83	2.0	4.5e-02	INV
587	SPNS1	Protein spinster homolog 1	Q9H2V7	2.0	3.0e-03	INV
588	MPRIP	Myosin phosphatase Rho-interacting protein	Q6WCQ1	2.0	4.0e-02	INV
589	EIF5B	Eukaryotic translation initiation factor 5B	O60841	2.0	1.6e-02	INV
590	HMOX2	Heme oxygenase 2	P30519	2.0	1.8e-02	INV
591	NOTCH2	Neurogenic locus notch homolog protein 2	Q04721	2.0	4.7e-02	INV
592	PLBD2	Putative phospholipase B-like 2	Q8NHP8	2.0	1.8e-02	INV
593	OTUB1	Ubiquitin thioesterase OTUB1	Q96FW1	2.0	5.0e-02	INV
594	OCIAD1	OCIA domain-containing protein 1	Q9NX40	2.0	4.3e-02	WT
595	DDRGK1	DDRGK domain-containing protein 1	Q96HY6	2.0	1.3e-02	INV
597	DYNC1I2	Cytoplasmic dynein 1 intermediate chain 2	Q13409	2.0	2.9e-02	INV
598	NCLN	Nicalin	Q969V3	2.0	2.1e-02	INV
599	POLR1E	DNA-directed RNA polymerase I subunit RPA49	Q9GZS1	2.0	2.1e-03	INV
600	NSFL1C	NSFL1 cofactor p47	Q9UNZ2	2.0	1.1e-02	INV
601	RPL24	60S ribosomal protein L24	P83731	2.0	1.1e-04	INV
602	ATAD3B	ATPase family AAA domain-containing protein 3B	Q5T9A4	2.0	3.5e-02	INV

Table S2. PANTHER protein classification of INV proteins The consolidated INV proteome with assigned class and subclass from PANTHER protein classification are shown ordered by class-subclass.

Gene name	Protein ID	Class	Subclass
ANXA2	P07355	calcium-binding protein	calcium-binding protein
ANXA1	P04083	calcium-binding protein	calcium-binding protein
ANXA11	P50995	calcium-binding protein	calcium-binding protein
CPNE8	Q86YQ8	calcium-binding protein	calcium-binding protein
CALU	O43852	calcium-binding protein	calmodulin-related
RCN2	Q14257	calcium-binding protein	calmodulin-related
RCN1	Q15293	calcium-binding protein	calmodulin-related
S100A9	P06702	calcium-binding protein	calmodulin-related
DSG2	Q14126	cell adhesion molecule	cadherin
CDH2	P19022	cell adhesion molecule	cadherin
CDH13	P55290	cell adhesion molecule	cadherin
TGFBI	Q15582	cell adhesion molecule	cell adhesion molecule
PVR	P15151	cell adhesion molecule	cell adhesion molecule
CSPG4	Q6UVK1	cell adhesion molecule	cell adhesion molecule
PODXL	O00592	cell adhesion molecule	cell adhesion molecule
CXCR4	P61073	cell adhesion molecule	cell adhesion molecule
THY1	P04216	cell adhesion molecule	cell adhesion molecule
MCAM	P43121	cell adhesion molecule	immunoglobulin superfamily cell adhesion molecule
ALCAM	Q13740	cell adhesion molecule	immunoglobulin superfamily cell adhesion molecule
L1CAM	P32004	cell adhesion molecule	immunoglobulin superfamily cell adhesion molecule
ITGB1	P05556	cell adhesion molecule	integrin
ITGA5	P08648	cell adhesion molecule	integrin
ITGAV	P06756	cell adhesion molecule	integrin
ITGA11	Q9UKX5	cell adhesion molecule	integrin
ITGA3	P26006	cell adhesion molecule	integrin
ITGB4	P16144	cell adhesion molecule	integrin
ITGA1	P56199	cell adhesion molecule	integrin
ITGA6	P23229	cell adhesion molecule	integrin
LIN7C	Q9NUP9	cell junction protein	cell junction protein
CALR	P27797	chaperone	chaperone
CANX	P27824	chaperone	chaperone
PDIA3	P30101	chaperone	chaperone
P4HB	P07237	chaperone	chaperone
DNAJC5	Q9H3Z4	chaperone	chaperone
DNAJC13	O75165	chaperone	chaperone
TXNDC5	Q8NBS9	chaperone	chaperone
PDIA6	Q15084	chaperone	chaperone
PDIA4	P13667	chaperone	chaperone
PPIA	P62937	chaperone	chaperone
FKBP4	Q02790	chaperone	chaperone
DNAJA1	P31689	chaperone	chaperone
HSPB1	P04792	chaperone	chaperone
DNAJB11	Q9UBS4	chaperone	chaperone
TMX3	Q96JJ7	chaperone	chaperone
CCT2	P78371	chaperone	chaperonin
CCT6A	P40227	chaperone	chaperonin
CCT4	P50991	chaperone	chaperonin
TCP1	P17987	chaperone	chaperonin
CCT7	Q99832	chaperone	chaperonin
CCT3	P49368	chaperone	chaperonin
CCT8	P50990	chaperone	chaperonin
CCT5	P48643	chaperone	chaperonin
HSPA5	P11021	chaperone	Hsp70 family chaperone
HYOU1	Q9Y4L1	chaperone	Hsp70 family chaperone
HSP90B1	P14625	chaperone	Hsp90 family chaperone
HSP90AB2P	Q58FF8	chaperone	Hsp90 family chaperone
HSP90AA1	P07900	chaperone	Hsp90 family chaperone
HSP90AB1	P08238	chaperone	Hsp90 family chaperone
MSN	P26038	cytoskeletal protein	actin or actin-binding cytoskeletal protein
CTNNA1	P35221	cytoskeletal protein	actin or actin-binding cytoskeletal protein
ACTN4	O43707	cytoskeletal protein	actin or actin-binding cytoskeletal protein
MYO1C	O00159	cytoskeletal protein	actin or actin-binding cytoskeletal protein
TLN1	Q9Y490	cytoskeletal protein	actin or actin-binding cytoskeletal protein
MYL12A	P19105	cytoskeletal protein	actin or actin-binding cytoskeletal protein
EPB41L2	O43491	cytoskeletal protein	actin or actin-binding cytoskeletal protein
CRIP2	P52943	cytoskeletal protein	actin or actin-binding cytoskeletal protein
CAP1	Q01518	cytoskeletal protein	actin or actin-binding cytoskeletal protein
ACTN1	P12814	cytoskeletal protein	actin or actin-binding cytoskeletal protein
VCL	P18206	cytoskeletal protein	actin or actin-binding cytoskeletal protein
ZYX	Q15942	cytoskeletal protein	actin or actin-binding cytoskeletal protein
MYH14	Q7Z406	cytoskeletal protein	actin or actin-binding cytoskeletal protein
EZR	P15311	cytoskeletal protein	actin or actin-binding cytoskeletal protein
PDLIM5	Q96HC4	cytoskeletal protein	actin or actin-binding cytoskeletal protein
MYH9	P35579	cytoskeletal protein	actin or actin-binding cytoskeletal protein
MYO1B	O43795	cytoskeletal protein	actin or actin-binding cytoskeletal protein
MYH10	P35580	cytoskeletal protein	actin or actin-binding cytoskeletal protein
LIMA1	Q9UHB6	cytoskeletal protein	actin or actin-binding cytoskeletal protein
MYO1E	Q12965	cytoskeletal protein	actin or actin-binding cytoskeletal protein
ACTR2	P61160	cytoskeletal protein	actin or actin-binding cytoskeletal protein
MPRIP	Q6WCQ1	cytoskeletal protein	actin or actin-binding cytoskeletal protein
CFL1	P23528	cytoskeletal protein	cytoskeletal protein
STOM	P27105	cytoskeletal protein	cytoskeletal protein
PLS3	P13797	cytoskeletal protein	cytoskeletal protein
FSCN1	Q16658	cytoskeletal protein	cytoskeletal protein

Gene name	Protein ID	Class	Subclass
CALD1	Q05682	cytoskeletal protein	cytoskeletal protein
TPM3	P06753	cytoskeletal protein	cytoskeletal protein
TPM4	P67936	cytoskeletal protein	cytoskeletal protein
PFN1	P07737	cytoskeletal protein	cytoskeletal protein
CORO1C	Q9ULV4	cytoskeletal protein	cytoskeletal protein
MAP4	P27816	cytoskeletal protein	cytoskeletal protein
CKAP5	Q14008	cytoskeletal protein	cytoskeletal protein
PLEC	Q15149	cytoskeletal protein	intermediate filament
DSP	P15924	cytoskeletal protein	intermediate filament
CTNND1	O60716	cytoskeletal protein	intermediate filament
EPPK1	P58107	cytoskeletal protein	intermediate filament
VIM	P08670	cytoskeletal protein	intermediate filament
TUBA4A	P68366	cytoskeletal protein	microtubule or microtubule-binding cytoskeletal protein
TUBB6	Q9BUF5	cytoskeletal protein	microtubule or microtubule-binding cytoskeletal protein
DYNC1H1	Q14204	cytoskeletal protein	microtubule or microtubule-binding cytoskeletal protein
TUBB8	Q3ZCM7	cytoskeletal protein	microtubule or microtubule-binding cytoskeletal protein
NUMA1	Q14980	cytoskeletal protein	microtubule or microtubule-binding cytoskeletal protein
NUDC	Q9Y266	cytoskeletal protein	microtubule or microtubule-binding cytoskeletal protein
TUBB	P07437	cytoskeletal protein	microtubule or microtubule-binding cytoskeletal protein
TUBB3	Q13509	cytoskeletal protein	microtubule or microtubule-binding cytoskeletal protein
TUBA1B	P68363	cytoskeletal protein	microtubule or microtubule-binding cytoskeletal protein
MAP1B	P46821	cytoskeletal protein	microtubule or microtubule-binding cytoskeletal protein
TUBB4B	P68371	cytoskeletal protein	microtubule or microtubule-binding cytoskeletal protein
CLASP2	O75122	cytoskeletal protein	microtubule or microtubule-binding cytoskeletal protein
MAPRE1	Q15691	cytoskeletal protein	microtubule or microtubule-binding cytoskeletal protein
DYNC1I2	Q13409	cytoskeletal protein	microtubule or microtubule-binding cytoskeletal protein
CD55	P08174	defense/immunity protein	complement component
GLIPR2	Q9H4G4	defense/immunity protein	defense/immunity protein
GLIPR1	P48060	defense/immunity protein	defense/immunity protein
NEGR1	Q7Z3B1	defense/immunity protein	immunoglobulin
PTGFRN	Q9P2B2	defense/immunity protein	immunoglobulin receptor superfamily
B2M	P61769	defense/immunity protein	major histocompatibility complex protein
XRCC5	P13010	DNA metabolism protein	DNA helicase
XRCC6	P12956	DNA metabolism protein	DNA helicase
TOP2A	P11388	DNA metabolism protein	DNA metabolism protein
RFC1	P35251	DNA metabolism protein	DNA metabolism protein
MCM4	P33991	DNA metabolism protein	DNA metabolism protein
PARP1	P09874	DNA metabolism protein	DNA metabolism protein
MCM6	Q14566	DNA metabolism protein	DNA metabolism protein
LEPRE1	Q32P28	extracellular matrix protein	extracellular matrix glycoprotein
LGALS1	P09382	extracellular matrix protein	extracellular matrix protein
TNC	P24821	extracellular matrix protein	extracellular matrix protein
COL8A1	P27658	extracellular matrix protein	extracellular matrix structural protein
NR3C1	P04150	gene-specific transcriptional regulator	DNA-binding transcription factor
HMX3	A6NHT5	gene-specific transcriptional regulator	DNA-binding transcription factor
GATAD2A	Q86YP4	gene-specific transcriptional regulator	DNA-binding transcription factor
PTHLH	P12272	intercellular signal molecule	peptide hormone
M6PR	P20645	membrane traffic protein	membrane traffic protein
VAMP3	Q15836	membrane traffic protein	membrane traffic protein
VAMP2	P63027	membrane traffic protein	membrane traffic protein
ERP29	P30040	membrane traffic protein	membrane traffic protein
VAMP8	Q9BV40	membrane traffic protein	membrane traffic protein
PTRF	Q6NZI2	membrane traffic protein	membrane traffic protein
BCAP31	P51572	membrane traffic protein	membrane traffic protein
EHD2	Q9NZN4	membrane traffic protein	membrane traffic protein
NSF	P46459	membrane traffic protein	membrane traffic protein
SEC61B	P60468	membrane traffic protein	membrane traffic protein
USO1	O60763	membrane traffic protein	membrane traffic protein
PDCD6IP	Q8WUM4	membrane traffic protein	membrane traffic protein
IGF2R	P11717	membrane traffic protein	membrane traffic protein
DNM2	P50570	membrane traffic protein	membrane traffic protein
EHD4	Q9H223	membrane traffic protein	membrane traffic protein
OCIAD1	Q9NX40	membrane traffic protein	membrane traffic protein
TPD52L2	O43399	membrane traffic protein	membrane trafficking regulatory protein
TPD52	P55327	membrane traffic protein	membrane trafficking regulatory protein
SYPL1	Q16563	membrane traffic protein	membrane trafficking regulatory protein
SYNGR2	O43760	membrane traffic protein	membrane trafficking regulatory protein
ATG9A	Q7Z3C6	membrane traffic protein	membrane trafficking regulatory protein
LAMP1	P11279	membrane traffic protein	membrane trafficking regulatory protein
TPD52L1	Q16890	membrane traffic protein	membrane trafficking regulatory protein
RTN4	Q9NQC3	membrane traffic protein	membrane trafficking regulatory protein
WDFY1	Q8IWB7	membrane traffic protein	membrane trafficking regulatory protein
CKAP4	Q07065	membrane traffic protein	membrane trafficking regulatory protein
ARL8A	Q96BM9	membrane traffic protein	membrane trafficking regulatory protein
ESYT1	Q9BSJ8	membrane traffic protein	membrane trafficking regulatory protein
SFT2D1	Q8WV19	membrane traffic protein	membrane trafficking regulatory protein
FOLR1	P15328	membrane traffic protein	membrane trafficking regulatory protein
SAR1A;SAR1B	Q9NR31;Q9Y6B6	membrane traffic protein	membrane trafficking regulatory protein
LAMTOR1	Q6IAA8	membrane traffic protein	membrane trafficking regulatory protein
SQSTM1	Q13501	membrane traffic protein	membrane trafficking regulatory protein
ESYT2	A0FGR8	membrane traffic protein	membrane trafficking regulatory protein
VAPA	Q9P0L0	membrane traffic protein	membrane trafficking regulatory protein
LAMP2	P13473	membrane traffic protein	membrane trafficking regulatory protein
SSR4	P51571	membrane traffic protein	membrane trafficking regulatory protein
SAR1B	Q9Y6B6	membrane traffic protein	membrane trafficking regulatory protein
RTN3	O95197	membrane traffic protein	membrane trafficking regulatory protein

Gene name	Protein ID	Class	Subclass
FLOT1	O75955	membrane traffic protein	membrane trafficking regulatory protein
SSR3	Q9UNL2	membrane traffic protein	membrane trafficking regulatory protein
SAR1A	Q9NR31	membrane traffic protein	membrane trafficking regulatory protein
ERLIN1	O75477	membrane traffic protein	membrane trafficking regulatory protein
FLOT2	Q14254	membrane traffic protein	membrane trafficking regulatory protein
SCARB1	Q8WTV0	membrane traffic protein	membrane trafficking regulatory protein
FYCO1	Q9BQS8	membrane traffic protein	membrane trafficking regulatory protein
COG5	Q9UP83	membrane traffic protein	membrane trafficking regulatory protein
VAMP7	P51809	membrane traffic protein	SNARE protein
SNAP23	O00161	membrane traffic protein	SNARE protein
COPB1	P53618	membrane traffic protein	vesicle coat protein
GANAB	Q14697	metabolite interconversion enzyme	hydrolase
DAGLB	Q8NCG7	metabolite interconversion enzyme	hydrolase
PLA2G4A	P47712	metabolite interconversion enzyme	hydrolase
EPHX1	P07099	metabolite interconversion enzyme	hydrolase
PLD1	Q13393	metabolite interconversion enzyme	hydrolase
PON2	Q15165	metabolite interconversion enzyme	hydrolase
GNS	P15586	metabolite interconversion enzyme	hydrolase
GDA	Q9Y2T3	metabolite interconversion enzyme	hydrolase
ARG1	P05089	metabolite interconversion enzyme	hydrolase
PLBD2	Q8NHP8	metabolite interconversion enzyme	hydrolase
GPI	P06744	metabolite interconversion enzyme	isomerase
TPI1	P60174	metabolite interconversion enzyme	isomerase
PGAM1	P18669	metabolite interconversion enzyme	isomerase
ACSL3	O95573	metabolite interconversion enzyme	ligase
GCLM	P48507	metabolite interconversion enzyme	ligase
ENO1	P06733	metabolite interconversion enzyme	lyase
ALDOA	P04075	metabolite interconversion enzyme	lyase
GAPDH	P04406	metabolite interconversion enzyme	metabolite interconversion enzyme
LDHA	P00338	metabolite interconversion enzyme	metabolite interconversion enzyme
LDHB	P07195	metabolite interconversion enzyme	metabolite interconversion enzyme
PHGDH	O43175	metabolite interconversion enzyme	metabolite interconversion enzyme
ALDH3B1	P43353	metabolite interconversion enzyme	metabolite interconversion enzyme
HSDL2	Q6YN16	metabolite interconversion enzyme	metabolite interconversion enzyme
HINT1	P49773	metabolite interconversion enzyme	metabolite interconversion enzyme
UGDH	O60701	metabolite interconversion enzyme	metabolite interconversion enzyme
EDIL3	O43854	metabolite interconversion enzyme	oxidoreductase
PRDX4	Q13162	metabolite interconversion enzyme	oxidoreductase
CYB5R3	P00387	metabolite interconversion enzyme	oxidoreductase
HSD17B10	Q99714	metabolite interconversion enzyme	oxidoreductase
PRDX1	Q06830	metabolite interconversion enzyme	oxidoreductase
CYB5B	O43169	metabolite interconversion enzyme	oxidoreductase
PRDX6	P30041	metabolite interconversion enzyme	oxidoreductase
CAT	P04040	metabolite interconversion enzyme	oxidoreductase
POR	P16435	metabolite interconversion enzyme	oxidoreductase
HMOX1	P09601	metabolite interconversion enzyme	oxidoreductase
PRDX2	P32119	metabolite interconversion enzyme	oxidoreductase
NQO1	P15559	metabolite interconversion enzyme	oxidoreductase
G6PD	P11413	metabolite interconversion enzyme	oxidoreductase
HMOX2	P30519	metabolite interconversion enzyme	oxidoreductase
PCYT1A	P49585	metabolite interconversion enzyme	transferase
DDOST	P39656	metabolite interconversion enzyme	transferase
RPN1	P04843	metabolite interconversion enzyme	transferase
PI4K2A	Q9BTU6	metabolite interconversion enzyme	transferase
GALNT2	Q10471	metabolite interconversion enzyme	transferase
NME2	P22392	metabolite interconversion enzyme	transferase
MTAP	Q13126	metabolite interconversion enzyme	transferase
RPN2	P04844	metabolite interconversion enzyme	transferase
PKM	P14618	metabolite interconversion enzyme	transferase
MAGT1	Q9H0U3	metabolite interconversion enzyme	transferase
PIPSL	Q99755	metabolite interconversion enzyme	transferase
PGK1	P00558	metabolite interconversion enzyme	transferase
CKB	P12277	metabolite interconversion enzyme	transferase
NAMPT	P43490	metabolite interconversion enzyme	transferase
DAD1	P61803	metabolite interconversion enzyme	transferase
PRPSAP1	Q14558	metabolite interconversion enzyme	transferase
ACLY	P53396	metabolite interconversion enzyme	transferase
MAT2A	P31153	metabolite interconversion enzyme	transferase
UCK2	Q9BZX2	metabolite interconversion enzyme	transferase
PCMT1	P22061	metabolite interconversion enzyme	transferase
UGGT1	Q9NYU2	metabolite interconversion enzyme	transferase
CDK1	P06493	protein modifying enzyme	non-receptor serine/threonine protein kinase
PRKCA	P17252	protein modifying enzyme	non-receptor serine/threonine protein kinase
CDK11B	P21127	protein modifying enzyme	non-receptor serine/threonine protein kinase
MARK2	Q7KZI7	protein modifying enzyme	non-receptor serine/threonine protein kinase
YES1	P07947	protein modifying enzyme	non-receptor tyrosine protein kinase
TFRC	P02786	protein modifying enzyme	protease
GGT1	P19440	protein modifying enzyme	protease
ECE1	P42892	protein modifying enzyme	protease
ANPEP	P15144	protein modifying enzyme	protease
SPCS2	Q15005	protein modifying enzyme	protease
CASP14	P31944	protein modifying enzyme	protease
PSMC3	P17980	protein modifying enzyme	protease
PSMA5	P28066	protein modifying enzyme	protease
CTSZ	Q9UBR2	protein modifying enzyme	protein modifying enzyme
PPT1	P50897	protein modifying enzyme	protein modifying enzyme

Gene name	Protein ID	Class	Subclass
CTSD	P07339	protein modifying enzyme	protein modifying enzyme
ASPH	Q12797	protein modifying enzyme	protein modifying enzyme
COLGALT1	Q8NBJ5	protein modifying enzyme	protein modifying enzyme
PRMT1	Q99873	protein modifying enzyme	protein modifying enzyme
P4HA1	P13674	protein modifying enzyme	protein modifying enzyme
POFUT1	Q9H488	protein modifying enzyme	protein modifying enzyme
P4HA2	O15460	protein modifying enzyme	protein modifying enzyme
USP5	P45974	protein modifying enzyme	protein modifying enzyme
OTUB1	Q96FW1	protein modifying enzyme	protein modifying enzyme
PTPRF	P10586	protein modifying enzyme	protein phosphatase
PTPRJ	Q12913	protein modifying enzyme	protein phosphatase
UBA1	P22314	protein modifying enzyme	ubiquitin-protein ligase
UBA5	Q9GZZ9	protein modifying enzyme	ubiquitin-protein ligase
UBR4	Q5T4S7	protein modifying enzyme	ubiquitin-protein ligase
RAB6A	P20340	protein-binding activity modulator	G-protein
RAB1B	Q9H0U4	protein-binding activity modulator	G-protein
GNAI2	P04899	protein-binding activity modulator	G-protein
RAB1A	P62820	protein-binding activity modulator	G-protein
RAB1C	Q92928	protein-binding activity modulator	G-protein
RAB14	P61106	protein-binding activity modulator	G-protein
RAB2A	P61019	protein-binding activity modulator	G-protein
RAP1B	P61224	protein-binding activity modulator	G-protein
GNAI3	P08754	protein-binding activity modulator	G-protein
GNB1	P62873	protein-binding activity modulator	G-protein
RAB10	P61026	protein-binding activity modulator	G-protein
RAB11B	Q15907	protein-binding activity modulator	G-protein
RAB7A	P51149	protein-binding activity modulator	G-protein
GNB2	P62879	protein-binding activity modulator	G-protein
GNA14	P29992	protein-binding activity modulator	G-protein
RAB5C	P51148	protein-binding activity modulator	G-protein
RAB8A	P61006	protein-binding activity modulator	G-protein
RAB11A	P62491	protein-binding activity modulator	G-protein
CDC42	P60953	protein-binding activity modulator	G-protein
NRAS	P01111	protein-binding activity modulator	G-protein
RAB8B	Q92930	protein-binding activity modulator	G-protein
GNAI1	P63096	protein-binding activity modulator	G-protein
RHOA	P61586	protein-binding activity modulator	G-protein
RAB5A	P20339	protein-binding activity modulator	G-protein
RAB5B	P61020	protein-binding activity modulator	G-protein
RAC1	P63000	protein-binding activity modulator	G-protein
ATL3	Q6DD88	protein-binding activity modulator	G-protein
ARF4	P18085	protein-binding activity modulator	G-protein
RAB34	Q9BZG1	protein-binding activity modulator	G-protein
RALA	P11233	protein-binding activity modulator	G-protein
RHOG	P84095	protein-binding activity modulator	G-protein
GNA13	Q14344	protein-binding activity modulator	G-protein
RAB21	Q9UL25	protein-binding activity modulator	G-protein
RHOB	P62745	protein-binding activity modulator	G-protein
GNB4	Q9HAV0	protein-binding activity modulator	G-protein
ATL2	Q8NHH9	protein-binding activity modulator	G-protein
ARFGAP1	Q8N6T3	protein-binding activity modulator	G-protein modulator
IQGAP1	P46940	protein-binding activity modulator	G-protein modulator
ARHGAP1	Q07960	protein-binding activity modulator	G-protein modulator
PRKAR2A	P13861	protein-binding activity modulator	kinase modulator
SERPINH1	P50454	protein-binding activity modulator	protease inhibitor
CD109	Q6YHK3	protein-binding activity modulator	protease inhibitor
CSTA	P01040	protein-binding activity modulator	protease inhibitor
PRKCSH	P14314	protein-binding activity modulator	protein-binding activity modulator
SERINC1	Q9NRX5	protein-binding activity modulator	protein-binding activity modulator
GNAS	P63092	protein-binding activity modulator	protein-binding activity modulator
ARHGEF2	Q92974	protein-binding activity modulator	protein-binding activity modulator
NSFL1C	Q9UNZ2	protein-binding activity modulator	protein-binding activity modulator
CD3EAP	O15446	RNA metabolism protein	DNA-directed RNA polymerase
POLR1E	Q9GZS1	RNA metabolism protein	DNA-directed RNA polymerase
DDX39B	Q13838	RNA metabolism protein	RNA helicase
DDX47	Q9H0S4	RNA metabolism protein	RNA helicase
DDX21	Q9NR30	RNA metabolism protein	RNA helicase
HDLBP	Q00341	RNA metabolism protein	RNA metabolism protein
SRP54	P61011	RNA metabolism protein	RNA metabolism protein
PCBP2	Q15366	RNA metabolism protein	RNA metabolism protein
SRP68	Q9UHB9	RNA metabolism protein	RNA metabolism protein
ADAR	P55265	RNA metabolism protein	RNA metabolism protein
PCBP3	P57721	RNA metabolism protein	RNA metabolism protein
NOP58	Q9Y2X3	RNA metabolism protein	RNA metabolism protein
DIMT1	Q9UNQ2	RNA metabolism protein	RNA methyltransferase
NSUN2	Q08J23	RNA metabolism protein	RNA methyltransferase
PTBP3	O95758	RNA metabolism protein	RNA processing factor
BSG	P35613	scaffold/adaptor protein	scaffold/adaptor protein
GPC1	P35052	scaffold/adaptor protein	scaffold/adaptor protein
CD63	P08962	scaffold/adaptor protein	scaffold/adaptor protein
LRRC59	Q96AG4	scaffold/adaptor protein	scaffold/adaptor protein
YWHAZ	P63104	scaffold/adaptor protein	scaffold/adaptor protein
SLC9A3R2	Q15599	scaffold/adaptor protein	scaffold/adaptor protein
TSPAN6	O43657	scaffold/adaptor protein	scaffold/adaptor protein
YWHAG	P61981	scaffold/adaptor protein	scaffold/adaptor protein
RRBP1	Q9P2E9	scaffold/adaptor protein	scaffold/adaptor protein

Gene name	Protein ID	Class	Subclass
PPFIBP1	Q86W92	scaffold/adaptor protein	scaffold/adaptor protein
SLC9A3R1	O14745	scaffold/adaptor protein	scaffold/adaptor protein
YWHAQ	P27348	scaffold/adaptor protein	scaffold/adaptor protein
SNTB2	Q13425	scaffold/adaptor protein	scaffold/adaptor protein
PLIN3	O60664	scaffold/adaptor protein	scaffold/adaptor protein
LRRC8A	Q8IWT6	scaffold/adaptor protein	scaffold/adaptor protein
GCN1L1	Q92616	scaffold/adaptor protein	scaffold/adaptor protein
SCRIB	Q14160	scaffold/adaptor protein	scaffold/adaptor protein
YWHAE	P62258	scaffold/adaptor protein	scaffold/adaptor protein
YWHAB	P31946	scaffold/adaptor protein	scaffold/adaptor protein
MPP6	Q9NZW5	scaffold/adaptor protein	scaffold/adaptor protein
NPTN	Q9Y639	scaffold/adaptor protein	scaffold/adaptor protein
CASK	O14936	scaffold/adaptor protein	scaffold/adaptor protein
DLG1	Q12959	scaffold/adaptor protein	scaffold/adaptor protein
ERBB2IP	Q96RT1	scaffold/adaptor protein	scaffold/adaptor protein
CAV1	Q03135	scaffold/adaptor protein	scaffold/adaptor protein
SCAMP3	O14828	transfer/carrier protein	transfer/carrier protein
SCAMP1	O15126	transfer/carrier protein	transfer/carrier protein
SLC25A5	P05141	transfer/carrier protein	transfer/carrier protein
SCAMP2	O15127	transfer/carrier protein	transfer/carrier protein
LCN1	P31025	transfer/carrier protein	transfer/carrier protein
SRPRB	Q9Y5M8	transfer/carrier protein	transfer/carrier protein
EPRS	P07814	translational protein	aminoacyl-tRNA synthetase
FARSA	Q9Y285	translational protein	aminoacyl-tRNA synthetase
KARS	Q15046	translational protein	aminoacyl-tRNA synthetase
QARS	P47897	translational protein	aminoacyl-tRNA synthetase
RPL14	P50914	translational protein	ribosomal protein
RPS29	P62273	translational protein	ribosomal protein
RPL23	P62829	translational protein	ribosomal protein
RPL21	P46778	translational protein	ribosomal protein
RPS13	P62277	translational protein	ribosomal protein
RPLP2	P05387	translational protein	ribosomal protein
RPL10A	P62906	translational protein	ribosomal protein
RPL8	P62917	translational protein	ribosomal protein
RPL4	P36578	translational protein	ribosomal protein
RPL24	P83731	translational protein	ribosomal protein
EEF2	P13639	translational protein	translation factor
EIF4E	P06730	translational protein	translation factor
EIF4G2	P78344	translational protein	translation factor
EIF2S3	P41091	translational protein	translation factor
EEF1A1	P68104	translational protein	translation factor
EIF4G1	Q04637	translational protein	translation factor
EEF1A1P5	Q5VTE0	translational protein	translation factor
EIF2B4	Q9UI10	translational protein	translation factor
EIF5B	O60841	translational protein	translation factor
EEF1B2	P24534	translational protein	translational protein
GPRC5A	Q8NFJ5	transmembrane signal receptor	G-protein coupled receptor
GPR56	Q9Y653	transmembrane signal receptor	G-protein coupled receptor
TMEM87A	Q8NBN3	transmembrane signal receptor	G-protein coupled receptor
CD97	P48960	transmembrane signal receptor	G-protein coupled receptor
ADRA2A	P08913	transmembrane signal receptor	G-protein coupled receptor
AGTRAP	Q6RW13	transmembrane signal receptor	transmembrane signal receptor
CD44	P16070	transmembrane signal receptor	transmembrane signal receptor
LMBRD2	Q68DH5	transmembrane signal receptor	transmembrane signal receptor
PGRMC1	O00264	transmembrane signal receptor	transmembrane signal receptor
TNFRSF10A	O00220	transmembrane signal receptor	transmembrane signal receptor
PGRMC2	O15173	transmembrane signal receptor	transmembrane signal receptor
EGFR	P00533	transmembrane signal receptor	transmembrane signal receptor
VASN	Q6EMK4	transmembrane signal receptor	transmembrane signal receptor
ENG	P17813	transmembrane signal receptor	transmembrane signal receptor
EPHA2	P29317	transmembrane signal receptor	transmembrane signal receptor
PLXNB2	O15031	transmembrane signal receptor	transmembrane signal receptor
SDC4	P31431	transmembrane signal receptor	transmembrane signal receptor
NPR3	P17342	transmembrane signal receptor	transmembrane signal receptor
SIRPA	P78324	transmembrane signal receptor	transmembrane signal receptor
VDAC2	P45880	transporter	ion channel
VDAC1	P21796	transporter	ion channel
CACNA2D1	P54289	transporter	ion channel
ANO6	Q4KMQ2	transporter	ion channel
CLIC1	O00299	transporter	ion channel
ATP1A1	P05023	transporter	primary active transporter
SLC1A5	Q15758	transporter	primary active transporter
ATP1B1	P05026	transporter	primary active transporter
ATP6V0A1	Q93050	transporter	primary active transporter
ATP6V0D1	P61421	transporter	primary active transporter
ATP1B3	P54709	transporter	primary active transporter
ATP2A2	P16615	transporter	primary active transporter
ATP2B1	P20020	transporter	primary active transporter
VCP	P55072	transporter	primary active transporter
ATP6V1A	P38606	transporter	primary active transporter
SLC12A4	Q9UP95	transporter	secondary carrier transporter
VAT1	Q99536	transporter	secondary carrier transporter
SLC39A6	Q13433	transporter	secondary carrier transporter
SLC39A10	Q9ULF5	transporter	secondary carrier transporter
MTCH2	Q9Y6C9	transporter	secondary carrier transporter
SLC12A2	P55011	transporter	secondary carrier transporter

Gene name	Protein ID	Class	Subclass
SLC4A7	Q9Y6M7	transporter	secondary carrier transporter
SLC3A2	P08195	transporter	transporter
SLC7A5	Q01650	transporter	transporter
SLC16A1	P53985	transporter	transporter
SLC2A13	Q96QE2	transporter	transporter
SLC16A3	O15427	transporter	transporter
CSE1L	P55060	transporter	transporter
SLC38A5	Q8WUX1	transporter	transporter
SLC7A11	Q9UPY5	transporter	transporter
SLC29A1	Q99808	transporter	transporter
TM9SF2	Q99805	transporter	transporter
NUP35	Q8NFH5	transporter	transporter
XPO1	O14980	transporter	transporter
KPNA3	O00505	transporter	transporter
ASNA1	O43681	transporter	transporter
SLC38A1	Q9H2H9	transporter	transporter
IPO7	O95373	transporter	transporter
SLC30A1	Q9Y6M5	transporter	transporter
AQP1	P29972	transporter	transporter
SPNS1	Q9H2V7	transporter	transporter
BASP1	P80723	Unclassified	Unclassified
AHNAK	Q09666	Unclassified	Unclassified
BST2	Q10589	Unclassified	Unclassified
JUP	P14923	Unclassified	Unclassified
TMEM179B	Q7Z7N9	Unclassified	Unclassified
CTNNB1	P35222	Unclassified	Unclassified
TAGLN2	P37802	Unclassified	Unclassified
HSD17B4	P51659	Unclassified	Unclassified
MYOF	Q9NZM1	Unclassified	Unclassified
ARL8B	Q9NVJ2	Unclassified	Unclassified
CD59	P13987	Unclassified	Unclassified
RPS27A	P62979	Unclassified	Unclassified
PHB	P35232	Unclassified	Unclassified
PHB2	Q99623	Unclassified	Unclassified
HDAC10	Q969S8	Unclassified	Unclassified
SDAD1	Q9NVU7	Unclassified	Unclassified
MARCKSL1	P49006	Unclassified	Unclassified
TMEM43	Q9BTV4	Unclassified	Unclassified
MARCKS	P29966	Unclassified	Unclassified
KTN1	Q86UP2	Unclassified	Unclassified
FAM129B	Q96TA1	Unclassified	Unclassified
PAICS	P22234	Unclassified	Unclassified
AHNAK2	Q8IVF2	Unclassified	Unclassified
PPIB	P23284	Unclassified	Unclassified
FERMT2	Q96AC1	Unclassified	Unclassified
FKBP10	Q96AY3	Unclassified	Unclassified
TPBG	Q13641	Unclassified	Unclassified
FKBP11	Q9NYL4	Unclassified	Unclassified
API5	Q9BZZ5	Unclassified	Unclassified
RCC2	Q9P258	Unclassified	Unclassified
EMC1	Q8N766	Unclassified	Unclassified
TMEM109	Q9BVC6	Unclassified	Unclassified
UBA52	P62987	Unclassified	Unclassified
NOMO1	Q15155	Unclassified	Unclassified
SND1	Q7KZF4	Unclassified	Unclassified
CCDC47	Q96A33	Unclassified	Unclassified
RAD50	Q92878	Unclassified	Unclassified
EEF1G	P26641	Unclassified	Unclassified
HNRNPM	P52272	Unclassified	Unclassified
IMMT	Q16891	Unclassified	Unclassified
CDC42SE2	Q9NRR3	Unclassified	Unclassified
MTDH	Q86UE4	Unclassified	Unclassified
LMNA	P02545	Unclassified	Unclassified
EMD	P50402	Unclassified	Unclassified
PARK7	Q99497	Unclassified	Unclassified
ZDHHC5	Q9C0B5	Unclassified	Unclassified
LMNB1	P20700	Unclassified	Unclassified
CLU	P10909	Unclassified	Unclassified
PEF1	Q9UBV8	Unclassified	Unclassified
ATAD3A	Q9NVI7	Unclassified	Unclassified
CLPTM1L	Q96KA5	Unclassified	Unclassified
CD70	P32970	Unclassified	Unclassified
CTNNBL1	Q8WYA6	Unclassified	Unclassified
YBX1	P67809	Unclassified	Unclassified
PSMD11	O00231	Unclassified	Unclassified
CYSRT1	A8MQ03	Unclassified	Unclassified
SYAP1	Q96A49	Unclassified	Unclassified
DBN1	Q16643	Unclassified	Unclassified
CMBL	Q96DG6	Unclassified	Unclassified
APMAP	Q9HDC9	Unclassified	Unclassified
PDXDC1	Q6P996	Unclassified	Unclassified
SMC1A	Q14683	Unclassified	Unclassified
RUVBL2	Q9Y230	Unclassified	Unclassified
TTLL12	Q14166	Unclassified	Unclassified
PIGS	Q96S52	Unclassified	Unclassified
TMEM165	Q9HC07	Unclassified	Unclassified

Gene name	Protein ID	Class	Subclass
PTK7	Q13308	Unclassified	Unclassified
UNC45A	Q9H3U1	Unclassified	Unclassified
ACACA	Q13085	Unclassified	Unclassified
MYADM	Q96S97	Unclassified	Unclassified
STIP1	P31948	Unclassified	Unclassified
PSMD6	Q15008	Unclassified	Unclassified
UNC13D	Q70J99	Unclassified	Unclassified
NOB1	Q9ULX3	Unclassified	Unclassified
TCF25	Q9BQ70	Unclassified	Unclassified
KPRP	Q5T749	Unclassified	Unclassified
RRP1	P56182	Unclassified	Unclassified
EFR3A	Q14156	Unclassified	Unclassified
PSME3	P61289	Unclassified	Unclassified
FASN	P49327	Unclassified	Unclassified
ST13	P50502	Unclassified	Unclassified
GNB2L1	P63244	Unclassified	Unclassified
ITFG1	Q8TB96	Unclassified	Unclassified
NOTCH2	Q04721	Unclassified	Unclassified
DDRGK1	Q96HY6	Unclassified	Unclassified
NCLN	Q969V3	Unclassified	Unclassified
ATAD3B	Q5T9A4	Unclassified	Unclassified